INVESTIGATION OF THE APPLICATIONS OF NANOFIBRILLATED CELLULOSE IN THE OIL INDUSTRY

A Dissertation

by

HAIYAN ZHAO

Submitted to the Office of Graduate and Professional Studies of
Texas A&M University
in partial fulfillment of the requirements for the degree of

DOCTOR OF PHILOSOPHY

Chair of Committee,	Hisham A. Nasr-El-Din
Committee Members,	Stephen A. Holditch
	Maria A. Barrufet
	Mahmoud El-Halwagi
Head of Department,	A. Daniel Hill

August 2015

Major Subject: Petroleum Engineering

ABSTRACT

Polymers, including biopolymers and synthetic polymers, are extensively used in oil industry. However, problems exist in these polymer fluids. Severe formation damage can be caused by most polymers. Moreover, thermal stability limits the applications of biopolymer-based fluids at high temperatures. Here, four nanofibrillated cellulose (NFC) have been evaluated as viscosifiers to prepare aqueous fluids, and compared to guar-based fluids.

The rheological properties and solid suspending ability of NFC-based fluids have been studied with the effects of temperature and salts. Formation damage of the new type of fluids in different formations has been evaluated. Degradation studies have been performed using different types of breakers.

The viscosity measurements have shown that the NFC-based fluids were stable as high as 350°F. For non-charged NFC, the fluids had a high tolerance to KCl and $CaCl_2$. Moreover, NFC-based fluids had a good solid suspending ability, which out-performanced guar-based fluids. Coreflood tests were run using cores of different permeability. As for NFC-based fluids, the regained permeabilities were 85% or higher of the initial permeabilities in low-permeability cores, suggesting that NFC caused a slight damage. However, guar and HPG fluids caused much more damage than NFC fluids under same conditions. Severe damage was caused to high-permeability cores (about 400 md or more) when treated by NFC-based fluids. The damage degree was related to the size of NFC fibers. Fibers of smaller sizes can invade the core and plug the pore throats more easily.

However, the new fluids were successfully degraded by different breakers, indicated by the significant decrease in the fluid viscosity. HPLC analyses have shown that the new viscosifiers can be mostly degraded into soluble products with low viscosity, which can be flowed back after the treatment.

This work has evaluated four nanofibrillated cellulose fibers as viscosifiers in fluids. These new fluids have better thermal stability and solid suspending ability than guar-based fluids under the same conditions. High regained permeability of low-permeability cores can be maintained when treated by the new fluids. Severe damage was caused in high-permeability cores, however, the damage can be removed because the fluids were degraded successfully.

DEDICATION

To my parents and my husband

ACKNOWLEDGEMENTS

I would like to thank my advisor and committee chair, Dr. Hisham Nasr-El-Din for giving me such a great study opportunity and supervising me through my graduate study. He is always helpful with enduring patience and kindness. Dr. Nasr-El-Din gives me great encouragement when I encounter challenges in research. I would also like to thank my committee members, Dr. S. Holditch, Dr. M. Barrufet, and Dr. M. El-Halwagi, for their guidance and support throughout the course of my research.

Thanks also go to all members of the Nasr-El-Din group. I would especially like to thank Dr. Guanqun Wang, and Dr. Lijun Zhou for their great help in my early years in the Nasr-El-Din group. I would also like to thank my friends in and out of the department, with whom I have had a great time when out of lab. Without these wonderful colleagues and friends, I would not have such enjoyable time during my graduate study.

Finally, I would like to thank my parents for their encouragement and support. I am extremely grateful to my husband, Yi Shu. His support and love accompany me to finish my PhD study.

TABLE OF CONTENTS

Page

Page

Page

LIST OF FIGURES

Page

Page

Page

Page

Page

Page

Page

LIST OF TABLES

Page

1. INTRODUCTION AND BACKGROUND

1.1. Polymers in oil industry

Organic polymers have wide applications in oil industry. They have been successfully used in many fluids/gels in drilling, acid stimulation, hydraulic fracturing, water and gas control, enhanced oil recovery (EOR), asphaltene control, and corrosion control, et al (Kelland 2014). Three types of polymers are used, polysaccharides (biopolymers), modified polymers, and synthetic polymers (polyacrylamides).

In water-based drilling fluids, polymers are added to provide solid carrying capacity, form filter cake, and control fluid loss. Partially hydrolyzed polyacrylamide (PHPA), guar gum, xanthan, starch, and cellulose derivatives were reported previously as important components in drilling fluids, due to the low toxicity of these polymers (Chatterji and Borchardt 1981; Talabani et al. 1993; Roger et al. 1993). In acid stimulations, polymers are used as diverting agents. Two types of diverting methods are developed. One is the injection of a polymer gel pill before main acid flush, and the other is the in-situ gelled acid. The acid diverters can slow down the reaction rate allowing deeper penetration and decrease the leak-off volume (Kelland 2014). In hydraulic fracturing fluids, polymers are added to increase the viscosity of the fluids, in order to enhance the propppant suspending ability and prevent fluid loss. More than 90% of the polymers used in fracturing fluid are guar and guar derivatives. These polymers can be crosslinked to form very viscous gel. The properties of polymer-based fluids will be discussed in the following part of this section.

1.2. Some background on hydraulic fracturing technique

With the development of shale gas/oil and horizontal wells, hydraulic fracturing becomes very important in well stimulation to enhance productivity. Historically, hydraulic fracturing has been applied to stimulate low-permeability formations with permeability in the millidarcy range by bypassing near-wellbore damage (Montgomery 2013). The first hydraulic fracturing treatment was performed in 1940s, but it did not increase production due to the lack of proppant (Howard and Fast 1970). The successful fracturing treatments were done by using oil-based fluids and proppant agents (Clark 1949). For example, a hydraulic fracturing treatment increased the productivity by injecting gelled lease crude, sand, and breaker in East Texas Field (Farris 1953). Hydraulic fracturing treatments showed superior performance over matrix treatments, because conductive paths into the production zone were created by hydraulic fracturing treatments. In 1990s, hydraulic fracturing found its applications for enhanced productivity in high-permeability unconsolidated formations (Meese et al. 1994; Parker et al. 1994; Parlar et al. 1995; Smith et al. 1996; Ellis 1998; Samuel et al. 2007). Nowadays, hydraulic fracturing has been used extensively to produce shale reservoir where the permeability is very low (McDaniel 2005). Three purposes are targeted for hydraulic fracturing operations: to create a conductive path and increase productivity, to bypass near-wellbore damage, and to alter fluid flow in the formation.

Fracturing fluids are injected into the formation through wellbore. Along with the fluid injection, the pressure builds up until the fracturing point is reached when the fractures are generated. The early fracture growth creates new formation area leading to

an increase in the leak-off rate of the injection fluid. However, the fracture can continue propagating as long as the pumping rate is higher than the fluid-loss rate. The contact area between the wellbore and formation is then enlarged. Proppant has to be transported into the fracture to keep the fracture open and maintain a conductive flow path during production (Economides and Nolte 2000). The first step of a hydraulic fracture treatment is to inject fluid only without proppant, termed as the pad, which is to initiate the fracture. After the pad, proppant-laden stages are performed to transport proppant to fractures. At the end, a final flush stage, one wellbore pore volume of fluid, is pumped to clean the proppant in the wellbore. The whole treatment will create one or more proppant-filled fractures. In some cases, one or more special stages are added for specific formations. For example, Salazar et al. (2013) incorporated a prepad of a viscosifier fluid of chelants and acid into their fracturing treatment design in water-sensitive formation where high clay contents.

1.2.1. Early development of fracturing to bypass damage and improve productivity

Near wellbore damage can be induced by several sources, such as drilling-induced damage, fines migration, and scale deposition. Historically, matrix treatments were used to remove formation damage. However, in some cases, matrix treatment may not be effective. For example, for the formation with high clay content, matrix acidizing is not sufficient to fully remove the damage. Hydraulic fracturing treatment has been tried to bypass the near wellbore damage by creating a conductive path in the damage region (Salazar et al. 2013).

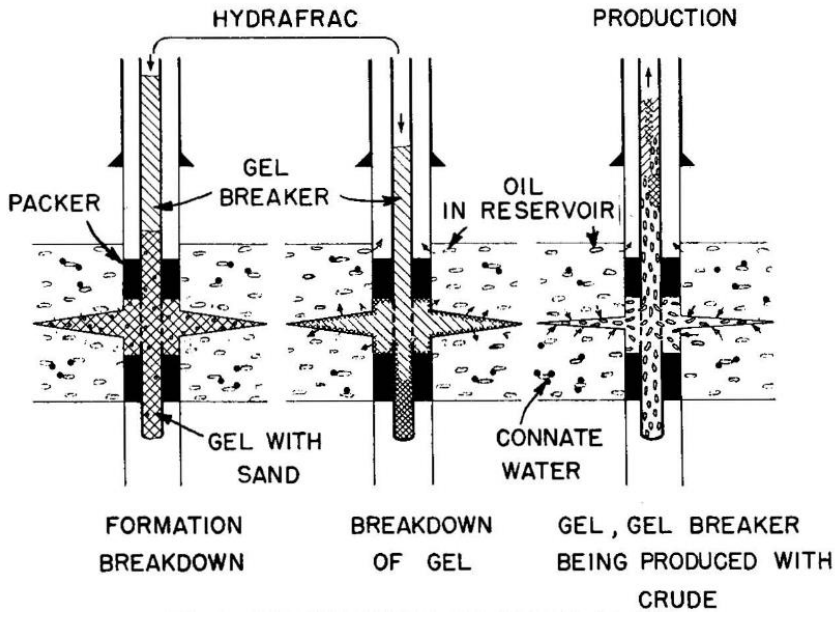

Fig. 1—Sequence of steps in hydrafrac process (after Clark 1949)

Moreover, the conductive path can be extended deep into the reservoir and enhance the productivity through increasing the formation flow area. The first hydraulic fracturing treatment was performed in the Hugoton gas field in Kansas in 1947, for stimulation purpose (Howard and Fast 1970). 1000 gallons of gelled gasoline was injected followed by the injection of gel breaker. Clark (1949) reported that the "hydrafrac" process increased production in 11 wells when such process was used in 32 jobs on 23 wells. This "hydrafrac" process was shown in **Fig. 1**, which consisted two steps: (1) formation breakdown was done with a viscous oil-based fluid loaded with sand as proppant; (2) the viscous fluid was broke down with a breaker solution. Later, the hydrafrac treatments were used to stimulate wells in different formations with higher chances of success (Grossman

1951; Padgett 1951; Ghauri 1960). Padgett (1951) reported that hydrafrac treatments on 316 wells showed 72.5 % success and enhanced production by an average of 45.8 barrels per day. Ghauri (1960) reported that a total of 53 hydraulic fracturing treatments were performed from 1953 to 1960 in the Los Angeles basin, and they were highly successful on an over-all basis.

During the early stage of hydraulic fracturing development, most applications were used for relatively high-permeability reservoir, because very low-permeability formation was not of interest with low oil prices (Smith and Hannah 1996). For example, **Fig. 2** shows the results of fracturing in a tight-gas reservoir and a moderate-permeability reservoir. The increased productivity in the moderate-permeability reservoir was larger in absolute number than low-permeability well. The applications of hydraulic fracturing grew rapidly and increased US oil supply significantly, with an estimation of at least 30% recoverable oil/gas reseves.

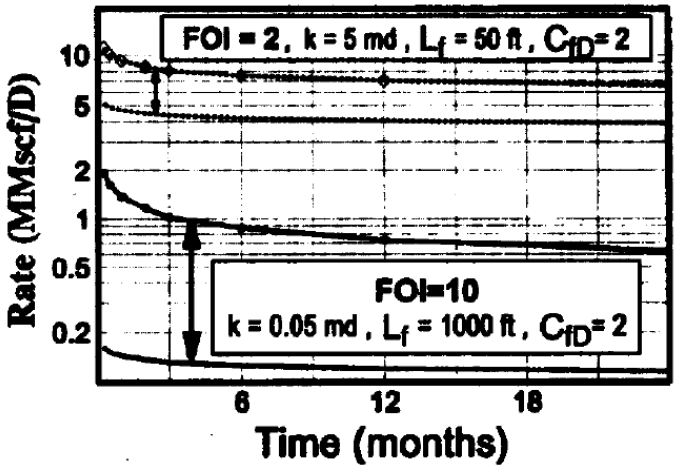

Fig. 2—Reason to fracture high-permeability wells (after Smith and Hannah 1996)

1.2.2. Hydraulic fracturing technique in moderate/high-permeability formations

Propped fracture width is the key factor for fracturing high-permeability formations. The development of tip-screenout (TSO) hydraulic fracturing technique can create wide and highly conductive fractures. TSO fracturing means to screen out the tip of the fracture intentionally with sand, and then to continue pumping slurry to increase the fracture width and to pack the fracture with proppant (Smith et al. 1987). TSO fracturing technique has been used extensively to stimulate soft formations (Ayoub et al. 1992; Martins et al. 1992). High proppant concentrations are necessary in soft formations, and TSO fracturing technique is essential to achieve the high proppant concentrations as well as large propped fracture width.

Frac pack is one major application of TSO-hydraulic fracturing technique in moderate/high-permeability formations, which is creating a revolution in well completion for sand control. Formation sand and fines can be produced with oil and gas, referred as sand production, which can cause erosion and wear of equipment and production loss. After applications of TSO hydraulic fracturing stimulations were successfully achieved, frac pack was developed in high-permeability, unconsolidated formations to prevent sand production (Ellis 1998). In many cases where fack pack treatments are applied, the vertical permeability of the formations limits the application of horizontal wells, or multiple target zone exist behind the casing (Weirich et al. 2013). Frac pack completion consists of TSO hydraulic fracturing stimulation and a gravel-pack screen-packer assembly (**Fig. 3**). TSO fracturing can create a high conductive fracture channel to bypass the near-wellbore damage and improve productivity. The gravel-pack screen assembly can prevent proppant

flowback. A stable barrier is established in the proppant/formation interface to prevent sand production. Therefore, the frac pack technique combines the advantages of hydraulic fracturing and gravel pack: the well stimulation from a highly conductive fracture and sand control from the gravel pack. Besides, frac pack is also an effective method to reduce drawdown and non-Darcy flow effects and to achieve complete zonal coverage (Roodhart et al., 1994).

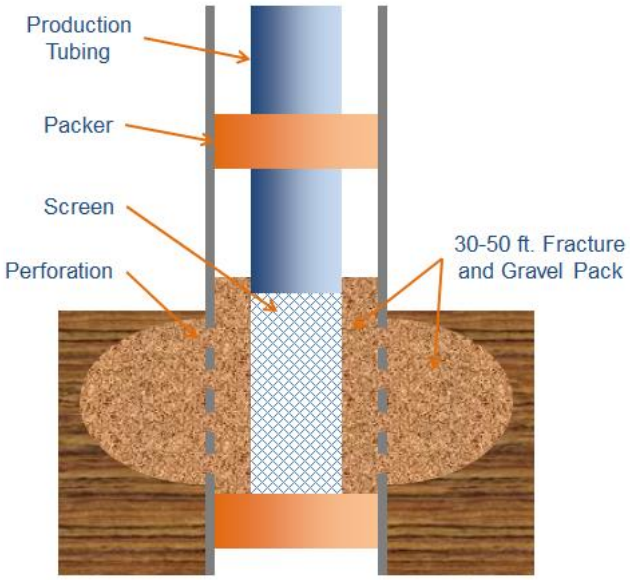

Fig. 3—The scheme of frac pack (after Suman et al. 1985)

The earliest use of frac pack idea went back to 1960s using “viscous-oil squeeze jobs”. In 1980s, a combination of TSO fracturing with gravel pack was reported to control sand production and improve oil/gas productivity. For example, Amoco did several frac pack completions in the Hackberry field, LA, and Trinidad, which were all successful.

Grubert showed that a small fracture job before gravel pack was better than stand-alone fracturing or gravel pack in sand control and production enhancement (Grubert 1991).

In 1990s, the application of frac pack was used with an increasing percentage of sand control completion methods in world wide. Case histories showed that frac pack increased productivity and controlled sand production effectively. Hainey and Troncoso (1992) reported successful field tests using crosslinked or linear gel in frac pack completions in the US Gulf coast, for productivity improvement and sand control. Other examples were also reported on frac pack completions in offshore Gulf Coast (Monus et al., 1992; Roodhart et al., 1994; Meese et al., 1994; Stewart et al. 1995). All showed successful stimulation as well as sand control.

From 1997 to 2006, an estimated 12,000 frac pack operations were done in worldwide, with proven superior to other sand-control methods (Weirich et al. 2013; Liu et al. 2006). In Gulf of Mexico (GOM), frac pack constitutes for over 70% of completions as shown in **Fig. 4**. Deepwater frac pack has additional challenges, such as higher rig costs, larger working-string volumes, fluid cool-down, and difficulty in prediction of fluid performance and work-string length changes (Malochee and Comeaux 2003). However, frac pack completion has shown improved flow efficiency as well as low failure rates compared to other sand-control methods (Vitthal 2003; Norman 2004).

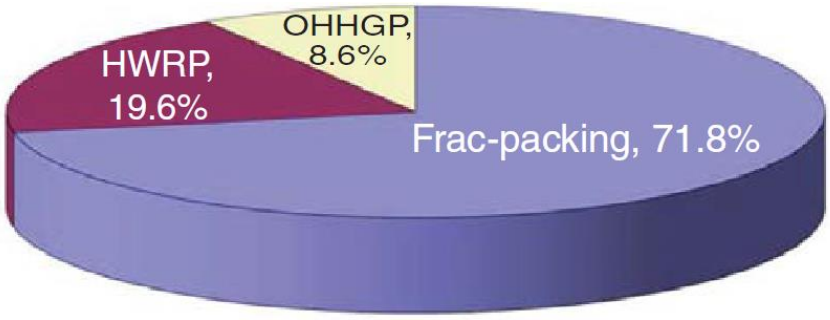

Fig. 4—The percentage of various completion methods in GOM (after Weirich et al. 2013).

In recent years, due to the developments of new techniques, frac pack has expanded to be applied in more types of formations. For example, Ibrahim et al. (2014) reported high angle frac pack operations in shallow sands in the gas field in the Malay Basin, Malaysia. The shallow vertical depth led to the injection pressure higher than overburden stress and thus creating a horizontal fracture. This made the screenout difficult. However, optimizations, including controlling pump rate, and decreasing the gel loading of fracturing fluid, were performed to induce a screenout eventually.

1.2.3. Hydraulic fracturing technique in low-permeability reservoir

Hydraulic fracturing is a key factor to promote the development of unconventional reservoirs, tight gas, shale gas, and coalbed methane. Due to the shortage of gas in mid 1970s, hydraulic fracturing began to stimulate low-permeability formations, which is the second age of hydraulic fracturing, massive hydraulic fracturing (MHF) (Smith and Hannah 1996). The massive hydraulic fracturing is to utilize hundreds of thousands gallons of fracturing fluid and 100,000 to 1,000,000 lb proppant to create long fractures

deep into the reservoirs (Jennings et al. 1977). The propped fracture length was the key in stimulating low-permeability formations. Sustained productivity increase was obtained by massive hydraulic fracturing treatments in low-permeability gas reservoirs in many fields. For example, massive hydraulic fracturing was applied successfully to stimulate the tight Muddy "J" formation, Wattenberg field, Colorado in 1970s (Fast et al. 1977). The permeability of Muddy "J" formation was quite low (0.05 to 0.005 md) with a pay zone of 50 ft thick at a depth of about 8000 ft. At the beginning, conventional hydraulic fracturing stimulation was operated and created fractures of 100 to 500 ft in length. The productivity was increased, but it declined very quickly. Later, massive hydraulic fracturing, with over 500,000 gal of fluid and 1,000,000 lbs sand, was performed by creating fractures extending 3000 ft in length. The field results showed that the massive hydraulic fracturing was effective in improving productivity economically. Other examples were also reported with successful MHF treatments in tight gas formations (Antoci and Anaya 2001; Nor-Azlan et al. 2003; Shaoul et al. 2007; Lei et al. 2008; Weng et al. 2011; Wang et al. 2012).

Massive hydraulic fracturing was also applied to stimulate low-permeability oil field. Irvine-Fortescue and Shoufi (2009) reported that multiple massive hydraulic fracturing treatments were performed in a south Oman oil field. The reservoir in this field mainly contains silica with a permeability of 0.02 md or lower. Sour crude is present in the reservoir with a thickness up to 400 meters. Three massive fractures in each well resulted in improved productivity in this field.

Shale reservoir can be produced economically due to the advancement in hydraulic fracturing techniques. Shale reservoir is of nanodarcy permeability, and may contain water-sensitive clays. The ultralow permeability in shale eliminates the requirement of high-viscosity fracturing fluids since leakoff is not an issue. Slickwater has been used in shale reservoirs. Slickwater means water with a drag friction reducer, which is injected at very high rates. The friction reducer, such as polyacrylamide polymers and low concentration linear gel, is to reduce the friction in the pipe during fluid transportation. The high velocity is the key factor to transport the proppant. Compared to other gelled fracturing fluids, slickwater has low viscosity and thus can only carry low concentrations of proppant, usually 0.25 to 3 lb/gal (Palisch et al 2010).

Mayerhofer et al. (1997) and Walker et al. (1998) pointed that "waterfrac" using water and very low proppant concentrations was very successful in tight gas reservoirs. The important characteristics of "waterfrac" were its substantial cost reduction, easier cleanup, and longer fractures compared to conventional hydraulic fracturing techniques. Due to the simple fluid system, slickwater can be reused, which can be very meaningful in places where water disposal is expensive or difficult. Slickwater fracturing came to the attention of engineers and was developed very quickly. Slickwater fracturing operations were used widely in early 2000s. For example, it constituted over 30% of stimulation treatments done in 2004 (Schein 2005). Slickwater fracturing was extensively applied to stimulate reservoirs in Texas as shown in **Fig. 5**.

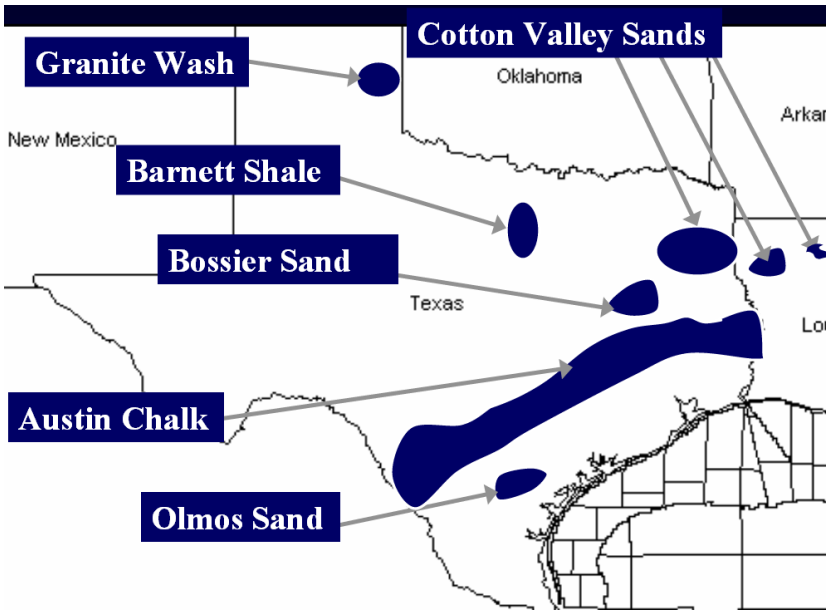

Fig. 5—The geographical areas with successful slickwater fracs (after Schein 2005).

However, later hybrid fracturing has come to engineers' attention. Hybrid is defined as the combination of slickwater with crosslinked gels or linear polymer fluids. Slickwater may be injected in initial stages and followed by crosslinked gels or linear polymer fluids in subsequent stages. A long thin fracture is created by the slickwater prepad. The following injection of crosslinked gel increases the width and height of the fracture. Hybrid fracturing started to increase its percentage in all fracturing operations in recent years. Robart et al. (2013) and Patel el al. (2014) showed that hybrid treatments using slickwater with crosslinked gels increased from 28 to 44% while slickwater decreased from 46 to 19% through analysis of over 55,000 hydraulic fracturing treatments between 2011 and the first half of 2013 (**Fig. 6**).

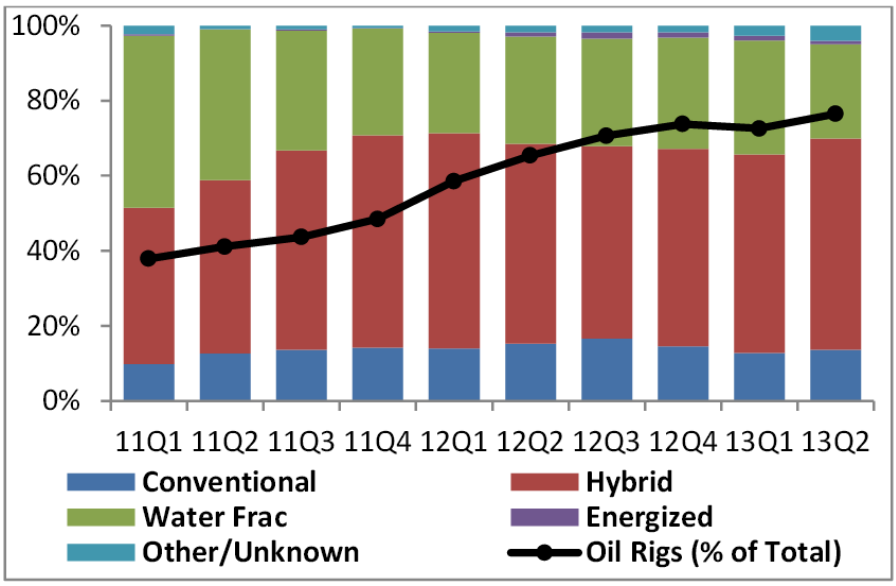

Fig. 6—US frac design trends (after Patel et al. 2014).

One important advantage of hybrid fracturing over conventional crosslinked gel is that hybrid fracturing can create longer and thinner fractures which is beneficial in low-permeability formations. Moreover, due to the cooldown effect induced by the slickwater prepad, lower chemical loadings are needed in the crosslinked gel of hybrid fracturing. This will lead to a more efficient break of gel, less formation damage, and reduced cost (Ramurthy et al. 2006; Coronado 2007). The advantage of hybrid fracturing over slickwater fracturing lies in the better proppant placement in the fracture of hybrid fracturing. The poor proppant suspending ability of slickwater may lead to an uneven distribution of proppant as shown in **Fig. 7**, which increases the screenout possibility. However, the hybrid fracturing can afford a more even distributed proppant placement (**Fig. 7**). Moreover, the hybrid fracturing is also cost effective compared to slickwater fracturing.

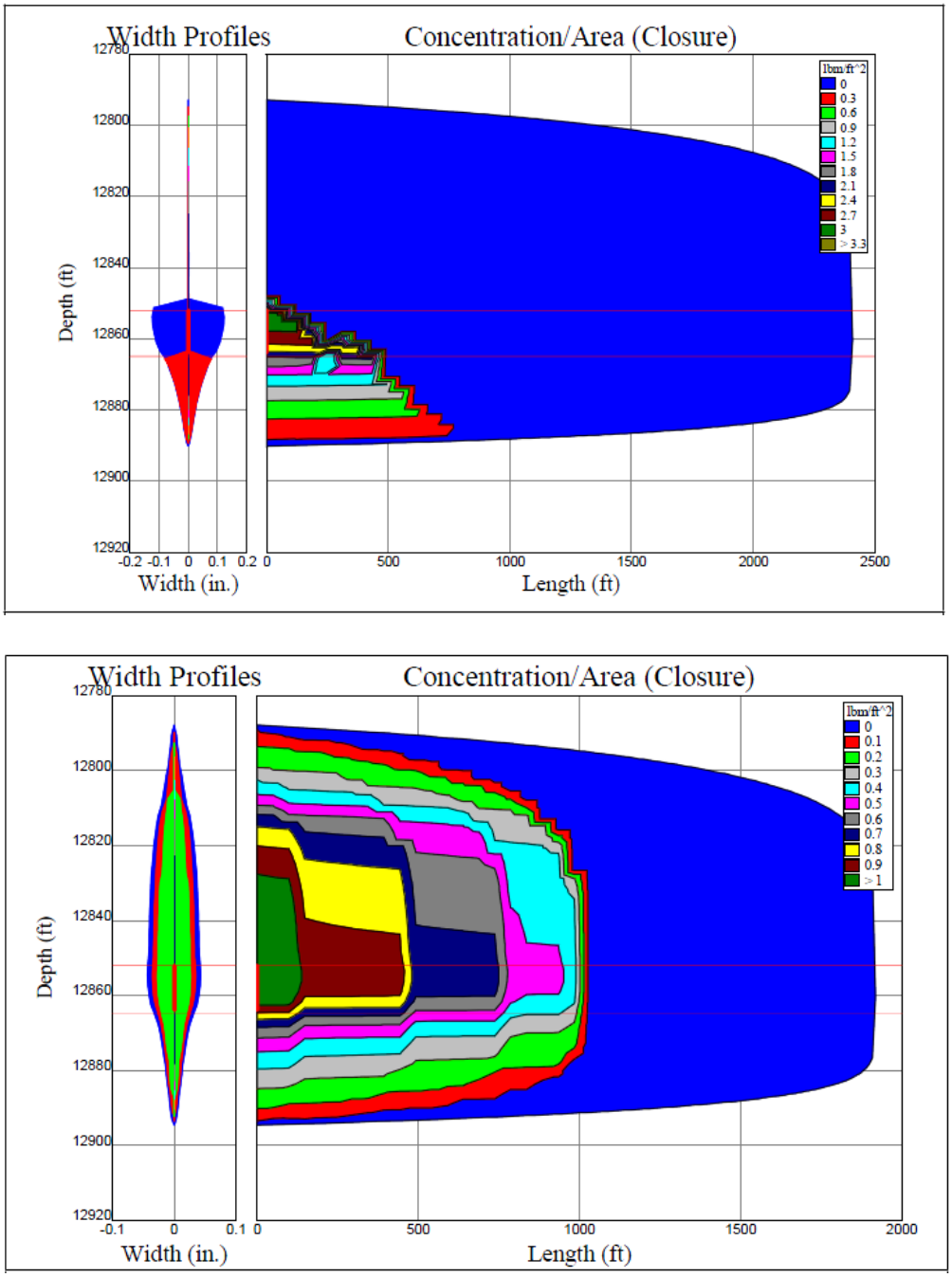

Fig. 7—Contour plots of slickwater fracturing (left) and hybrid fracturing (right) (after Coronado 2007).

1.3. Properties of polymer fluids

Biopolymers can increase the viscosity of aqueous fluids through hydration. Guar and guar derivatives are most commonly used as viscosifiers to prepare water-based fracturing fluids (Ely 1989; Nasr-El-Din et al., 2007; Al-Muntasheri, 2014). 90% of gelled fracturing fluids use guar and its derivatives as viscosifiers.

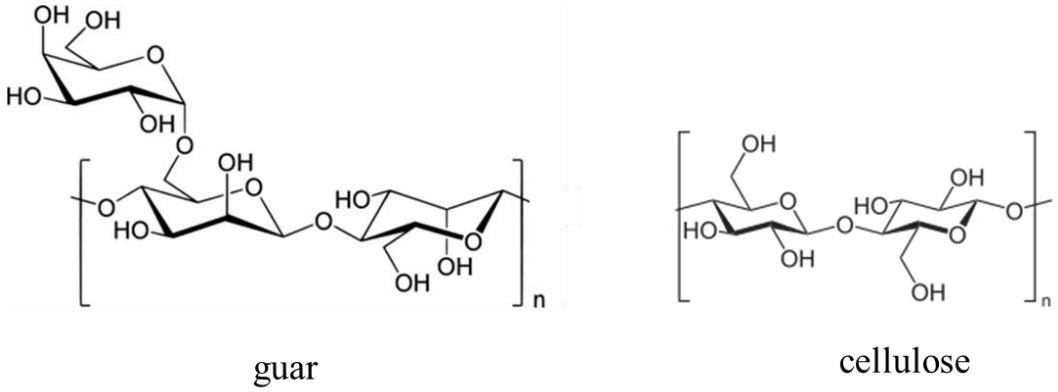

Fig. 8—The structures of guar gum and cellulose

Guar gum is a polygalactomannan produced from seeds of the plant Cyamopsis tetragonolobus (Kapoor et al., 2013). The structure is shown above, consisting of mannose and galactose monomer units (**Fig. 8**). The mannose units, which form the main linear chain of the polymer, are linked by β-1,4 glycosidic bonds. The galactose units are linked to mannose by α-1,6 glycosidic bonds, forming the pendant branches. Guar gum can form intermolecular hydrogen bonding, leading to high solvation and thus increased viscosity. The rheological properties will be discussed in detail later.

The native guar gum has some disadvantages. For example, its excessive hydrophobicity and high molecular weight prevents complete solvation or hydration of the polymer. Low thermal and shear stability also limits its applications in harsh conditions. Guar gum contains 10-14% insoluble residue. In addition, the intermolecular hydrogen bonding will cause the guar molecules to form aggregates, resulting in formation damage (Cheng et al., 2002). Therefore, guar derivatives, modified by the functionalization of the hydroxyl groups on guar backbone, find wide applications in industry. Two terms are used to describe the substitution of hydroxyl groups. Molar substitution (MS) means the average number of moles of substituent groups per mole of anhydro sugar units. Degree of substitution (DS) is defined as the average number of substituent groups per sugar unit. Hydroxyethyl guar (HEG), hydroxypropyl guar (HPG), and carboxymethyl guar (CMG) are three examples for modified guar polymers. These guar polymers are more soluble in water with less insoluble residues. Cheng et al. (2002) studied the effects of hydroxypropyl (HP) substitution. HP substitution decreases the intermolecular hydrogen bonding interactions between guar molecules, by sterically blocking the hydrogen bonding sites on the guar backbone. When temperature increases, it is more likely for HPG to collapse through intramolecular hydrophobic attractions, rather than aggregating through intermolecular interactions. Moreover, the steric hindrance from the substituted groups will restrict the rotation of the polymer backbone bonds, resulting in greater chain rigidity.

1.3.1. Rheological properties of polymer solutions

1.3.1.1. Viscosity

The high viscosity of polymer solutions arises from the high molecular weight, physical entanglement due to molecule overlapping, and intermolecular association (hyperentanglement) through hydrogen bonding (Morris et al., 1981; Goycoolea et al., 1995; Cheng et al., 2002). The hyperentanglement are specific interactions between the mannan backbones, leading to high zero shear viscosity. Polymer fluids are shear-thinning (Bataweel and Nasr-El-Din, 2012). A typical shear-viscosity behavior is shown in **Fig. 9** with a log-log scale. In lower and upper Newtonian flow regions, the viscosity remains constant when shear rate changes, which means that the viscosity is independent of shear rate. In the middle region, the viscosity decreases as shear rate increases. This relationship could be described by the power-law model as expressed in eq. *1*. The non-Newtonian behavior results from the uncoiling and aligning of polymer chains when shearing is applied.

$$\mu = k\gamma^{n-1}. \quad \text{eq. 1}$$

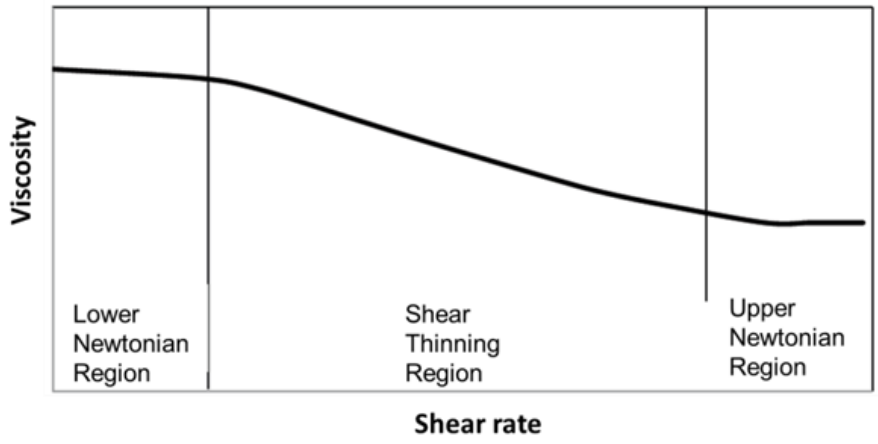

Fig. 9—Shear-viscosity behavior of shear-thinning fluids (after Bataweel and Nasr-El-Din, 2012).

The viscosity of a polymer solution exhibits an exponential increase as a function of concentration (Lei and Clark, 2007). Three regions are shown in the viscosity-concentration curve when the log of specific viscosity is plotted against the log of the concentration (**Fig. 10**). The specific viscosity is:

$$\eta_{sp} = \frac{\eta_0 - \eta_s}{\eta_s} \quad \text{.....eq. 2}$$

Where η_{sp} is the specific viscosity; η_0 is the zero shear viscosity; and η_s is the solvent viscosity.

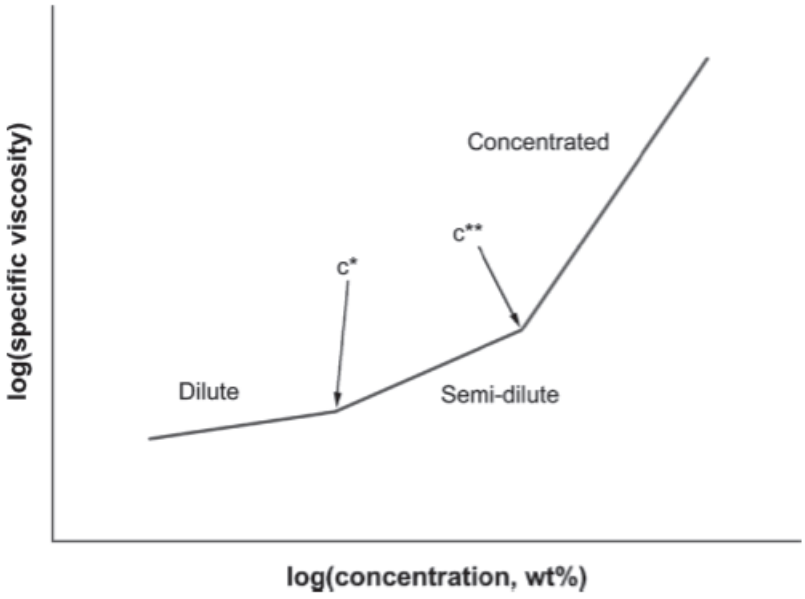

Fig. 10—The relationship between specific viscosity and concentration for polymer solutions (after Lei and Clark, 2007).

In dilute solutions the average distance between polymer chains is larger than their size. Therefore, no interaction exists between polymer molecules, and the viscosity is hydrodynamic (Rubinstein and Colby, 2003). When the concentration reaches the overlap concentration, c*, the polymer molecules begin to weakly interact and chains begin to overlap. Starting this point, the physical properties of semidilute solutions (such as viscosity) will be dominated by the polymer. Thus, the addition of the polymer to a solvent can form a solution with a much higher viscosity than the solvent only. As the concentration increases further above c**, the polymer molecules begin to strongly interpenetrate, and another slope change occurs in **Fig. 10**. Lei and Clark (2007) reported that the c* values are all lower than 0.1 wt% and c** are between 0.36 and 0.42 wt% for

HPG, CMG, and CMHPG. These studies have indicated that a small amount of polymer can afford a solution with a very high viscosity.

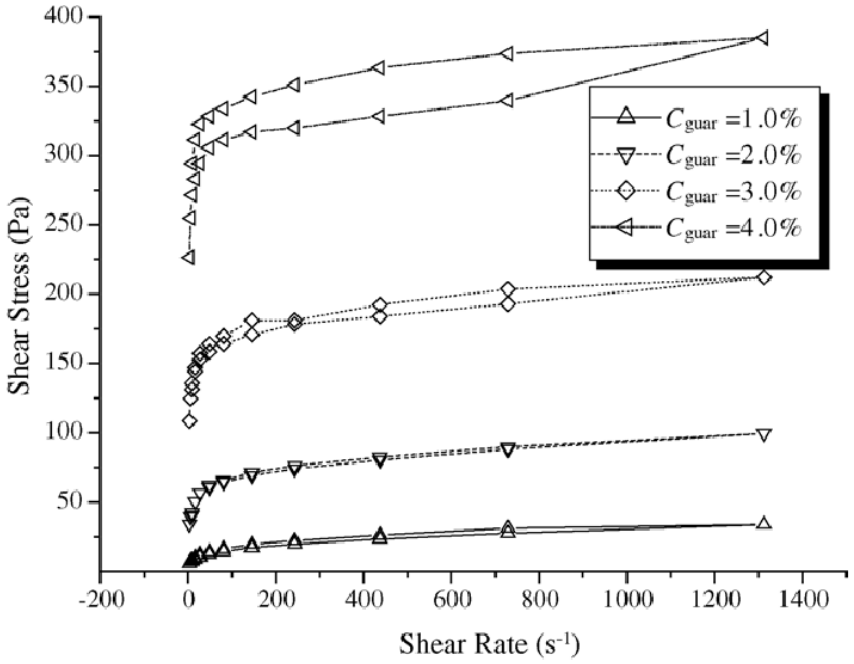

Fig. 11—Thixotropic response of CMHPTG solutions with various concentrations (after Zhang et al., 2005).

The thixotropy of a material is the ability to regain the gel structure when the polymer is allowed to rest after attaining the sol phase (Zhang et al., 2005). Guar and cellulose-based polymers have such an ability to build up their structure from sol to gel. The thixotropic behavior is dependent on the concentration as shown in **Fig. 11**. At low concentrations (<2%), the thixotropic behavior usually is not noticeable, while it becomes obvious at high concentrations (≥3%).

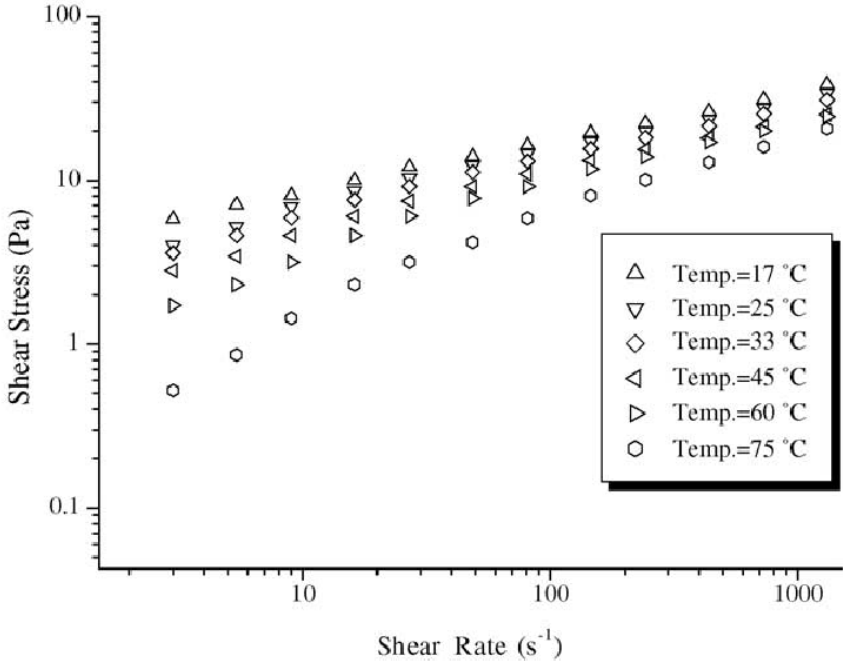

Fig. 12—Effect of temperature on the flow behavior of CMHPTG solutions (1.0%, pH 7) (after Zhang et al., 2005)

The increase of temperature usually weakens the thickening properties of polymer solutions (Zhang et al., 2005). As shown in **Fig. 12**, the viscosity at the same shear rate decreases as temperature increases. The difference in viscosity becomes more obvious at low shear rates. Several studies have shown that the consistency coefficient (*k*) decreased and the flow behavior index (*n)* value increased with temperature.

The effects of salts on the polymer solutions depend on the salt type, salt concentration, and polymer type. As for non-ionic polysaccharides, such as native guar gum, the presence of salts does not affect the viscosity significantly. Ma and Pawlik (2007) studied the effect of lithium, sodium, potassium, and cesium chlorides on the properties of dilute guar gum solutions. The intrinsic viscosity of guar gum is not significantly

affected by the salts up to an electrolyte concentration of 4.1 mol/L. In the range of low salt concentrations, guar gum stays in an aggregated state regardless of the salt type. However, high concentrations of kosmotropic ions (Li^+ and Na^+) can enhance the aggregation of guar gum because of these strongly hydrated cations decrease the amount of free water available for polymer solubilization. On the other hand, chaotropic ions (K^+ and Cs^+, water-structure breaking ions) seems to induce the dissolution of guar gum aggregates into individual molecules.

As for anionic and cationic polysaccharides, the addition of salts can decrease the viscosity of their solutions (Zhang et al., 2005). The anionic or cationic polymers can display high viscosity as a result of the electrostatic repulsion between charges along the polymer chains. However, the addition of salts would shield the charge-charge repulsion, resulting in a collapse of the polymers and thus a decrease in viscosity.

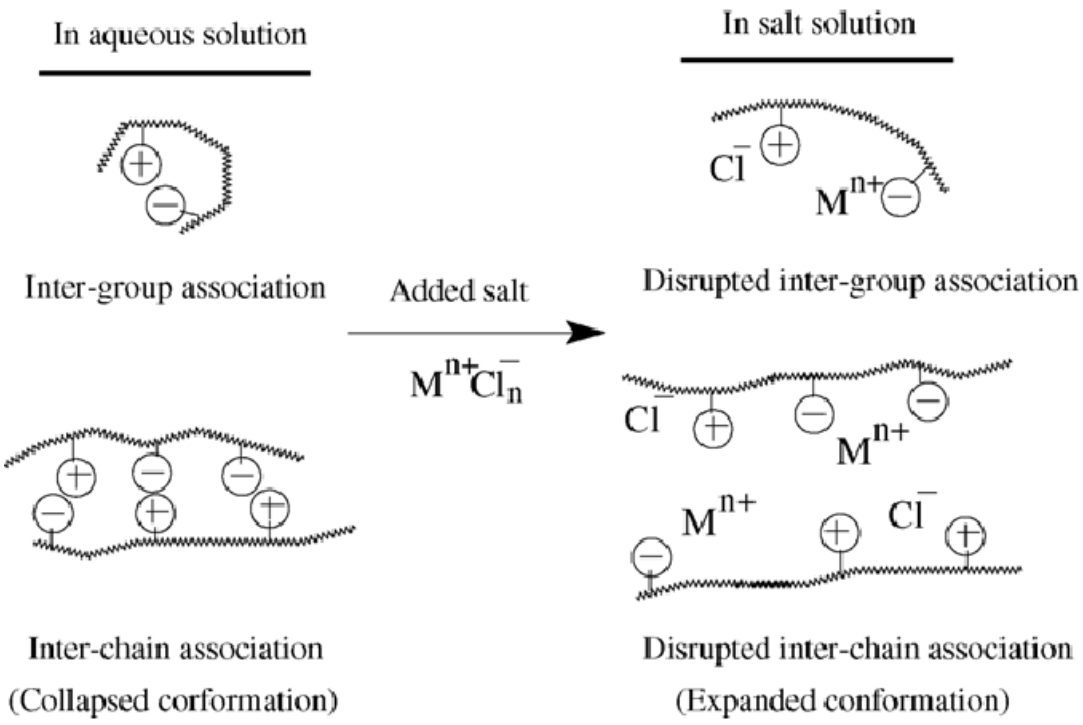

Fig. 13—The proposed model for the effect of salts on amphoteric polymer CMHTPG (after Zhang et al., 2005)

The effects of salts on amphoteric polysaccharides are very different. Salts, such as NaCl, $MgCl_2$, and $CaCl_2$, can lead to an increase in viscosity of CMHTPG. A schematic model was proposed to explain this phenomenon as shown in **Fig. 13**. This amphoteric polymer, with one cationic and one anionic charge in one unit, has extensive inter and intro molecular interactions. Such interactions are from the electrostatic attractions between cationic ammonium groups and anionic carboxymethyl groups of same or different CMHTPG chains. These interactions would lead to a collapsed structure. However, the presence of salts can disrupt the inter and intro interactions, and thus the polymer expands. This will result in an increase in the viscosity.

1.3.1.2. Viscoelastic properties

Polymers are viscoelastic, which means that they have intermediate properties between Newtonian liquids and Hookean solids. The simplest model of viscoelasticity is the Maxwell model by linearly combining a perfectly elastic spring and a perfectly viscous damper in series. Dynamic oscillatory measurements are usually used to evaluate the viscoelastic properties. The complex modulus G* in eq. 3 represents the total resistance of the polymers against the applied strain.

$$G* = \sqrt{(G'2 + G''2)} \quad \text{eq. 3}$$

where G', storage modulus, is the elastic response to quantify the ability of the polymers to store elastic energy which can be recovered finally. G'', the loss modulus, quantified the mechanical energy transferred into heat (i.e., energy loss) because of viscous force. Currently, dynamic rheology is the most popular method to characterize gel strength.

The guar-based gels, most used as hydraulic fracturing fluids, are viscoelastic fluids. The evaluation of elasticity has been used to correlate with the proppant transportation behavior of both linear and crosslinked guar gels (Acharya 1986; de Kruijf et al. 1993; Zhao et al. 1995; Goel et al 2002; Harris et al 2009). De Kruijf et al. (1993) concluded that G' is a controlling parameter to affect the proppant settling velocity in the static proppant settling tests using borate-crosslinked gels. Gheissary and van den Brule (1996) showed that elastic effects of non-Newtonian fluids could cause particle dispersion

and thus delay the partile settling. Goel et al (2002) showed that G' can correlate the rheological properties of a fluid with the solid transport behavior better than G".

1.3.2. Formation damage

Polymer or polymer residue can bridge pores of the rock (**Fig. 14**) and cause formation damage by reducing fracture conductivity and formation permeability (DeVine et al., 1998). The degree of damage can be related to many factors, such as polymer type, polymer concentration, crosslinker, breaker type, breaker concentration, rock permeability and so on. Guar-based fluids can cause more damage than cellulose-based fluids (Almond, 1982). A higher polymer loading usually causes more damage to the permeability (Siddiqui et al., 2004). Gels crosslinked with borate can afford a better cleanup result than those crosslinked with Ti and Zr ions. As for the effect of permeability, a correlation between rock permeability and the damage degree was reported from previous studies. In general, the higher the permeability is, the greater the formation damage is. A higher regained permeability can be obtained for the rock with a higher permeability. The effects of breakers will be discussed in the following part.

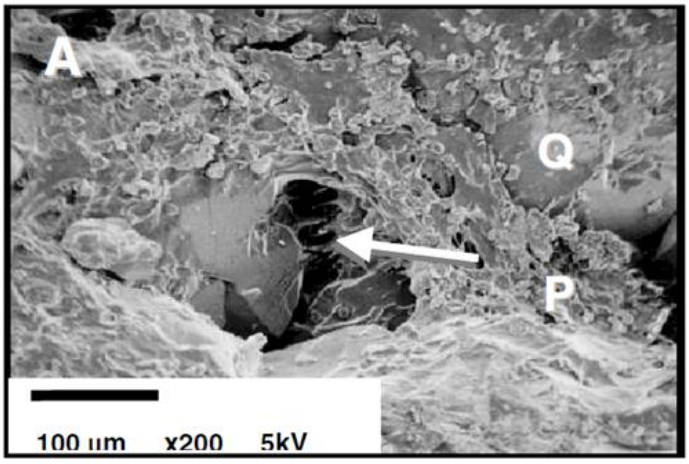

Fig. 14—Polymer damage to a core is illustrated in a scanning electron micrograph. The pore (arrow) was bridged by polymers (after Devine et al., 1998).

Therefore, polymers must be removed to avoid or minimize formation damage after the fractures are created. Breakers are used to degrade polymers by cleaving the polymers into small fragments, and thus to remove the formation damage of polymers. However, the inadequate degradation would also lead to formation damage when polymer fragments are still large enough to bridge pores or plug pore throats. Moreover, polymers used in hydraulic fracturing fluids may leave insoluble residues after breaking, which can cause a reduction in reservoir permeability and fracture conductivity.

1.4. Breakers

Two types of breakers have been investigated to degrade biopolymers: chemical breakers and enzymatic breakers. The chemical breakers include strong acids and oxidizers, in which the former is usually hydrochloric acid and the latter are persulfate salts, bromate salts, and chlorous acid. Enzymatic breakers include conventional enzymes

and polymer-linkage-specific enzymes. The conventional enzymes could degrade the polysaccharide, through a random hydrolysis reaction of the base polymer, into short-chain polysaccharides with low concentrations of monosaccharide and disaccharide. Polymer-linkage-specific enzymes, which have shown a superior performance over conventional enzymes, have been receiving extensive investigations since 1992.

1.4.1. Acid breakers

Acid breakers degrade polysaccharides through hydrolysis at some specific carbon sites (**Fig. 15**). Hydrolysis includes three consecutive steps:

- Protonation of either one of the acetalic oxygen atoms leads to the formation of a conjugate acid.
- The C-O bond cleaves to form a carbonium cation.
- The product is formed by heterolysis of a water molecule.

Another possible mechanism is a partial protonation of both acetalic oxygen atoms in the first step (**Fig. 15**) (Hayatdavoudi et al., 1994; Philipp et al., 1979).

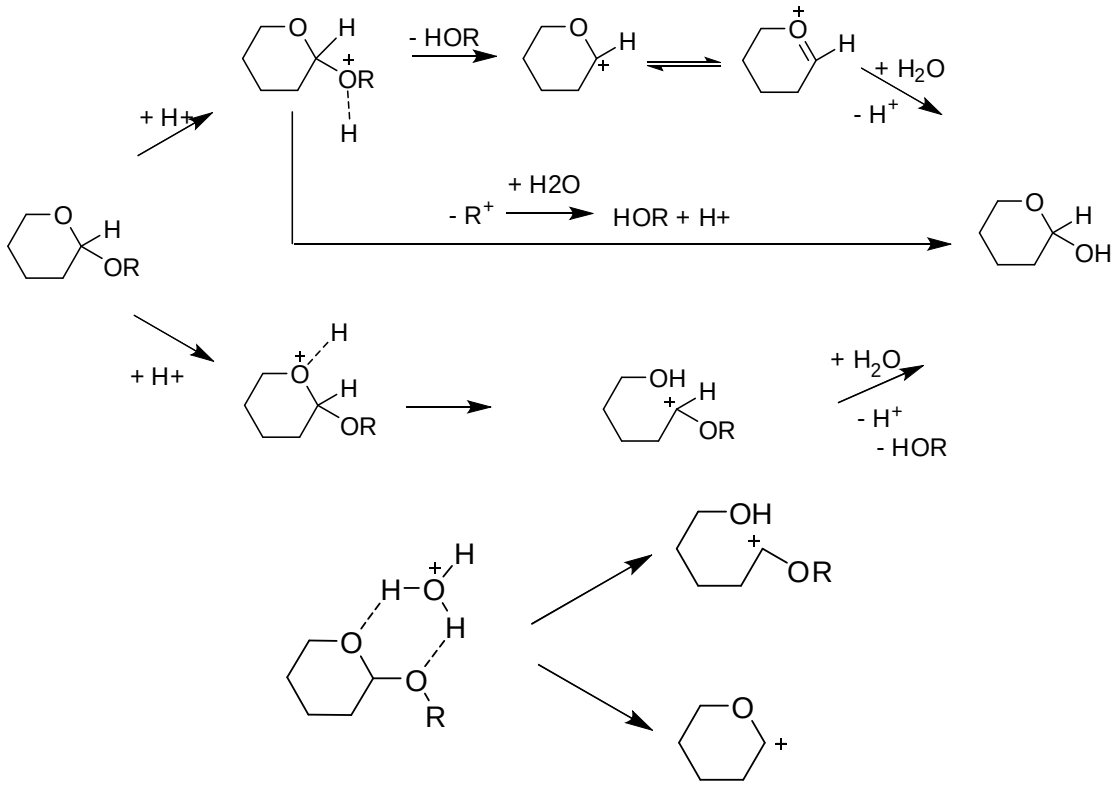

Fig. 15—Mechanism of acid hydrolysis of glycosidic bonds (after Philipp et al., 1979).

The most common acid used in the oil field is hydrochloric acid, partially because it is cost effective. However, formation damage can occur when the formation is acid sensitive and the corresponding acid-reaction products are incompatible with the formation. Moreover, the acid contact can cause corrosion of tubular goods, which becomes significant at high temperatures.

1.4.2. Oxidative breakers

The process of oxidative breakers reacting with polymers has two steps. The breakers decompose to release free radicals; the radicals attack polymer chains, create

radicals on the polymer, and produce a chain reaction (Economides and Nolte, 2000). At low temperatures, the initiators, including tertiary amines, organic esters, and transition metal salts, are added to initiate the production of radicals. At high temperatures, the oxidative breakers may be too active. This leads to the development of encapsulation. The breakers are coated by a low-permeability film to slow down the dissolution of the breakers and their release to polymer fluids (Rae and di Lullo, 1996). This process could also be used in acid and enzyme breakers.

Oxidative breakers can be used in a wide range of temperature from room temperature up to 300ºF (Sarwar et al., 2011). Sodium bromate can be used to remove the damage of borate-crosslinked guar gels successfully up to 300ºF in the laboratory as well as the oil field (Siddiqui et al., 2004). A more comprehensive study on the degradation of borate-crosslinked guar gels with ammonium persulfate, chlorous acid, and sodium bromate provided good information on how to choose breakers based on reservoir conditions (Nasr-El-Din et al. 2007). The comparison among sodium persulfate, ammonium persulfate, magnesium oxide, and sodium bromate indicated that each breaker had a temperature range to maintain good activity. Among those oxidative breakers, ammonium persulfate was the most effective breaker (Sarwar et al., 2011). The disadvantage of the oxidative breakers is that the oxidizers can be consumed by many competing reactions occurring downhole, which reduce their availability for polymeric degradation (DeVine et al., 1998; Tjon-Joe-Pin et al., 1993). Moreover, the reaction with oxidative breakers is too fast at elevated temperatures, which could lead to an early viscosity reduction of polymer fluids.

1.4.3. Enzymatic breakers

1.4.3.1. Kinetics of enzyme degredation

Enzymes are biocatalysts, which allow a single enzyme molecule to react with many substrate molecules. These enzymes, belonging to proteins, have three-dimensional (3D) structures with active sites. In the process of catalysis, the substrate fits into the active site of the enzyme, like a key fitting into a lock. The enzyme-substrate complex lowers the activation energy for a reaction and thus increases the reaction rate. For each enzyme, only molecules which can become properly oriented at the enzyme's active site can be catalyzed by the enzyme. Therefore, enzymes are specific to their substrates (Economides and Nolte, 2000).

Three types of glycosidic bonds exist in guar: then endo- and exo-β-1,4 linkages on the mannose backbone, and the α-1,6 linkages between mannose and galactose unit. The corresponding enzymes to cleave these bonds are β-mannosidase, β-mannanase and α-galactosidase (Cheng and Prud'homme, 2000; Mahammad et al., 2007). β-mannosidase only cleaves the mannose unit from the end of the guar molecule. β-mannanase cleaves interior glycosidic bonds between adjacent mannose units, and α-galactosidase cleaves the galactose side branches off the guar (**Fig. 16**). To design enzymes with good properties, it is important to understand the kinetics of enzymatic hydrolysis in guar solutions.

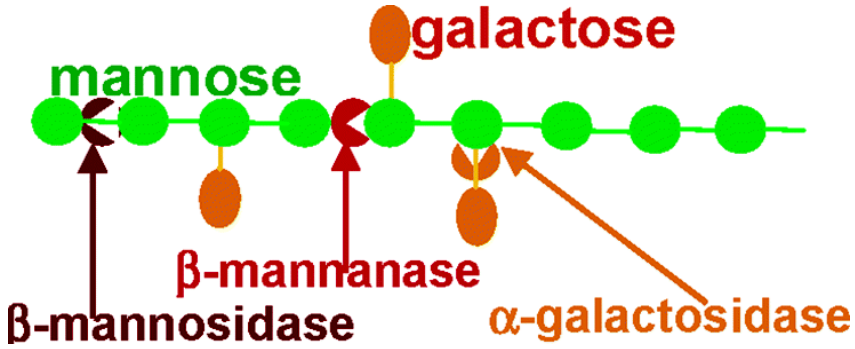

Fig. 16—The scheme of three types of enzymes to cleave the different bonds in guar (after Mahammad et al., 2007)

Mahammad et al. (2007) studied the rheological properties of guar solutions with these enzymes. β-mannanase can decrease the viscosity much more significantly than the other two enzymes under the same conditions as shown in **Fig. 17**. The residual viscosity obtained on complete degradation by a combination of β-mannanase and α-galactosidase is consequently lower when compared to that obtained on complete degradation of native guar by β-mannanase enzyme. The galactose branches attached to guar backbone obstruct the β-mannanase enzyme approaching β-1,4-linkages between the mannose units. The debranching of the guar by α-galactosidase makes the β-1,4-linkages easily accessible by the β-mannanase enzyme, increasing the rate of hydrolysis.

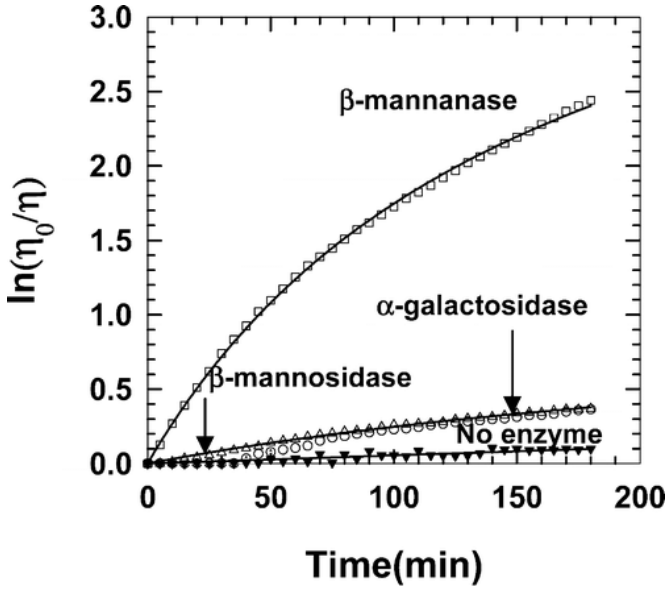

Fig. 17—Degradation of a 1% guar solution by individual enzymes, monitored in terms of the viscosity ratio of undegraded guar (η0) to degraded guar (η).

The kinetics of the reaction between β-mannanase and guar polymers have been investigated (Cheng and Prud'homme, 2000). Michaelis-Menton model is commonly used to describe the reaction between enzyme and substrate:

$$\mathrm{S} + \mathrm{E} \underset{k_2}{\overset{k_1}{\rightleftharpoons}} \mathrm{ES} \overset{k_{cat}}{\rightarrow} \mathrm{P} + \mathrm{E}$$

In the catalytic process, the enzyme (E) first attached to the polymer substrate (S) to form an enzyme-substrate complex (ES). The enzyme cuts the substrate to release the product (P) and enzyme itself. The degradation kinetics are:

$$\frac{dL}{dt} = -\frac{k_{cat}C_eL}{K_m+L} \quad \text{.....eq. 4}$$

where k_{cat} and K_m are the rate constant and the Michaelis−Menton constant, respectively. C_e is the concentration of the enzyme. L represents the molar concentration of cleavable bonds in the system.

When $L << K_m$, eq. *4*will be a first-order reaction:

$$\frac{dL}{dt} = -\frac{k_{cat}C_eL}{K_m} \quad \text{.....eq. 5}$$

When $L >> K_m$, eq. *4* will be a zero-order reaction:

$$\frac{dL}{dt} = -k_{cat}C_e \quad \text{.....eq. 6}$$

As the guar concentration is low, the reaction rate increases with the substrate concentration, a first-order reaction. In this case, the polymer concentration is much lower than the overlap concentration, c*. As the polymer concentration is high enough, the reaction rate is independent of substrate concentration, a zero-order reaction. This is because at high polymer concentrations, sufficient substrate sites bind all enzymes to form enzyme-substrate complexes. Therefore, the increase of the polymer concentration does not lead to an increase in the number of enzyme-substrate complexes. The reaction is now limited by the enzyme kinetics, not the substrate concentration.

Guar derivatives usually feature a slower enzyme hydrolysis process. For different substituent groups, different mechanisms apply. Three derivatized guars were studied in

the kinetics of β-mannanase hydrolysis: hydroxypropyl guar (HPG), carboxymethyl guar (CMG), and hydroxypropyl trimethylammonium guar (HPTMAG) (Cheng and Prud'homme, 2000). For HPG, the hydrolysis is slower than the native guar at pH 7. Higher molar substitution affords an even lower hydrolysis rate. This arises from the steric effects of hydroxypropyl groups on the polymer chains. The hydroxypropyl groups hinder the enzyme from attaching to the polymer, and thus decrease the hydrolysis rate. CMG provides similar results as HPG, resulting from a combination of steric effects and electrostatic effects. At pH 7, both CMG and β-mannanase are negatively charged. Therefore, the electrostatic repulsion between the carboxyl groups of the polymers and the enzyme further decreases the hydrolysis. More interestingly, the hydrolysis rate is quite low for HPTMAG at pH 7. During the first 20 hour, the viscosity of this polymer solution with β-mannanase remained almost the same as the initial value. The triggering mechanism was proposed in this study. At high pH, HPTMAG is cationic while the enzyme is anionic. Therefore, the electrostatic attraction leads to the formation of an enzyme-polymer complex, which is inactive towards the hydrolysis reaction. At low pH, enzyme will be released and activated.

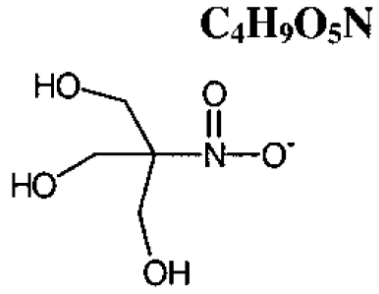

Fig. 18—The structure of Tris.

A pH-dependent inhibitor, tris(hydroxymethyl)aminomethane (Tris, in **Fig. 18**), was used to control the hydrolysis of guar by β-mannanase (Burke and Khan, 2000; Khan et al., 2002). As shown in **Fig. 19,** at pH 9, the viscosity of guar solutions did not decrease after 5 hours in the presence of β-mannanase and Tris (25 mM or 50 mM). Without the addition of Tris, the viscosity of the same solutions decreased significantly in the presence of β-mannanase under the same conditions. These results indicated that Tris inhibited the hydrolysis of guar polymers by β-mannanase at pH 9. When the concentration of Tris was high enough, the hydrolysis was stopped completely in the tested time. However when pH is below 6, the degradation of guar solutions proceeded in a same rate in the tested range of Tris concentrations (0-50 mM). More interestingly, when the initial pH was maintained at 9 for 5 hours, the degradation of guar was inhibited by Tris. However, adjusting the pH of this solution to 4, the degradation was initiated and proceeded normally. These results have shown that the onset of enzyme degradation can be controlled by adjusting the pH in the presence of Tris. A guar solution can be prepared with β-mannanase and Tris at high pH. The degradation will not occur until the pH drops below 6.

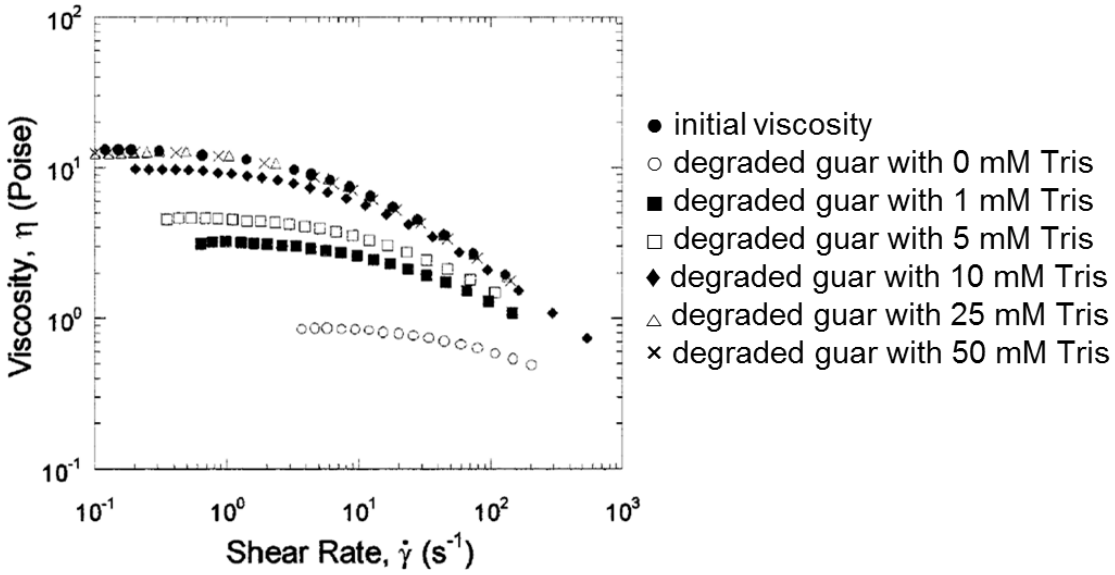

Fig. 19—The effect of Tris on the viscosity of 7 mg/ml guar solutions degraded by β-mannanase (8.3×10-4 U/ml) for 5 hours at pH 9 (after Burke and Khan, 2000).

The inhibition mechanism was proposed to be a result of electrostatic interactions between the Tris molecule and the histidine residue in the active site of the enzyme as shown in **Fig. 20**. At pH 7, the Tris molecule is protonated featuring a cationic charge, and the catalytic histidine residue in the enzyme is negatively charged. Therefore, an ion pair between the Tris molecule and the enzyme can be formed due to the electrostatic interactions, resulting in an inhibition of the enzyme activity. Once pH drops to 4, the histidine residue now is neutral, and the Tris molecule remains protonated. The enzyme will be released and reactivated because of the absence of the electrostatic interactions. At low concentrations of Tris (≤ 5 mM), the inhibition effect is more effective at pH 7 than at pH 9, because the electrostatic interactions are more significant at pH7. However, at high concentrations (≥ 10 mM) of Tris, the inhibition becomes more effective at pH 9.

Burke and Khan (2000) proposed that the increased inhibition at pH 9 and high Tris concentrations may arises from a combined inhibition and destabilizing effect on the enzyme by the abundance of Tris in solution. However, this is somewhat unclear and needs more studies.

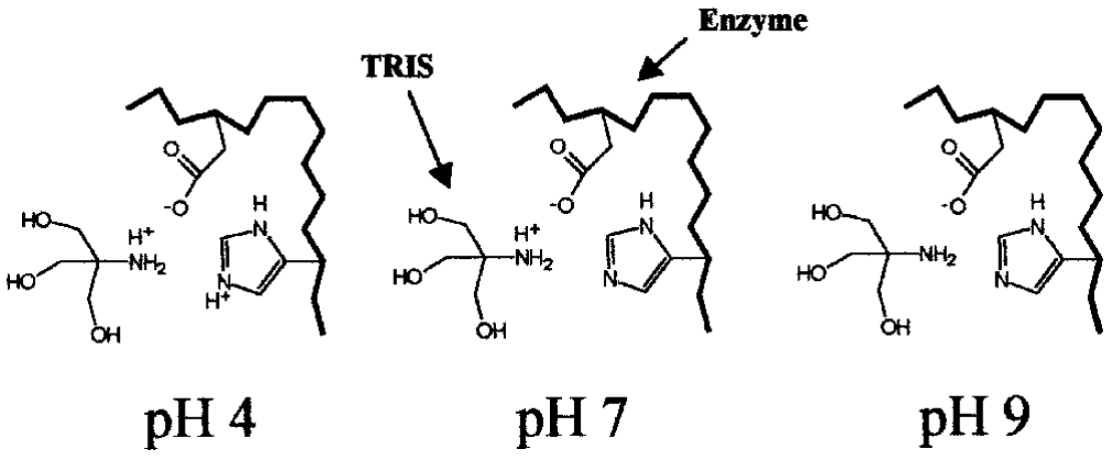

Fig. 20—The proposed representation of the interaction between Tris and the active site of enzyme (after Burke and Khan, 2000).

Other methods were also reported to control the enzyme degradation of guar molecules with a same mechanism (Khan et al., 2002). For example, a polymeric additive with a negative charge can be used to decrease the activity of a positively charged enzyme under specific conditions. Reducing pH to protonate the polymeric additive can reactivate the enzyme. Or increasing the ionic strength of the solution can also promote the enzyme activity, because the high ionic strength will screen the electrostatic attraction between the enzyme and the inhibitor. The salts used to increase the ionic strength do not affect the enzyme activity without the inhibitor.

1.4.3.2. Development of enzyme breakers in oilfield

Two types of enzyme breakers have been used in the oil field: conventional enzymes and polymer-specific enzymes. The conventional enzymes, a nonspecific mixture of hemicellulase, cellulase, amylase, and pectinase, randomly hydrolyze polymers (Brannon et al., 2003). Each enzyme can only react with one specific polymer. For example, hemicellulase can only catalyze the hydrolysis of guar polymers, and cellulase is specific to cellulose polymers. However, all enzymes can bind with any polymer. The "wrong" enzyme bound to the polymer will block the "right" enzyme from breaking it. This phenomenon may lead to incomplete degradation and thus severe formation damage. Therefore, conventional enzymes are not recommended now.

Since 1992, polymer-linkage-specific enzymes (PLSE) have been attracting a great deal of attention. Many studies have supported that PLSEs outperformed the oxidative breakers and conventional enzymes (Sarwar et al., 2011). PLSEs are specific to the linkages between the units of polymers. Advantages of PLSE include:

- Substrate-specific enzyme complexes could hydrolyze the polymers to as little residue as possible.
- Enzymes are not consumed in the reaction and can continue working during their life time, thus providing a more complete degradation with fewer residues than oxidative breakers.
- Neither the crosslinker type nor the degree of polymer derivatization interferes with the ultimate degree of enzymatic degradation of the polymer.
- PLSE are nonreactive with anything other than the targeted polymer.

- Enzymes exhibit the unique ability of maintaining their structures during the reactions they initiate.
- Enzymes are also known for their tendency to catalyze reactions at extraordinary rate.

Initially, PLSEs could only work under mild conditions, where pH and temperature are the key factors to limit the activity of enzymes. For example, Tjon-Joe-Pin et al. (1993) developed an effective enzyme treatment to remove polymeric damage from guar, cellulose, and starch, but this treatment could only work up to 120ºC with a narrow pH range. Similar PLSE systems have been reported on guar-based polymers and cellulose gels, respectively. The commercial Gamanase enzyme was highly effective in degrading guar at slightly acidic conditions (pH 5) and at low temperatures (25 to 60ºC). The thermophilic TN5068 enzymes were significantly more effective in reducing polymer viscosity at high temperatures (85ºC). However, they had limited activity at lower temperatures (Tayal et al., 1997). The enzyme treatment developed to remove cellulose-based blocking gels was very effective and economic; however, this method was also limited to use at temperatures of 140ºF and below(Rickards et al., 1993).

More recently, the PLSE technology has found its utility and effectiveness in extreme environments, such as a wide range of pH and/or temperature. An effective enzyme-based method developed by DeVine et al. (1998) was applied to remove damage of guar-based polymers in high temperatures exceeding 250ºF and over a wide pH range. With the development of proprietary evolution technologies and an ultrahigh-throughput screening platform, the temperature and pH profiling of enzyme systems has been further

improved. An exceptionally thermo-stable cellulase enzyme can break linear and crosslinked guar polymers under broad ranges of temperature and pH (Zhang et al., 2012).

1.5. Research objectives

Formation damage caused by guar is a serious problem with detrimental effects on production enhancement. Fluid invasion to the formation causes internal damage. Polymers can bridge pores of the rock and thus reduce the formation permeability (Parker et al. 1994; DeVine et al. 1998). The degree of damage can be related to many factors, such as polymer type and concentration, crosslinker, breaker type and concentration, and rock permeability. Guar-based fluids can cause more damage than cellulose-based fluids, due to a larger amount of insoluble residue from guar polymers (Almond 1982). A higher polymer loading usually causes more damage to the permeability. External damage is caused by the formation of filter cake (Vitthal et al. 1996). Filter cake is formed on the fracture face where there is highest polymer concentration due to fluid loss (Parlar et al. 1995).

Therefore, polymers must be removed to avoid or minimize formation damage after the fractures are created. Breakers are used to degrade polymers by cleaving the polymers into small fragments, and thus to remove the formation damage of polymers. However, the inadequate degradation would also lead to formation damage when polymer fragments are still large enough to bridge pores or plug pore throats. Moreover, polymers used in hydraulic fracturing fluids may leave insoluble residues after breaking, which can cause a reduction in reservoir permeability and fracture conductivity.

One guar alternative is viscoelastic surfactant (VES)-based fluid (Samuel et al. 1997; Whalen 2000; Zhang 2002; Centurion et al. 2006; Crews et al. 2008). The advantages of VES-based fracturing fluids include simple operation, rapid flowback for clean-up, tolerance with various water sources, and no need for biocides (Fredd 2004; Gomaa 2011). However, the disadvantage of VES-based fluids lies in the weak thermal stability. For VES with good solubility in water, it may degrade quickly at temperatures higher than 200ºF. Addition of organic alcohols was found to increase the thermal stability of VES-based fluids (Norman 1996; Whalen 2000). VES stabilizer was also developed for VES applications between 180 and 300ºF (Fig. 21, Crews et al. 2008).

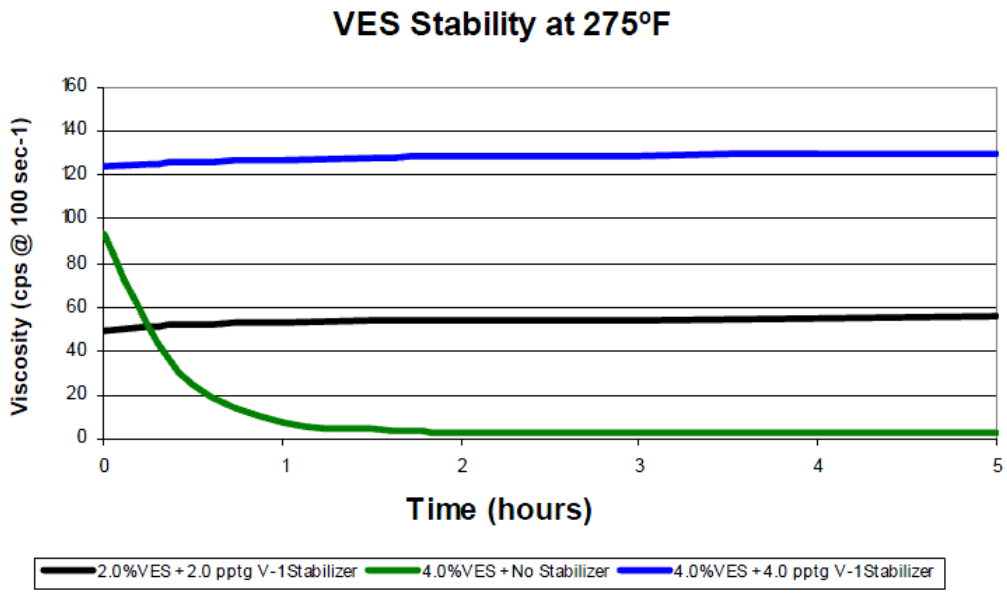

Fig. 21—The effect of stabilizer in VES fluids (after Crews et al., 2008).

Fiber-laden fluids have been developed since 2005. (Bulova et al., 2006; Bustos et al., 2007; Oussoltsev et al., 2008; Samuel et al., 2007; Sitdikov et al., 2009). Samuel et al. 2007 reported an engineered fiber for the fracturing of unconsolidated sand in the Tali field of Bruner. Fiber was added in linear guar fluids with low viscosity. The presence of fibers can transport high proppant concentrations to the fracture and control the sand flowback during production. This fiber technology is physical rather than chemical. The fibers can mechanically holding proppant or sand pack in the fracture by forming a good network between the fibers and proppants as shown in **Fig. 22**. Therefore, the viscosity of base fluid can be significantly reduced while still generating enough fracture width.

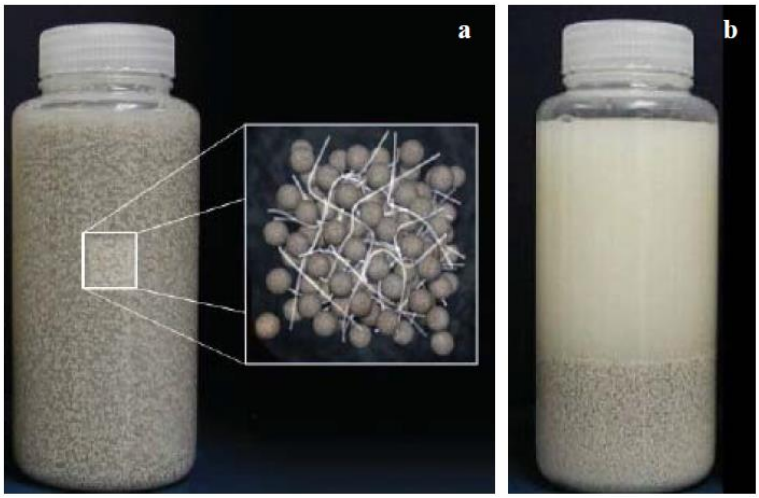

Fig. 22—Solids suspension experiments with (a) and without (b) the fiber (after Samuel et al., 2007)

Fiber-laden fluid system has been also used to improve proppant transport for hydraulic fracturing in low-permeability tight gas reservoir. The entanglement of proppant

by fibers creates a good network, which significantly reduces proppant settling. Moreover, the fiber used in this technique can decompose with time, leaving a non-damaged fracture conductivity. An average 24% production improvement has been reported since fiber-laden fluids were implemented.

Cellulose derivative polymers were also used as a replacement for guar in hydraulic fracturing fluids due to the residue-free property. The most common example is carboxymethyl cellulose (CMC, **Fig. 23**), which is soluble in water and yields highly viscous fluids. However, CMC is salt-sensitive because it contains anionic charges. Besides water-soluble cellulose derivatives, the insoluble cellulose fibers were reported to improve the fluid performance. For example, one type of cellulose fiber, with an inter-tangled structure (**Fig. 23**), was added to guar fluids in order to improve the temperature stability and proppant suspending ability (Westland et al. 1993). Micronized cellulose fibers are loss control agents in drilling fluids (Verret et al 2000).

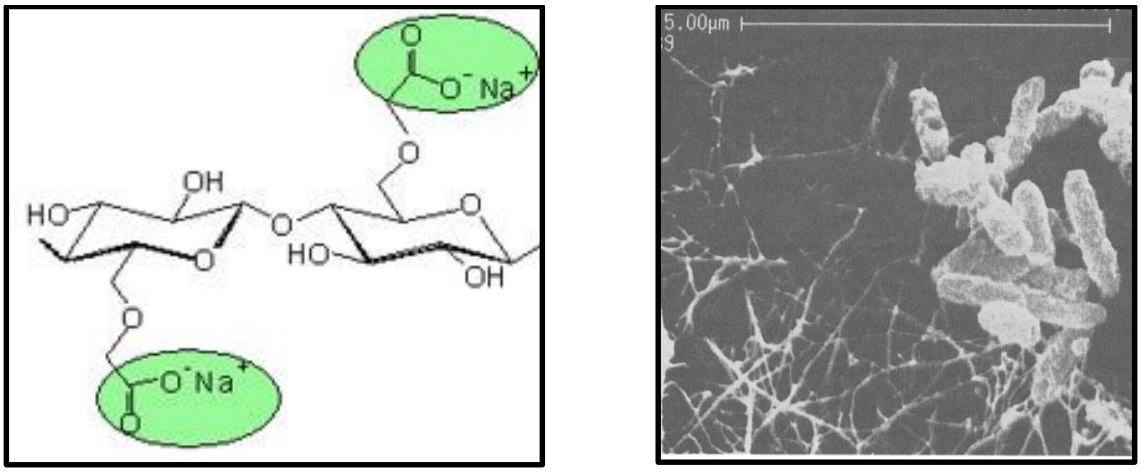

Fig. 23—The structure of CMC (left) and the insoluble cellulose fiber (right, after Westland et al., 1993)

However, all reported fiber-laden fluids used guar polymer or VES as a base fluid with a polymer loading from 18 to 40 lb/1000gal. In this work, four nanofibrillated cellulose fibers were evaluated as a guar alternative to develop guar-free hydraulic fracturing fluid. Nanofibrillated cellulose has found wide applications in nanocomposites, paper making, coating additives, and food packaging (Abdul Khalil et al. 2014). However, this is the first time to investigate the potential applications of nanofibrillated cellulose (NFC) fibers in oilfield fluids. NFC forms an aqueous gel at low concentrations due to its large specific surface. The objective of this work is to evaluate this new type of fiber-based fluids, including rheological properties, solid suspending ability, formation damage, and degradation studies, and compare it with other viscosifier-based fluids, including guar, HPG, and VES.

2. RHEOLOGICAL PROPERTIES OF NANOFIBRILLATED CELLULOSE FLUIDS

2.1. Introduction

In order to evaluate the new viscosifiers of nanofibrillated cellulose (NFC) fibers, rheological properties of the fiber-based fluids should be studied. Viscosity is required to improve the ability to suspend solids. For hydraulic fracturing fluids, a high viscosity is desired to increase the fracture width and improve the proppant placement in the fracture. A high viscosity is obtained through increasing the polymer loading or using crosslinkers. However, high polymer loading or crosslinked gels may cause severe damage to fracture conductivity and/or formation permeability.

For non-Newtonian fluids, viscosity decreases with increasing shear rate, which is referred to shear thinning fluids. Most reported polymer-based fluids are shear thinning. In this work, the viscosity of NFC-based fluids were measured at different shear rates to determine if they are shear thinning. Moreover, the viscosity stability of the fluids as a function of temperature and time is also a crucial factor. Many wells have high bottom-hole temperatures. Therefore, viscosity measurements of the new fluids were performed at high temperatures for extended time.

Dynamic properties, including elastic and viscous moduli, are also important criteria to evaluate fracturing fluids. Elasticity is developed due to the network of structure in fluids. The elastic characteristics of linear guar fluid results from the entanglements of polymer chain. Therefore, crosslinked gels always give a high elasticity compared to linear

gels. Dynamic oscillatory tests were designed to evaluate the viscous and elastic properties of fluids by measuring the viscous (G") and elastic (G') moduli as a function of frequency. These tests provided information to determine if the fluid is solid-like or liquid-like.

2.2. Experimental methods

2.2.1. Materials

Four nanofibrillated cellulose, ENZ-NFC (slurry, 0.94 wt%), TEMPO-NFC (slurry, 0.98 wt%), ME-NFC (slurry, 0.91 wt%), and KS-NFC (slurry, 2.1 wt%) were from Elkem Materials Company. Other viscosifiers, guar (solid), HPG (solid), and VES (liquid) were obtained from oil service companies. VES was a mixture liquid of an amphoteric amide oxide surfactant and a solvent (Li et al. 2011 for composition), and used as received. KCl (ACS grade) and $CaCl_2$ (ACS grade) were from Sigma Aldrich, and used as received. Deionized water (18.2 MΩ·cm at 25ºC) was used to prepare all fluids.

2.2.2. Fluid systems

The formulations of all fluids are given in **Table 1**. An overhead mixer was used for all fluids. NFC-based fluids (40 or 67 lb/1000gal) were prepared by mixing each NFC slurry and deionized water. KCl (5 wt%) was added when necessary. The concentration of NFC fluids (40, 50 or 67 lb/1000gal) was calculated as active NFC loading. Guar/HPG fluids were prepared by adding guar/HPG solid into deionized water slowly when the fluid was stirring. Hydration time was 30 min. KCl (5 wt%) was added to the polymer fluids if necessary. The concentration of guar/HPG fluids (40, 50 or 67 lb/1000gal) was calculated

as the active guar or HPG polymer loading. The VES fluid was made by mixing VES liquid with 5 wt% KCl solution. Air bubbles trapped in the fluids were removed by centrifuge at 2500 rpm for 30 minutes. The concentration of VES fluid (40 gal/1000gal) was calculated as the VES liquid (a mixture liquid as received) loading.

Table 1—Formulation of NFC fluids based on 1000 gal for rheological measurements.

	Viscosifier Concentration	Water, gal	Viscosifier
ENZ Fluid	40 ppt[a]	490	510 gal
ENZ Fluid	50 ppt	362	638 gal
ENZ Fluid	67 ppt	150	850 gal
TEMPO Fluid	40 ppt	510	490 gal
TEMPO Fluid	67 ppt	184	816 gal
ME Fluid	40 ppt	473	527 gal
ME Fluid	67 ppt	121	879 gal
KS Fluid	40 ppt	771	229 gal
KS Fluid	67 ppt	619	381 gal
Guar Fluid	40 ppt	1000	40 lb
Guar Fluid	50 ppt	1000	50 lb
Guar Fluid	67 ppt	1000	67 lb
HPG Fluid	40 ppt	1000	40 lb
VES Fluid	40 gpt[b]	960	40 gal

a. ppt: lb/1000gal; b. gpt: gal/1000gal

Fig. 24—Rotational HP/HT rheometer, Grace M5600 (left) and aging cell (right).

2.2.3. Viscosity and oscillatory measurements

A rotational rheometer, Grace M5600, was used to measure the apparent viscosity of all fluids at different temperatures (75, 245, 295, and 350ºF). Both rotor and bob of the rheometer were made of Hastelloy C. A B5 bob was used, which required a sample volume of 52 cm^3. Two sequences were used. One was that the viscosity measurements were performed as a function of shear rate (from 0.1 to 935 s^{-1}). This measurement provided the relationship between viscosity and shear rate. The other sequence was to measure the viscosity at a fixed shear rate (40 s^{-1}). This method provided some information on the viscosity stability under some specific conditions. The dynamic properties (elastic and viscous moduli, G' and G") of NFC and guar-based fluids were also measured at a frequency range of 0.01 to 5 Hz at 75ºF. A HB5 bob was used, which required a sample volume of 65 cm^3.

2.2.4. Viscosity stability tests using aging cell

The fiber fluids (40 lb/1000gal) were put in the aging cell (), and pressurized with nitrogen to 300 psi. An oven was preheated to a target temperature. Then the aging cell was kept in the oven for 4 hours. After 4 hours, the aging cell was taken out and cooled down to room temperature. Then the nitrogen was released and the fluid was taken out. The viscosity of the fluid was measured and compared to the original fluid without heating.

2.2.5. Zeta potential measurements

The samples were prepared by mixing each fiber, TEMPO-NFC (1.905 g, 1.05%), KS-NFC (1.02 g, 1.95%) or ME-NFC (1.13g, 1.77%), 0.1000 g of KCl with deionized water to prepare a NFC fluid (0.02 wt%). Each 10 ml sample was put into a plastic tube, and its pH was adjusted with HCl or NaOH according to the target pH value. Samples were left at room temperature at least 2 hours to reach equilibrium. When pH is between 7 and 9, the pH value decreases slowly during the waiting time for all three fibers. When pH is higher than 9 or lower than 7, pH is relatively stable. pH was measured using Oakton pH 510 meter (Oakton Instruments). Zeta potential (ξ) was measured using ZetaPALs (Brookhaven Company). All measurements were performed at room temperature and atmospheric pressure. Each sample was measured 5 times, and the average was taken to give the final ξ value. ENZ-NFC is non-charged, therefore the measurement was only performed at pH 7, and the zetal potential showed a low value close to zero.

2.3. Rheological properties of ENZ-NFC and guar fluids

2.3.1. Viscosity properties of ENZ-NFC and guar fluids

The viscosities of ENZ-MFC, guar, HPG, and VES based fluids were measured at different shear rates at room temperature. For guar, HPG, and VES based fluids, the viscosity/shear-rate relationship could be described by the power-law model in the range of 0.1 to 1000 s^{-1} (**Fig. 25, Fig. 26, Fig. 27**), indicating that these fluids are non-Newtonian fluids. As the shear rate increased, the viscosity decreased. However, the viscosity/shear-rate relationship for the ENZ-based fluid can be separated into two parts. At shear rates from 0.1 to 100 s^{-1}, this relationship can be described by the power-law model as shown in **Fig. 28**. As the shear rate increased, the viscosity decreased. At shear rates higher than 100 s^{-1}, the viscosity became relatively constant due to the aligning of the fiber chains at high shear rates.

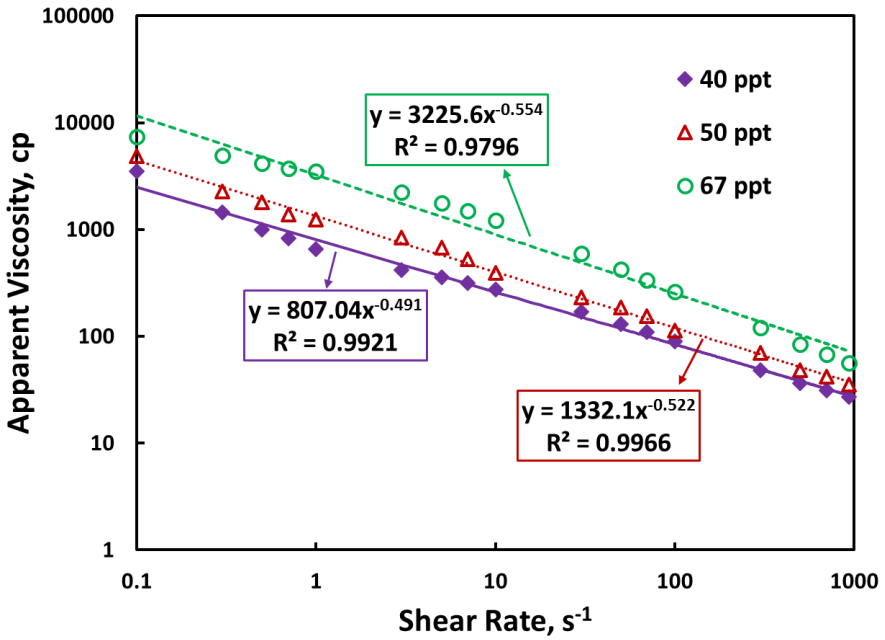

Fig. 25—The viscosity of guar fluids as a function of shear rate at 75°F.

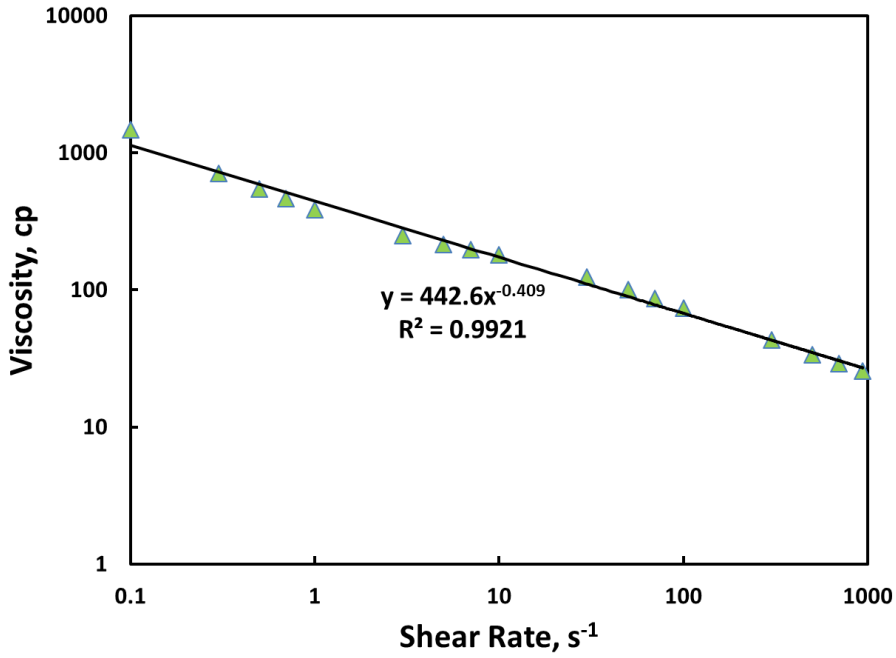

Fig. 26—The viscosity of HPG (40 lb/1000gal) fluid as a function of shear rate at 75°F.

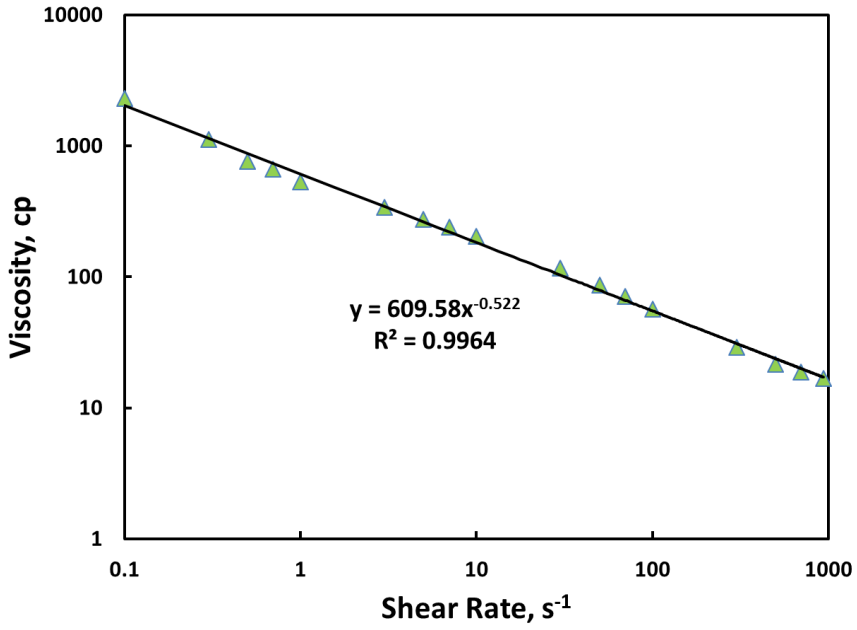

Fig. 27—The viscosity of VES (4 gal/1000gal) fluid as a function of shear rate at 75ºF.

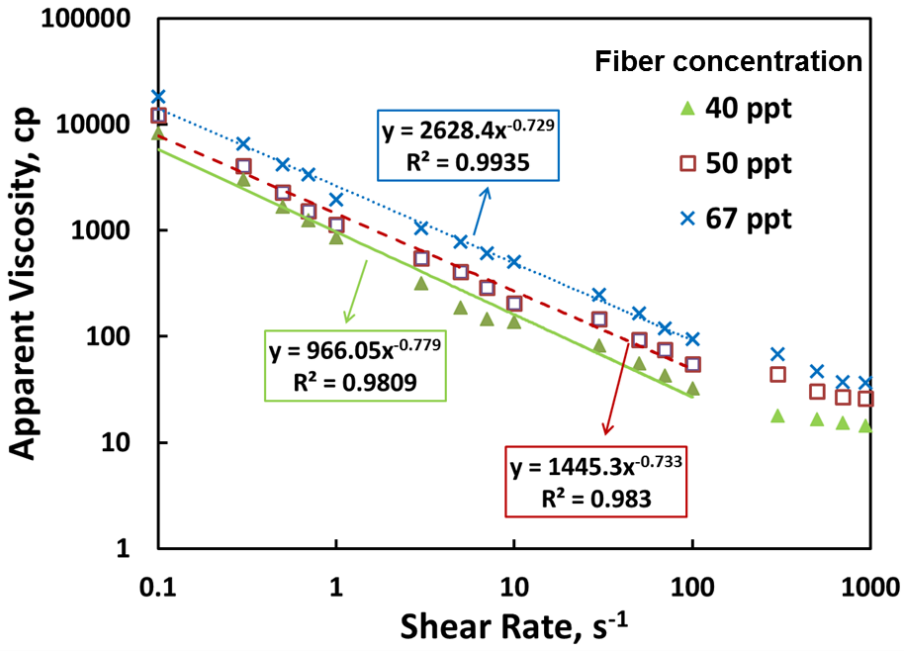

Fig. 28—The viscosity of ENZ-NFC fluids as a function of shear rate at 75ºF.

The effect of viscosifier concentration is shown in **Fig. 28**. A higher concentration of ENZ-NFC gave a higher viscosity, which is similar to the guar-based fluids (**Fig. 25**). The viscosities of ENZ-NFC-based fluids at elevated temperatures were also studied. As shown in **Fig. 29**, the viscosity of guar-based fluid (40 lb/1000gal) was reduced to 1 cp at 40 s^{-1} very quickly at 245^{o}F. However, the viscosity of ENZ-NFC-based fluid (40 lb/1000gal) decreased at the beginning as the temperature increased, and kept above 23 cp at 40 s^{-1} for at least 200 minutes when the temperature reached 245^{o}F. Similar phenomena were observed at 295^{o}F (**Fig. 30**). For ENZ-NFC-based fluid (40 lb/1000gal), the viscosity was stable at nearly 17 cp at 40 s^{-1}. The increase of ENZ-NFC concentration to 67 lb/1000gal led to an increase in viscosity to 70 cp at 40 s^{-1}, which was stable at 295ºF for at least 200 minutes.

The viscosity of ENZ-NFC fluid (50 lb/1000gal) was measured at 350ºF. As shown in **Fig. 31**, the viscosity of ENZ-NFC fluid dropped quickly as the temperature increased to 350ºF. After temperature reached 350ºF, the viscosity kept decreasing slowly from nearly 30 to 5 cp within 200 minutes. There results indicate that ENZ-NFC-based fluid can maintain its viscosity at temperatures up to 350ºF.

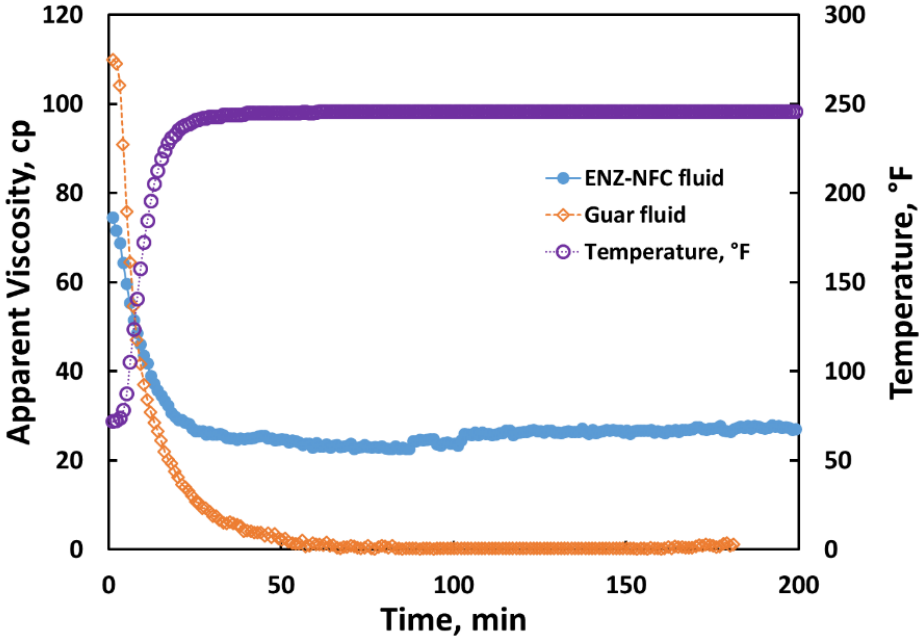

Fig. 29—The viscosity of ENZ-NFC and guar (40 lb/1000gal) fluids at 245ºF and a shear rate of 40 s^{-1}.

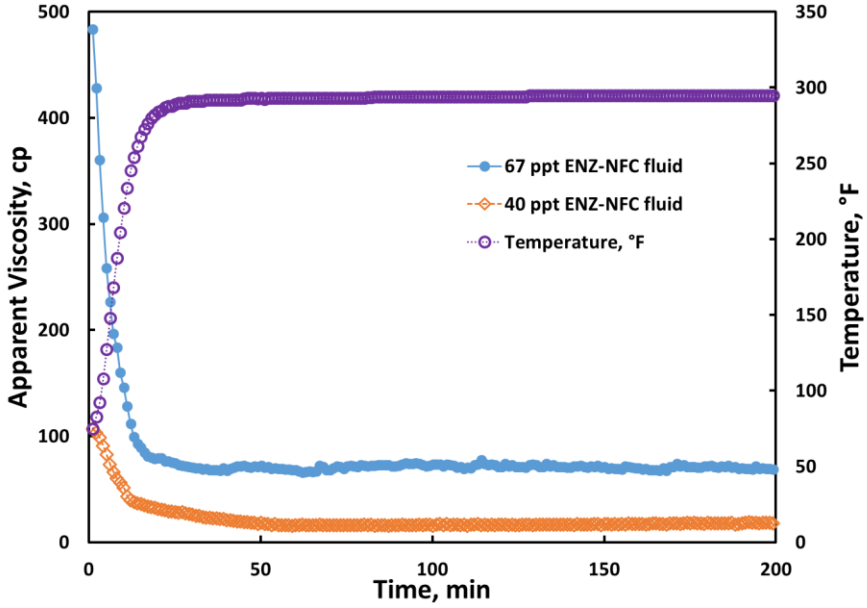

Fig. 30—The viscosity of ENZ-NFC (40 and 67 lb/1000gal) fluids at 295ºF and a shear rate of 40 s^{-1}.

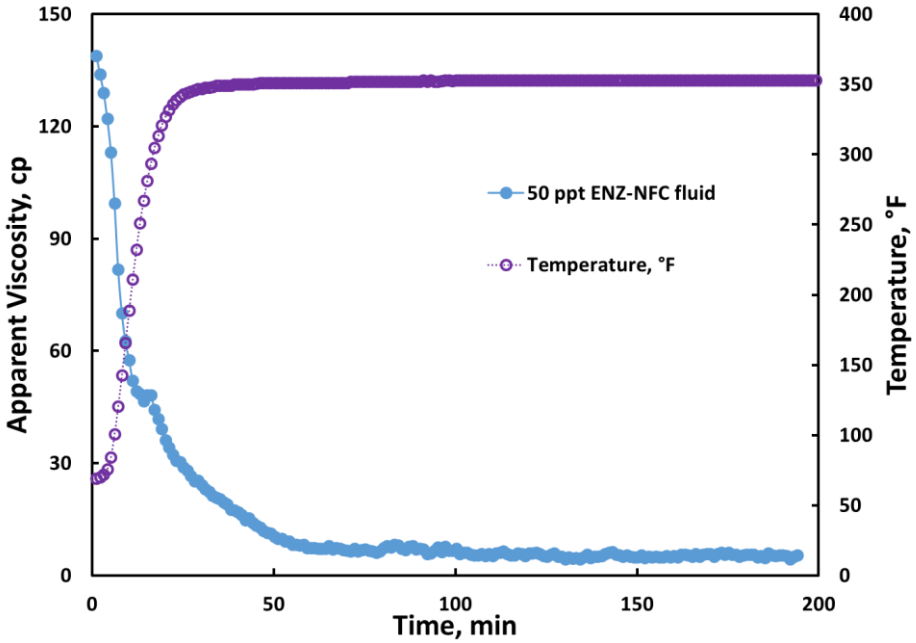

Fig. 31—The viscosity of ENZ-NFC (50 lb/1000gal) fluids at 350ºF and a shear rate of 40 s^{-1}.

The effect of KCl was examined by measuring the viscosity of ENZ-NFC -based fluid with the presence of 5 and 10 wt% KCl at 75ºF. The addition of KCl to ENZ-NFC -based fluid did not change the viscosity significantly (**Fig. 32**). A similar test was performed in the presence of 10 wt% $CaCl_2$. The viscosity of ENZ-NFC fluid with 10 wt% $CaCl_2$ was close to that of ENZ-NFC fluid without $CaCl_2$ at 75ºF (**Fig. 33**). These results indicate that ENZ-NFC is stable in brine solutions at 75ºF. The viscosity stability of ENZ-NFC fluids in the presence of KCl and $CaCl_2$ were also examined at 295ºF (**Fig. 34**). With 10 wt% KCl, the viscosity of ENZ-NFC fluid was as stable as the fluid without KCl. The addition of 10 wt% $CaCl_2$, the viscosity decreased slowly, which was slightly different from the fluid without $CaCl_2$. Such difference became obvious after 1 hour at 295ºF.

However, the viscosity was still above 40 cp after 200 minutes. The viscosity of ENZ-NFC fluid in the presence of 10 wt% $CaCl_2$ was also measured at 350ºF. The viscosity was similar to the fluid without the addition of $CaCl_2$ (**Fig. 35**). In conclusion, ENZ-NFC fluid has a high tolerance to KCl and $CaCl_2$ salts at high temperatures up to 350ºF.

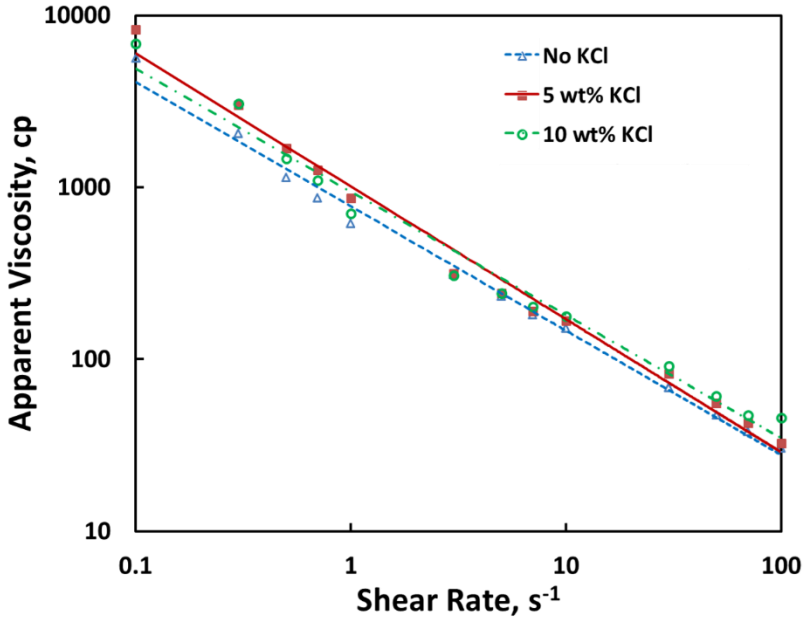

Fig. 32—The viscosity of ENZ-NFC (40 lb/1000gal) fluid without KCl and with 5 or 10 wt% KCl at 75ºF.

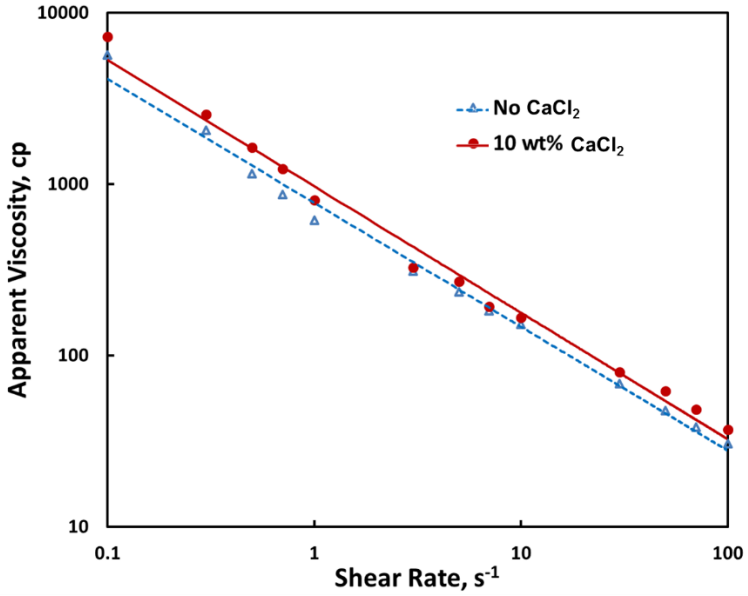

Fig. 33—The viscosity of ENZ-NFC (40 lb/1000gal) fluid without $CaCl_2$ and with 10 wt% $CaCl_2$ at 75ºF.

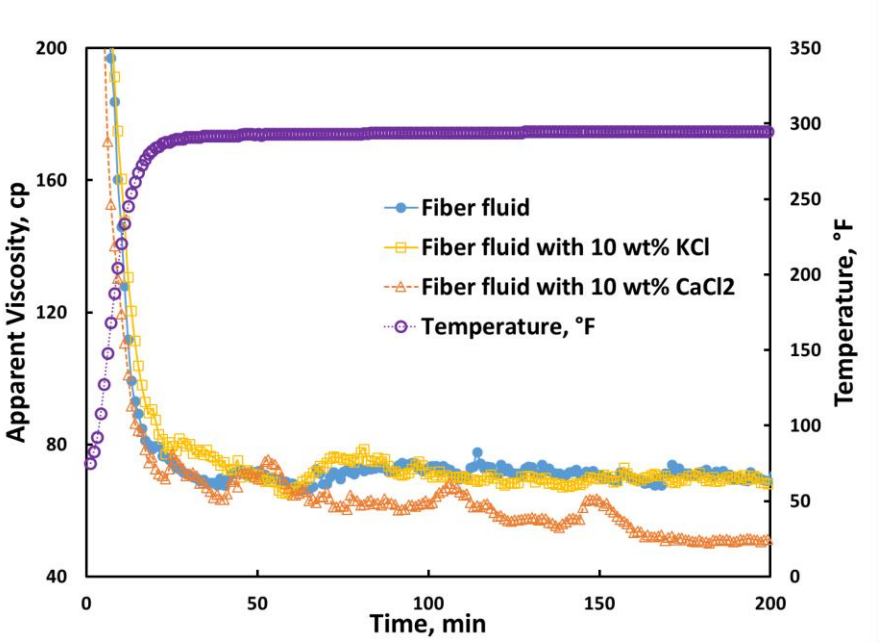

Fig. 34—The viscosity of ENZ-NFC (67 lb/1000gal) fluids with KCl or CaCl2 (10 wt%) at 295ºF and a shear rate of 40 s^{-1}.

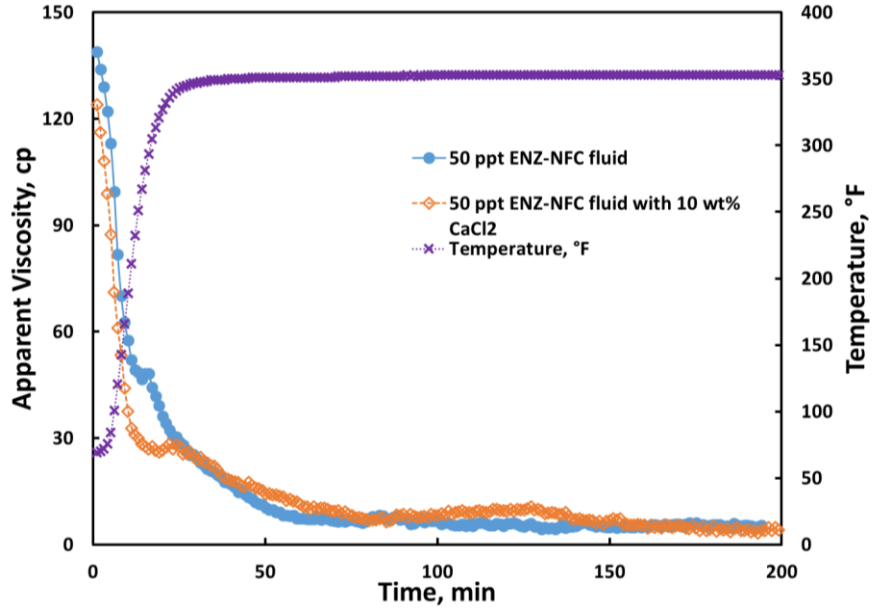

Fig. 35—The viscosity of ENZ-NFC (50 lb/1000gal) fluids with $CaCl_2$ (10 wt%) at 350°F and a shear rate of 40 s^{-1}.

2.3.2. Viscoelastic properties of NFC-based fluids

The elastic (G') and viscous (G") moduli were measured at a frequency range of 0.01 to 5 Hz to determine the frequency limits of elastic or viscous regimes of ENZ-NFC and guar fluids at 75ºF. The elastic modulus (G') is the stress in phase with the strain during a shear deformation, which is a measure of stored elastic energy. The viscous modulus (G") is the stress 90 degrees out of phase with the strain, which is a measure of the energy lost as heat during the shear deformation (Li et al. 1988).

In this work, the dynamic properties of ENZ-NFC-based fluid (40 lb/1000gal) was measured (**Fig. 36**) and compared to guar fluid under the same conditions. For ENZ-NFC-based fluid (40 lb/1000gal), both G' and G" increased when frequency increased.

However, G’ increased more quickly than G”, therefore, the crossover point of G’ and G” was achieved at a frequency of 0.3 Hz. When the frequency is lower than 0.3 Hz, G” was dominant, and the fiber fluid behaved like viscous fluid. At a frequency higher than 0.3 Hz, G’ was higher than G”. In this elastic regime, the fiber fluid behaved as an elastic material. Both G’ and G” of guar-based fluid (40 lb/1000gal) also increased with the frequency. The difference lied in that the crossover frequency of guar-based fluid was at 2.3 Hz, which was much higher than that of ENZ-NFC fluid (0.3 Hz). In the range of the frequency from 0.1 to 5 Hz, the elastic modulus G’ of guar-based was lower than that of V1-based fluid as shown in **Fig. 36**. The viscoelastic properties of the fiber fluid, which was different from guar fluid, indicate that a better network formed by the entanglement of the long NFC fiber chains.

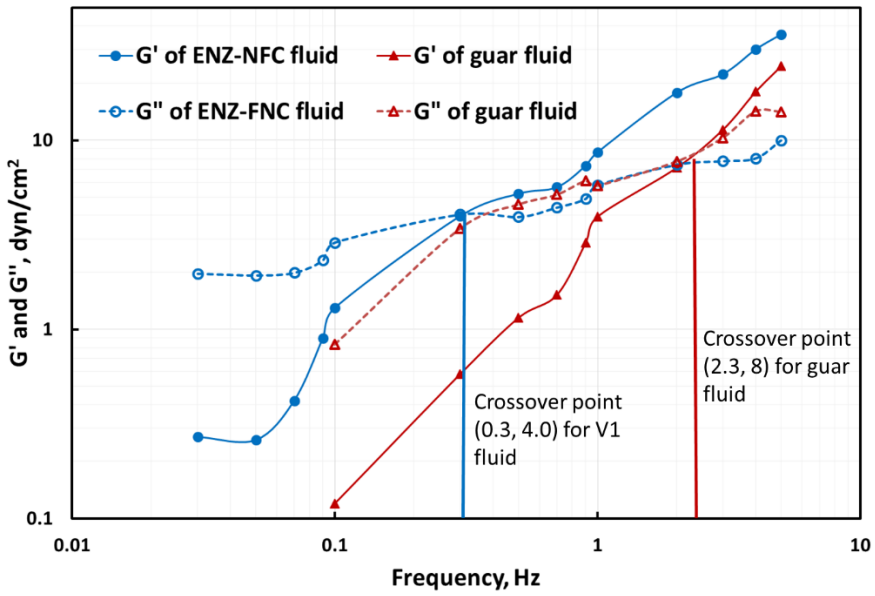

Fig. 36—The elastic (G’) and viscous (G”) moduli of ENZ-NFC and guar (40 lb/1000gal) fluids at different frequencies.

2.4. Rheological properties of other NFC-based fluids

2.4.1. Viscosity properties of other three NFC-based fluids

The viscosity of other three NFC fibers, TEMPO-NFC, ME-NFC, and KS-NFC, was also measured as a function of shear rate at 75ºF. The relationship of viscosity and shear rate shows that all fluids are non-Newtonian, where the viscosity decreases as the shear rate increases. These results are very similar to that of ENZ-NFC fluid.

Addition of 5 wt% KCl resulted in a significant decrease in the viscosity for TEMPO-NFC fluid (**Fig. 37**). TEMPO-NFC is negatively charged and the fiber chains are expanding due to the electrostatic repulsion among the fiber chains. However, the presence of KCl can cause the collapse of the fiber chain by shielding the repulsion between the negatively charge fiber chains (Zhang et al., 2005). Zeta potential of TEMPO-NFC fluid was then measured (**Fig. 38**). In all cases, the zeta potential of TEMPO-NFC fluid was negative, indicating the negatively charged nature of the fiber. Without KCl, the zeta potential was below -30 mV from pH 5 to 10, which suggested that TMEPO-NFC suspension was stable. In the presence of KCl, the absolute value of zeta potential decreased to about 20 mV, because K^+ shielded the negative charge of the fiber surface.

Similar results have been obtained for KS-NFC, which was incorporated with methylcarboxylate groups carrying negative charge (**Fig. 39** and **Fig. 40**). However, the absolute value of zeta potential of KS-NFC was smaller than that of TEMPO-NFC, especially when no KCl was added in KS-NFC fluid from pH 5 to 10. These results indicated that the surface charge amount of KS-NFC was less than that of TEMPO-NFC.

The effect of KCl to the viscosity of ME-NFC was not significant. The addition of 5% KCl to ME-NFC fluid (40 lb/1000gal) reduced the viscosity of the fluid (**Fig. 41**). However, the viscosity reduction was not as obvious as that of TMEPO-NFC and KS-NFC fluids under the same conditions. This is because ME-NFC has lower surface charge density than the other two fibers, TMEPO-NFC and KS-NFC, which can be supported by the results of zeta potential measurements (**Fig. 42**). The zeta potential of ME-NFC at pH 7 was -18 mV, the absolute value of which was much smaller than that of TMEPO-NFC (-52 mV) and KS-NFC (-39 mV).

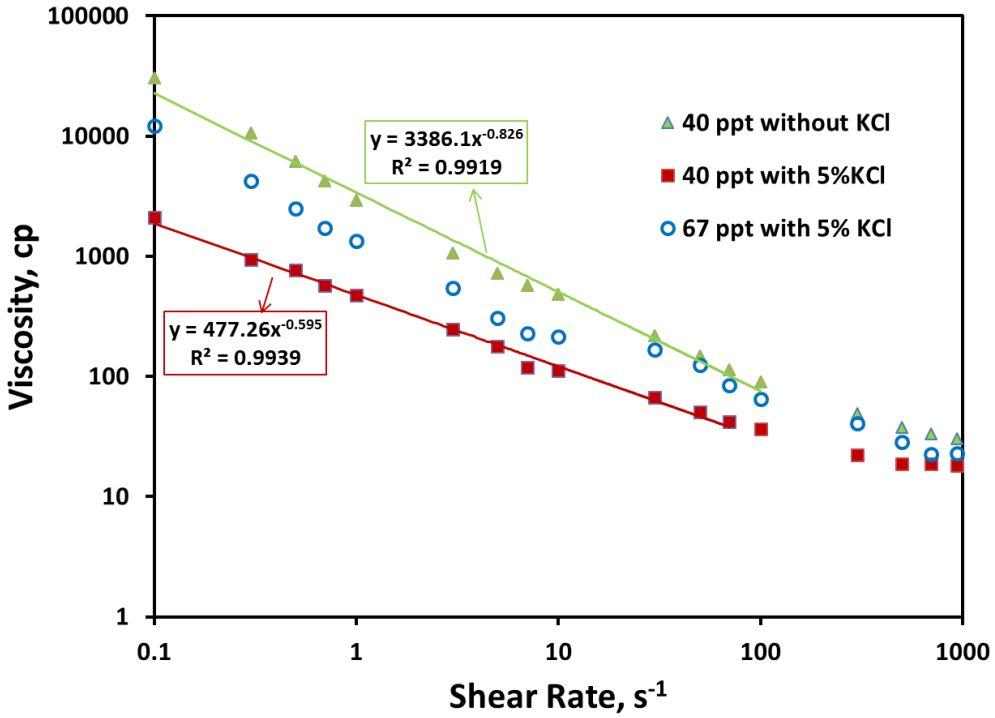

Fig. 37—The viscosity of TEMPO-NFC fluids as a function of shear rate at 75ºF.

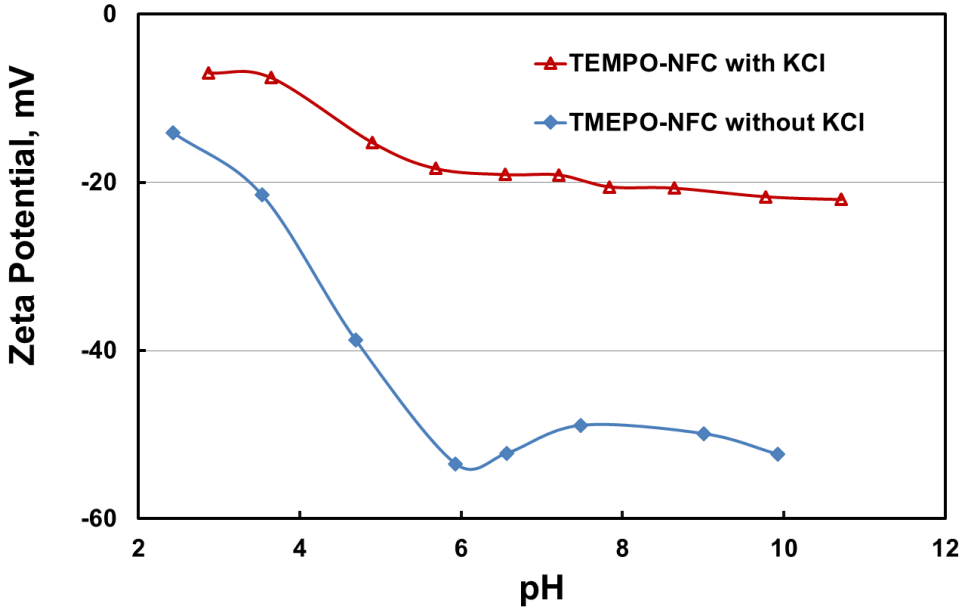

Fig. 38—The zeta potential of TEMPO-NFC fluid (0.02 wt%) with and without KCl.

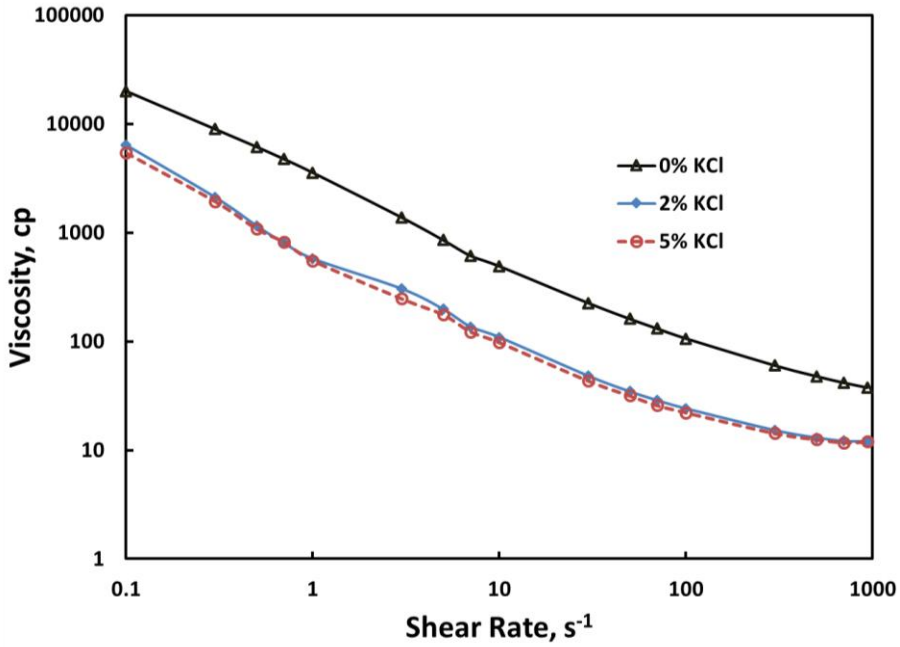

Fig. 39—The viscosity of KS-NFC fluid (40 lb/1000gal) as a function of shear rate at 75°F.

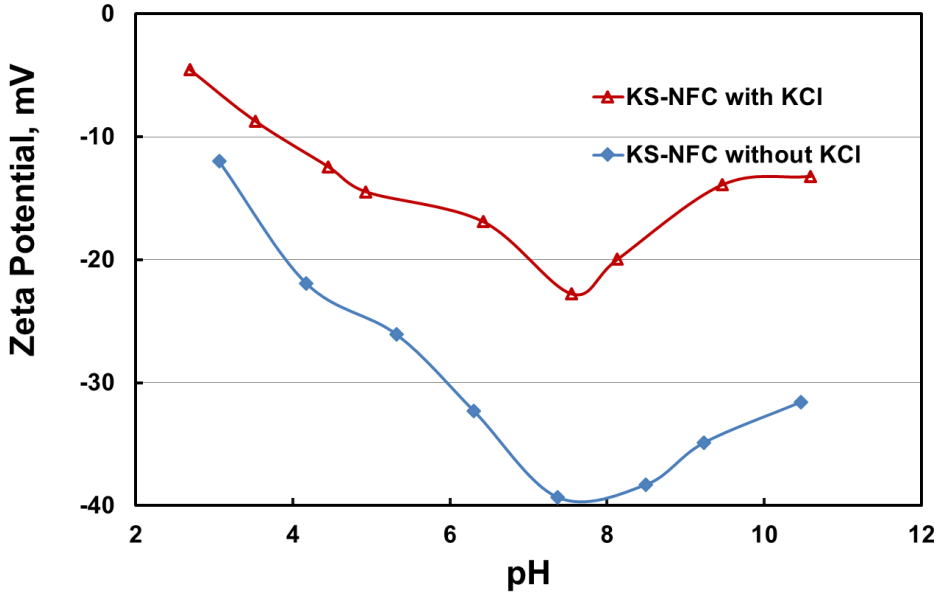

Fig. 40—The zeta potential of KS-NFC fluid (0.02 wt%) with and without KCl.

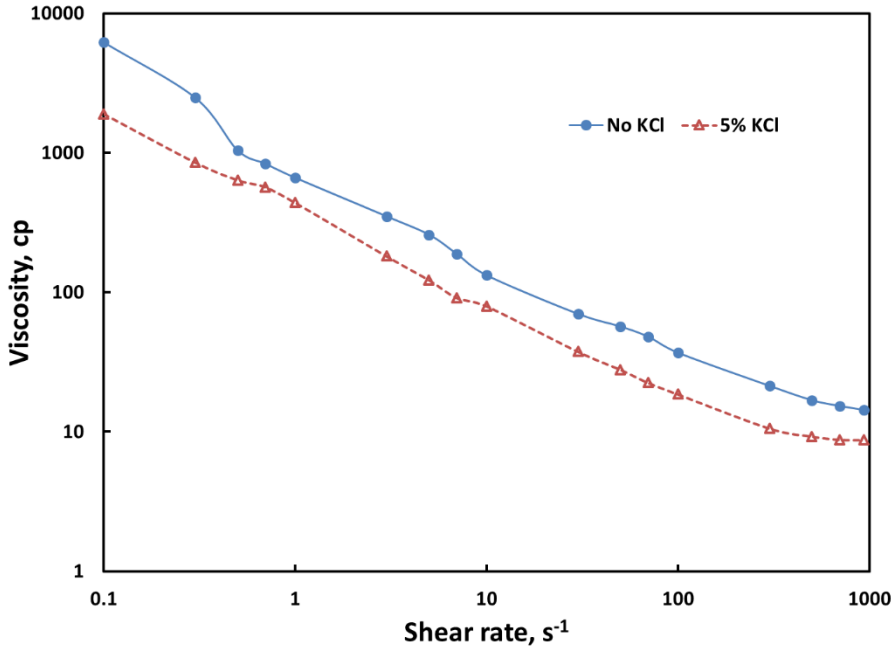

Fig. 41—The viscosity of ME-NFC fluid (40 lb/1000gal) with 5% KCl or without KCl as a function of shear rate at 75ºF.

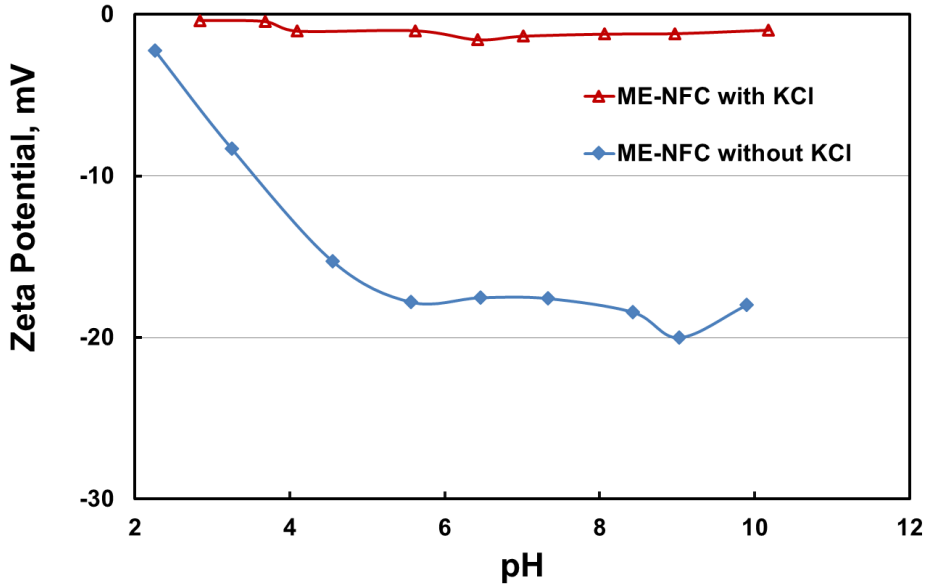

Fig. 42—The zeta potential of ME-NFC fluid (0.02 wt%) with and without KCl.

The viscosity stability of three NFC-based fluids, ME-NFC, TEMPO-NFC, and KS-NFC, were also studied at 350ºF. As shown previously, ENZ-NFC fluid was relatively stable up to 350ºF. Therefore, the temperature of 350ºF was tested for other three fibers, ME-NFC, TEMPO-NFC, and KS-NFC fluids at a concentration of 67 lb/1000gal (**Fig. 43**). The viscosity of each fluid was measured at a shear rate of 40 s^{-1} for 200 minutes. As the temperature increased from room temperature to 350ºF, the viscosity dropped significantly within 30 minutes at the beginning of each test. However, when the temperature was relatively stable at about 350ºF, the viscosity of all fluids also became relatively stable within 200 minutes. For ME-NFC fluid, the viscosity was stabilized at about 9 cp. TEMPO-NFC fluid had a stable viscosity of around 11 cp. KS-NFC fluid provided the highest viscosity of about 18 cp.

There was a disadvantage of the viscosity measurement method using the rotational rheometer, Grace M5600. In the whole process, a fixed shear rate of 40 s^{-1} was applied. The fiber suspended in the fluid tended to climb up the bob and stay on the top of the bob (**Fig. 43**), which may reduce the measured viscosity. Therefore, the measured viscosity may be lower than the real viscosity of the fluid.

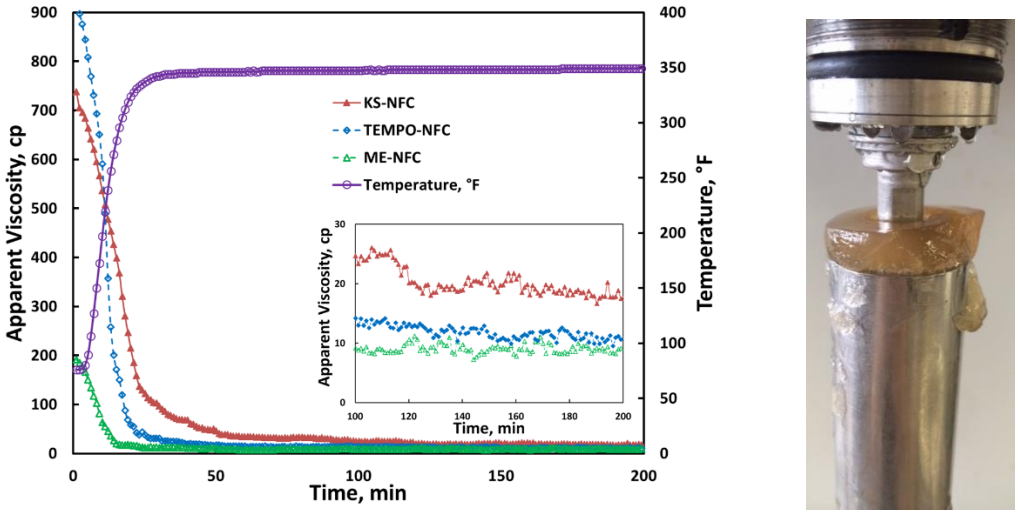

Fig. 43—The viscosity of three fiber fluids (67 lb/1000gal) fluids at 350°F and a shear rate of 40 s^{-1} (left), and the fiber residue on top of the bob after 200 minutes for ME-NFC fluid.

2.4.2. Viscoelastic properties of other three NFC-based fluids

Dynamic oscillatory tests were also performed using three NFC-based fluids, ME-NFC, KS-NFC, and TEMPO-NFC, to measure the elastic and viscous moduli, G' and G" at room temperature. Combining the same test for ENZ-NFC fluid in the previous section, the viscoelastic properties of the four fiber fluids (40 lb/1000gal) have been shown in **Fig. 44** and **Fig. 45**. The four fluids can be divided into two sets: ENZ-NFC and ME-NFC, KS-

NFC and TEMPO-NFC. ENZ-NFC and ME-NFC fluids showed similar viscoelastic properties, while the viscoelasticity behavior of KS-NFC fluid was close to TEMPO-NFC fluid. Both G' and G" of KS-NFC and TEMPO-NFC fluids were much larger than those of ENZ-NFC and ME-NFC fluids under the same conditions. The crossover frequency points, where G' is equal to G", have been shown in the following two figures. The order of the crossover frequency points for the four fiber fluids are as follows: ENZ-NFC > ME-NFC >> KS-NFC > TEMPO-NFC. Therefore, TEMPO-NFC showed the best viscoelastic property. These differences in the moduli and crossover points among the four fiber fluids resulted in different results in the proppant settling tests in the next section.

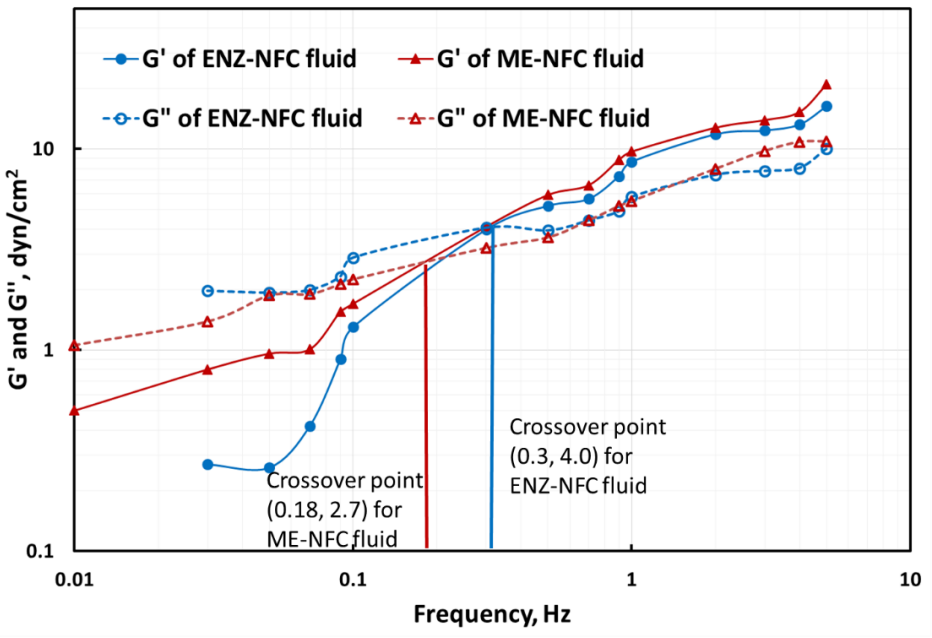

Fig. 44—The elastic (G') and viscous (G") moduli of ENZ-NFC and ME-NFC (40 lb/1000gal) fluids at different frequencies.

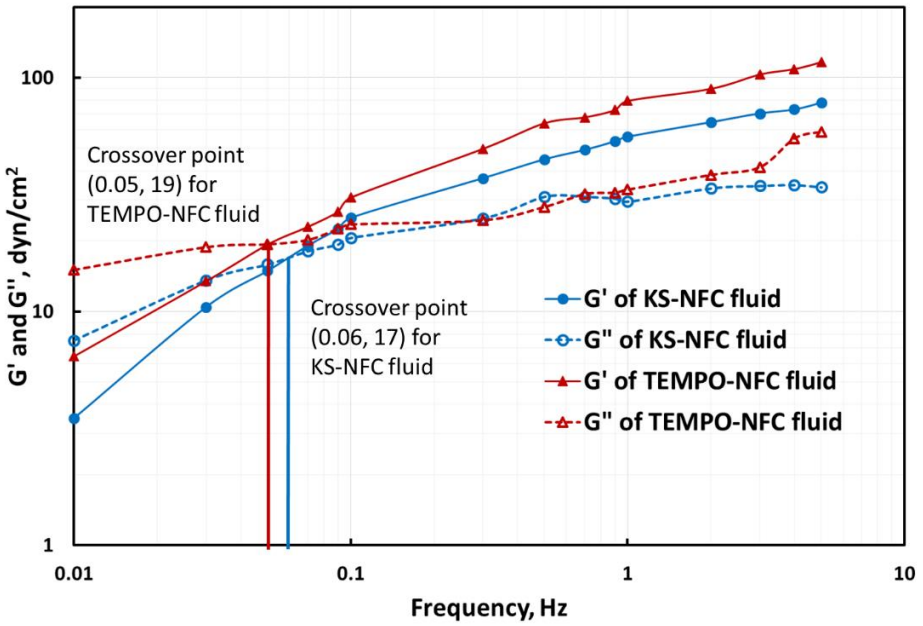

Fig. 45—The elastic (G') and viscous (G") moduli of KS-NFC and TEMPO-NFC (40 lb/1000gal) fluids at different frequencies.

2.5. Conclusion

In this section, the rheological properties of ENZ-NFC fluids were carefully studied using a rotational rheometer, Grace M5600. The viscosity measurements were performed to evaluate the effects of shear rate, salts, and temperature. The viscoelastic properties were examined by dynamic oscillatory tests. The ENZ-NFC fluid was non-Newtonian. This type of fluid had high thermal stability up to 350ºF, which was much better than guar fluid. The viscosity of ENZ-NFC was stable in the presence of 10 wt% KCl or $CaCl_2$. The dynamic oscillatory tests have shown that the fiber fluid behaved as an elastic material when the frequency was higher than 0.3 Hz. However, viscous modulus was still dominant for guar fluid until 2.3 Hz.

The rheological properties of other three NFC fluids, ME-NFC, TEMPO-NFC, and KS-NFC, were also investigated. All fiber-based fluids are non-Newtonian, which can be described by the power-law model. The presence of KCl resulted in an obvious reduction of the viscosity of ME-NFC, TEMPO-NFC, and KS-NFC fluids. The zeta potential profiles of the fiber fluids confirmed that the fibers have negative charge and the presence of KCl reduced the zeta potential of the fibers significantly. Therefore, the viscosity reduction in the presence of KS is resulted from that KCl can cause the collapse of the fiber chains by shielding the electrostatic repulsion between the negatively charged fiber chains. These three fiber fluids, ME-NFC, TEMPO-NFC, and KS-NFC, have also shown high stability at 350ºF. TEMPO-NFC fluid had the highest viscosity within 200 minutes at 350ºF with 40 lb/1000gal fiber added. The viscoelasticity behavior of four fiber fluids were compared. TEMPO-NFC fluid has shown the best viscoelasticity behavior under the same conditions. This can account for the difference in the sand settling tests of the four fiber fluids in Section 3.

3. PROPPANT SUSPENDING ABILITY OF NFC-BASED FRACTURING FLUIDS

3.1.Introduction

One important function of the fracturing fluid is to transport proppant into the fracture. However, proppant settles down when the gravity vector is larger than the forces to suspend the proppant. Therefore, it is necessary to evaluate the proppant suspending ability of the fracturing fluid and prevent proppant settling. Viscosity and network structure are the key parameters to afford good proppant suspending ability of fracturing fluids. Crosslinked fluids have excellent proppant suspending ability due to the high viscosity as well as the good network resulted from crosslinking of the polymers. However, one big disadvantage of crosslinked fluids is that severe damage may be caused to the fracture and formation due to the polymer residue. In contrast, slickwater does not have such problem. Moreover, slickwater has low cost and can create more complex fractures. But slickwater has poor proppant suspending ability due to the lack of viscosity and structure. Therefore, the proppant loading is usually very low in slickwater fracturing (0.25 to 2.5 lb/gal). The proppant can be transported mainly due to the high velocity. However, the high-velocity proppant-loaded fluid can cause blasting of the pumping equipment and reduce the service life of the equipment (Sahai et al. 2014). Linear gel has been used to replace slickwater with low polymer loadings. A synthetic polymer was sued to prepare guar-free fracturing fluid with low polymer loading and non-damaging property (Sun et al. 2013).

Proppant settling velocity can be described by Stoke's Law (eq. 7),

$$V = \frac{d^2 g(D_p - D_f)}{18\mu}. \quad \text{eq. 7}$$

where V is the proppant settling velocity, d is the proppant diameter, g is acceleration of gravity, D_p is the density of the proppant, D_f is the density of the fluid, and μ is the viscosity of the fluid. The methods to reduce the proppant settling involve reducing proppant size and proppant density, and increasing the viscosity of the fluid (Rickards et al. 2006; Brannon and Starks, 2009; dos Santos et al. 2009; Cawiezel and Gupta, 2010; Jardim Neto et al. 2012). Other efforts have also been performed. Kostenuk and Browne (2010) reported that a proppant transportation modifier used in slickwater fluid can help proppant travel further distances into the formation by creating micro-bubbles on the surface around the proppant grains.

Different methods have been developed to evaluate the proppant suspending ability of fracturing fluids. Harris et al. (2005) constructed a proppant viscometer to measure fracturing fluids containing propping agents. The measurements were used not only to evaluate the capability of the fracturing fluids to support proppant, but also to distinguish different types of fluids having either viscous or elastic components. Slot flow test is one important method to visualize the proppant transportation as the fracturing fluid travels from perforation into the fracture (Loveless et al. 2011). The model of slot flow test is shown in **Fig. 46**. The whole process can be video recorded when the proppant-loaded fluid flows through the pipe. Sahai et al. 2014 reported an experimental setup to evaluate the proppant transport and placement in the complex fracture networks in slickwater fracturing (**Fig. 47**).

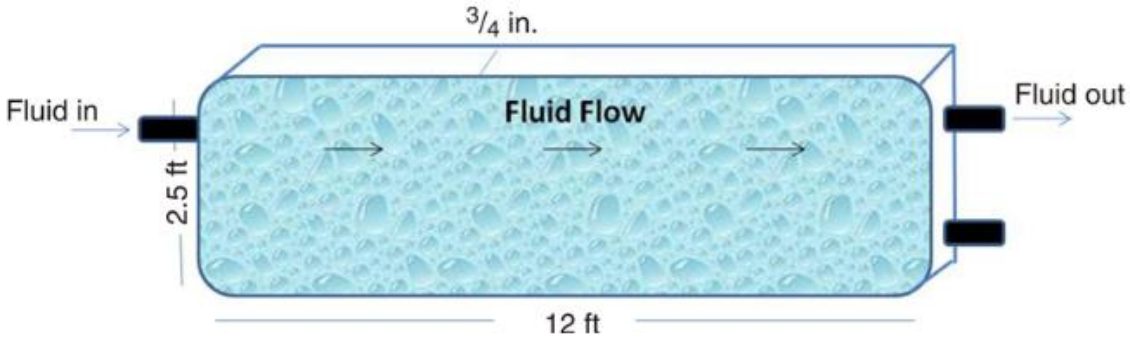

Fig. 46—The scheme of lot flow test model (after Loveless et al. 2011).

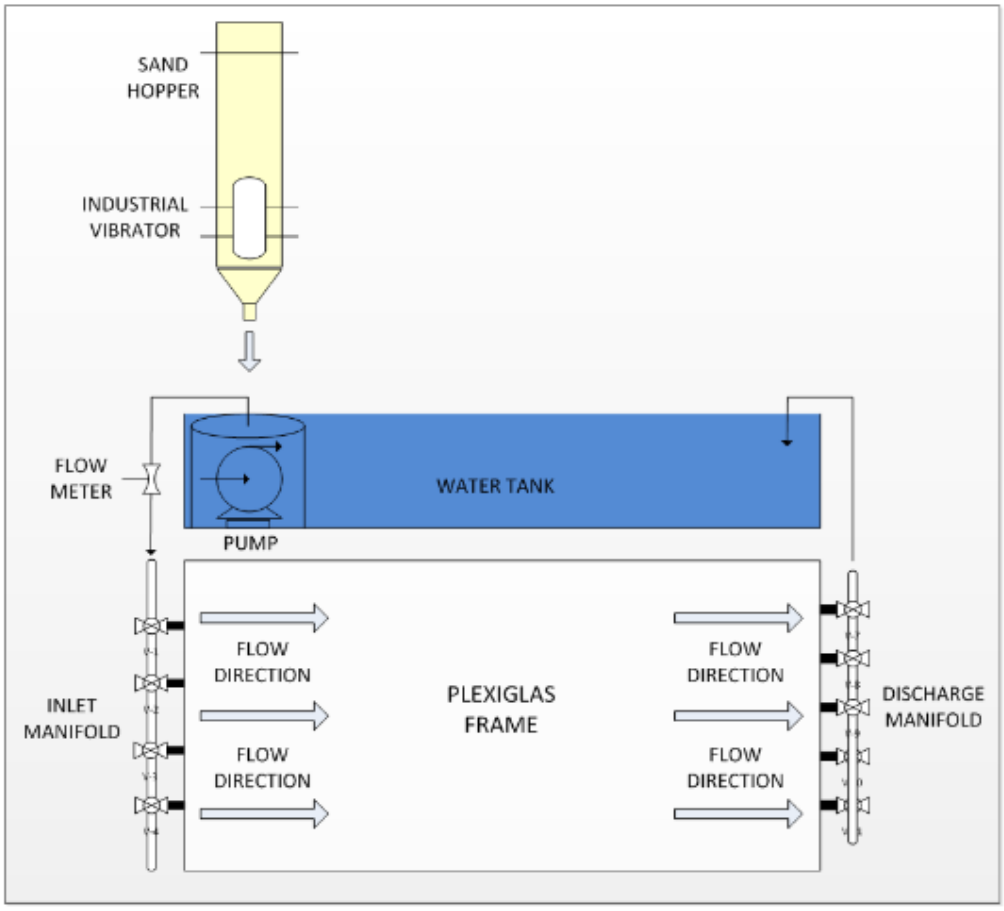

Fig. 47—The scheme of the experimental setup to evaluate proppant transport in the complex fracture networks (after Sahai et al. 2014).

Another method to evaluate proppant suspending ability of fracturing fluids is to measure the settling velocity of proppant in fluids (Liu and Sharma 2005; Malhotra and Sharma 2011). One container (usually a glass cylinder/tube) is filled with the fluid, where one proppant particle is immersed in the fluid and start to settle down. The time for the particle to travel from the surface of the fluid to the bottom is recorded by a stopwatch, and the settling velocity can be calculated based on Stokes' law. In many cases, Stokes equation is not sufficient/accurate to predict the settling velocity in non-Newtonian fracturing fluids. Therefore, extensive studies were performed on the settling velocity of spherical particles in Newtonian and non-Newtonian fluids (Novotny 1977; Roodhart 1985; Acharya 1986; Gadde et al. 2004).

Static proppant/sand settling test is also an easy way to measure the proppant suspending ability of fracturing fluids (Goel et al. 2002; Haghshenas and Nasr-El-Din 2014). This method allows to observe the proppant settling in the proppant-loaded slurry. The details are described in the following part of this section since it was used in this project.

3.2. Experimental methods

3.2.1. Materials

Four nanofibrillated cellulose, ENZ-NFC (slurry, 0.94 wt%), TEMPO-NFC (slurry, 0.98 wt%), ME-NFC (slurry, 0.91 wt%), and KS-NFC (slurry, 2.1 wt%) were from Elkem Materials Company. Deionized water (18.2 MΩ·cm at 25ºC) was used to prepare all fluids. Proppant, 100-mesh and 40/70-mesh Ottawa sand, was from US Silica Company

and used as received. The proppant has an average diameter of 0.2150 mm (100-mesh) and 0.3669 mm (40/70-mesh), and a density of 2.65 g/cm^3.

3.2.2. Fluid Systems

The formulations of all fluids are given in **Table 2**. An overhead mixer was used for all fluids. NFC fluids (40 or 67 lb/1000gal) were prepared by mixing NFC suspension and deionized water. The concentration of NFC fluids (40, or 67 lb/1000gal) was calculated as active NFC loading. Guar fluids were prepared by adding guar solid into deionized water slowly when the fluid was stirring. Hydration time was 30 min. The concentration of guar fluids (40 lb/1000gal) was calculated as the guar powder loading. Air bubbles trapped in the fluids were removed by centrifuge.

3.2.3. Proppant settling tests

The static proppant settling tests were conducted at 75 and 250ºF. A 100 cm^3 graduated cylinder was filled with fracturing fluids (NFC or guar fluid) and 4 lb/gal proppant. The viscosifier concentrations of fluids were 40 or 67 lb/1000gal. This method can allow to compare the proppant settling for NFC and guar fluids visually. When proppant settled down, there was a separation in the cylinder. The proppant-loaded fluid stayed at the bottom, leaving the proppant-free fluid on top. The height of the proppant-loaded fluid was measured every 5 minutes. For the test at 250ºF, the graduated cylinder was put inside the see-through cell (**Fig. 48**), which was kept at 250ºF at a pressure of 500 psi. The glass window on the see-through cell allowed to observe the proppant settling.

Table 2—Formulation of NFC fluids based on 1000 gal for proppant settling tests.

	Viscosifier Concentration	Water, gal	Viscosifier
ENZ Fluid	40 ppt[a]	490	510 gal
ENZ Fluid	67 ppt	150	850 gal
TEMPO Fluid	40 ppt	510	490 gal
TEMPO Fluid	67 ppt	184	816 gal
ME Fluid	40 ppt	473	527 gal
ME Fluid	67 ppt	121	879 gal
KS Fluid	40 ppt	771	229 gal
KS Fluid	67 ppt	619	381 gal
Guar Fluid	40 ppt	1000	40 lb

a. ppt: lb/1000gal

Fig. 48—See-through cell for the proppant settling test at high temperature.

3.3. Proppant suspending ability of NFC and guar fluids

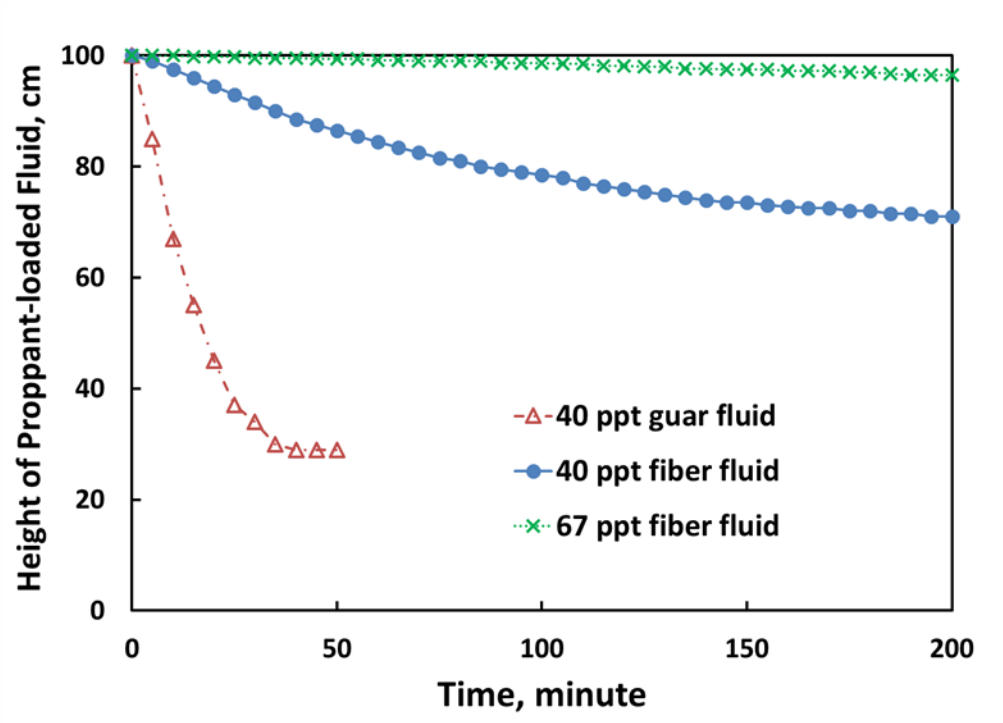

Fig. 49—The proppant settling tests of ENZ-NFC (V1) fluids (40 and 67 lb/1000gal) and guar fluid (40 lb/1000gal) with 4 lb/gal proppant at 75ºF.

The proppant suspending ability of ENZ-NFC fluids was evaluated at 75 and 250ºF. For all tests, 4 lb/gal proppants were added to the fluids. At 75ºF, guar fluid (40 lb/1000gal) was also tested. All proppants settled down in the guar fluid within 40 minutes. The height was about 30 cm, because the dry proppant had a volume of around 30 ml. However, most proppants were still suspended after 40 minutes in ENZ-NFC fluid (40 lb/1000gal). After 200 minutes, the height of the proppant-loaded fluid was 71 cm in ENZ-NFC fluid (40 lb/1000gal) as shown in **Fig. 49**, indicating that more than 50% proppant

was still suspended. Therefore, the proppant suspending ability of ENZ-NFC fluid has out-performanced guar fluid at 75ºF. This result can be correlated with the viscoelastic properties of the fiber and guar fluids. In Section 2, dynamic oscillatory tests were performed to measure G' and G" of ENZ-NFC fluid (40 lb/1000gal). The crossover frequency, where G' is equal to G", was 0.3 Hz, which is much lower than that of guar fluid (40 lb/1000gal). Harris et al. (2009) established a correlation between the crossover frequency with the elastic transport time of the proppant particle in the polymer fluids. Basically, they showed that the crossover frequency and the settling time could be correlated with a power-law function. As the crossover frequency decreased, the settling time increased. This relationship was consistent with the results of ENZ-NFC and guar fluids. The lower crossover frequency of ENZ-NFC fluid predicted a better propant suspending ability than guar fluid.

An increase of ENZ-NFC concentration improved the proppant suspending ability. A similar test was performed using 67 lb/1000gal ENZ-NFC fluid. After 200 minutes, the height of proppant-loaded fluid was 96.5 cm, indicating that most proppants in 67 lb/1000gal ENZ-NFC fluid were suspended after 200 minutes at 75ºF. Along with the settling of proppants, the viscosifier ENZ-NFC also settled down, leaving water-like consistency on top of the cylinder as shown in **Fig. 50**. The concentrated viscosifier ENZ-NFC in the proppant-loaded fluid slowed down the proppant settling rate further.

The proppant suspending ability of ENZ-NFC fluid was tested at 250ºF using see-through cell. As shown in **Fig. 51**, after 100 minutes, the height of proppant-loaded fluid

was 66.5 cm at 250ºF while it was 78.5 cm for the fluid at 75ºF. Therefore, a rise in temperature resulted in a higher proppant settling velocity in ENZ-NFC fluids.

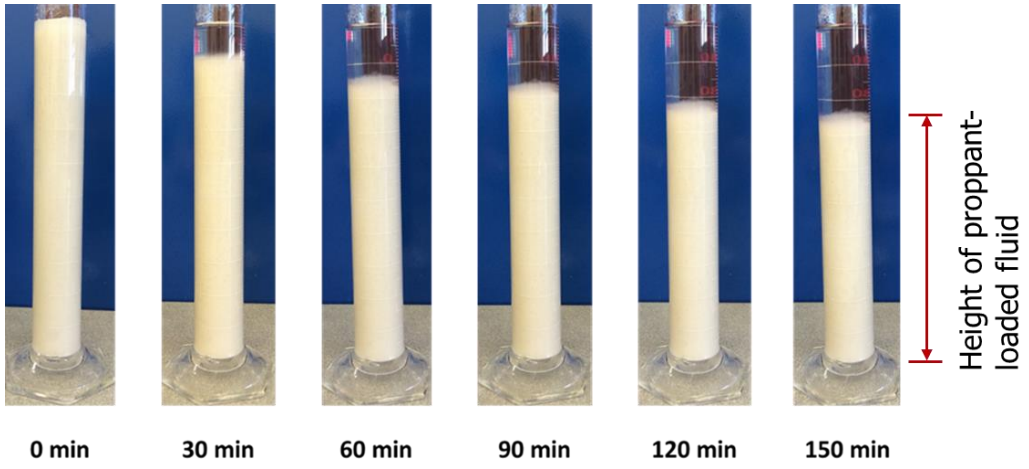

Fig. 50—The proppant settling test of ENZ-NFC fluid (40 lb/1000gal) with 4 lb/gal proppant at 75ºF.

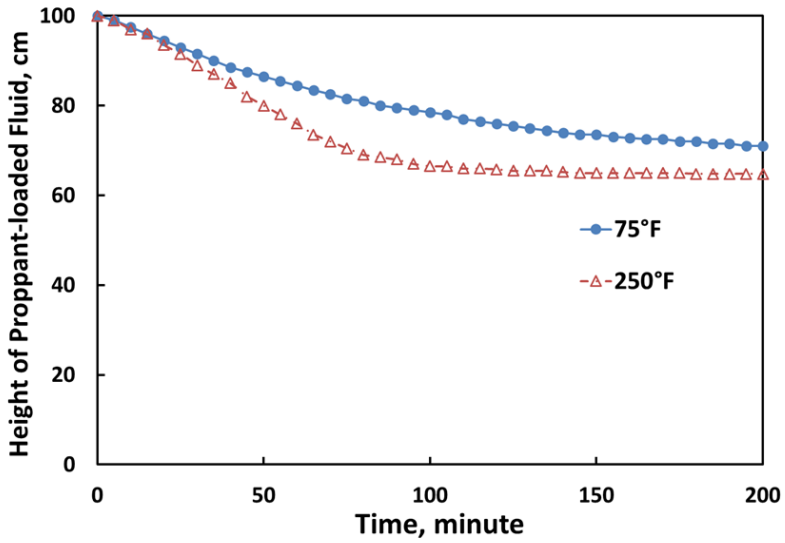

Fig. 51—The proppant settling tests of ENZ-NFC fluid (40 lb/1000gal) with 4 lb/gal proppant at 75 and 250ºF.

Other NFC fluids were also evaluated using the same method. Four types of NFC fluids were tested and compared under similar conditions. ME-NFC, KS-NFC, and TEMPO-NFC fluids (40 lb/1000gal) were loaded with 4 lb/gal 100-mesh Ottawa sand. The height of the proppant-loaded fluids were recorded and compared with that of ENZ-NFC fluid under the same conditions. As shown in **Fig. 52**, after 100 minutes, the height of the proppant-loaded ENZ-NFC fluid was 78.5 cm, while it was 83.2 cm for ME-NFC fluid. Starting from 10 to 200 minutes during the tests, the height of the proppant-loaded fluid was higher for ME-NFC fluid than ENZ-NFC fluid. These two tests have shown that the proppant suspending ability of ME-NFC is better than that of ENZ-NFC fluid under the same conditions. When KS-NFC or TEMPO-NFC fluid (40 lb/1000gal) was loaded with 4 lb/1000gal 100-mesh Ottawa sand, all proppant was suspended for at least 200 minutes and no obvious settling was observed. Therefore, the proppant suspending ability for four fiber fluids was as follows: ENZ-NFC < ME-NFC < KS-NFC/TEMPO-NFC.

In order to tell apart the proppant suspending ability between KS-NFC and TEMPO-NFC fluids, 33 lb/1000gal fiber and 4 lb/gal 40/70-mesh Ottawa sand were used in the static sand settling tests. For KS-NFC fluid, the sand settled down slowly. After 200 minutes, the height of the proppant-loaded fluid was 94.5 cm (**Fig. 53**). However, the sand did not move in TEMPO-NFC fluid under the same conditions. The height of the proppant-loaded fluid was kept at 100 cm. Therefore, the proppant suspending ability of TEMPO-NFC fluid was better than KS-NFC fluid under the same conditions. Therefore, the proppant suspending ability for the four fluids was as follows: ENZ-NFC < ME-NFC < KS-NFC < TEMPO-NFC.

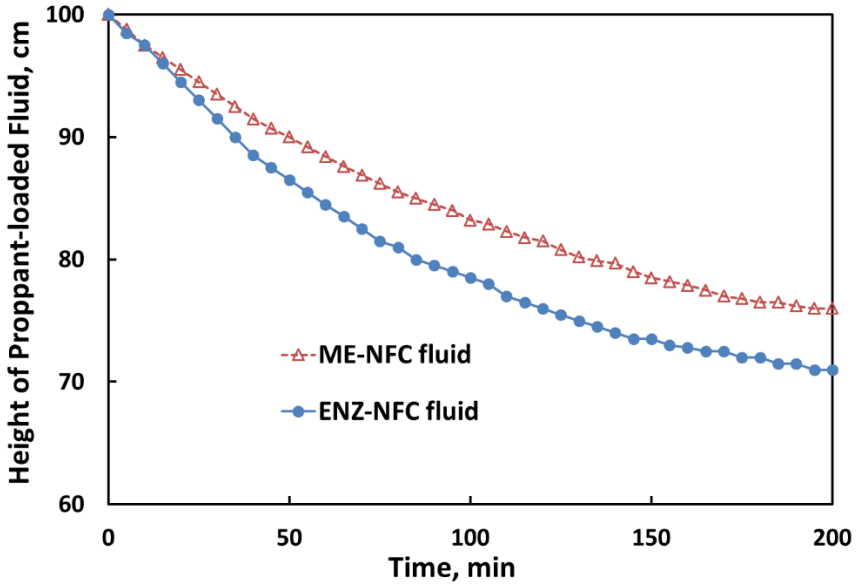

Fig. 52—The proppant settling tests of ENZ-NFC fluid (40 lb/1000gal) and ME-NFC fluid (40 lb/1000gal) with 4 lb/gal 100-mesh proppant at 75°F.

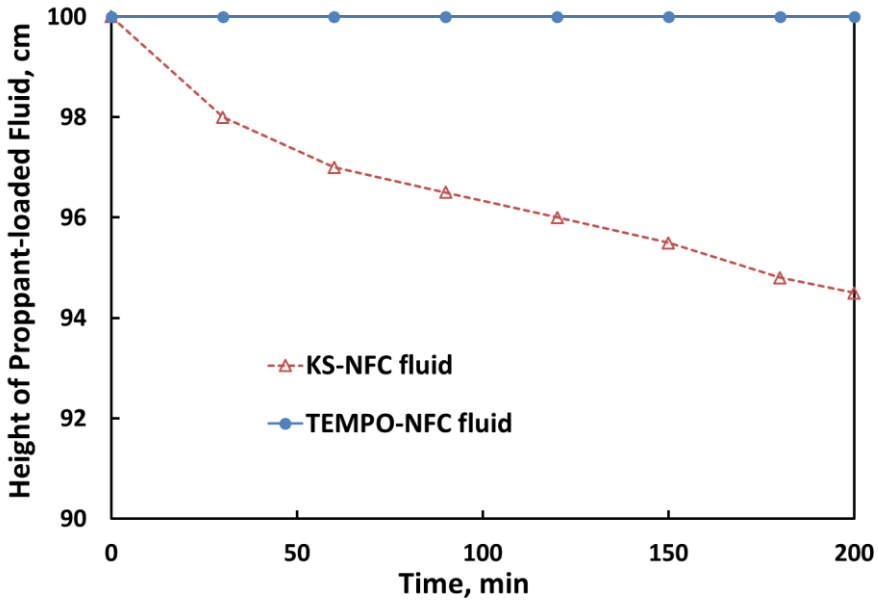

Fig. 53—The proppant settling tests of KS-NFC fluids (33 lb/1000gal) and ME-NFC fluid (33 lb/1000gal) with 4 lb/gal 40/70-mesh proppant at 75°F.

The proppant suspending ability of the fiber fluids can be correlated to their viscoelastic properties. The viscoelastic properties of the four fiber fluids and guar (40 lb/1000gal) have been studied in the previous section by measuring G' and G" at different frequencies from 0.01 to 5 Hz. The crossover frequency was obtained where G' was equal to G" for each fluid (**Table 3**). Harris et al. (2009) established a correlation between the crossover frequency and the proppant settling time for different fluids with the same proppant. As the crossover frequency decreased, the proppant settling time became longer and thus the fluid had a better proppant suspending ability. Similar trend has been shown when we compared the four fiber fluids and guar fluid. The crossover frequency for the five fluids decreased in the following order: guar > ENZ-NFC > ME-NFC > KS-NFC > TEMPO-NFC. Correspondingly, the proppant suspending ability of these five fluids were as follows: guar < ENZ-NFC < ME-NFC < KS-NFC < TEMPO-NFC.

Table 3—The frequency of crossover point for four fiber fluids

	Guar	ENZ-NFC	ME-NFC	KS-NFC	TEMPO-NFC
Crossover Frequency, Hz	2.3	0.3	0.18	0.06	0.05

3.4. Conclusion

In this section, the proppant suspending ability of four fiber fluids have been evaluated and compared to guar fluid using static sand settling tests. Fiber fluids had a

much better proppant suspending ability than guar fluid under the same conditions. An increase in the fiber concentration led to the improvement in the proppant suspending ability. However, the temperature increase resulted in a faster sand settling. A correlation was found between the viscoelastic properties and the proppant suspending ability for the fiber and guar fluids. The crossover frequency for the five fluid decreased in the following order: guar > ENZ-NFC > ME-NFC > KS-NFC > TEMPO-NFC. Correspondingly, the proppant suspending ability of these five fluids were as follows: guar < ENZ-NFC < ME-NFC < KS-NFC < TEMPO-NFC.

4. FORMATION DAMAGE EVALUATION OF NFC-BASED FLUIDS

4.1. Introduction

Guar gum contains 10-14% insoluble residue. In addition, the intermolecular hydrogen bonding will cause the guar molecules to form aggregates, resulting in formation damage (Cheng et al., 2002). Polymers can bridge pores of the rock and cause formation damage by reducing fracture conductivity and formation permeability (DeVine et al., 1998). The degree of damage can be related to many factors, such as polymer type, polymer concentration, crosslinker, breaker type, breaker concentration, and rock permeability. Guar-based fluids can cause more damage than cellulose-based fluids (Almond, 1982). A higher polymer loading usually causes more damage to the permeability (Siddiqui, Nasr-El-Din, Al-Anazi, and Bartko, 2004). Gels crosslinked with borate can afford a better cleanup result than those crosslinked with Ti and Zr ions. As for the effect of permeability, a correlation between rock permeability and the damage degree was reported from previous studies. In general, the higher the permeability is, the greater the formation damage is.

To develop potential applications of new chemicals in the oilfield, it is necessary to evaluate the possible formation damage they may cause. Most research in developing chemicals has reported the formation damage studies (Okoye et al. 1991; Parlar et al. 1995; Krilov et al. 1996; Audibert, et al. 1999; Al-Yami et al. 2008; Salazar et al. 2013). In this section, the formation damage of fiber-based hydraulic fracturing fluids in different formations have been evaluated and compared with guar, hydroxypropyl guar (HPG) and

viscoelastic surfactant (VES) fluids. The effects of temperature, viscosifier type, viscosifier concentration, and formation permeability were investigated.

4.2. Experimental methods

4.2.1. Materials

Four nanofibrillated cellulose, ENZ-NFC (slurry, 0.94 wt%), TEMPO-NFC (slurry, 0.98 wt%), ME-NFC (slurry, 0.91 wt%), and KS-NFC (slurry, 2.1 wt%) were from Elkem Materials Company. Other viscosifiers, guar (solid), HPG (solid), and VES (liquid) were obtained from oil service companies. VES was a mixture liquid of an amphoteric amide oxide surfactant and a solvent (Li et al. 2011 for composition), and used as received. KCl (ACS grade) was from Sigma Aldrich, and used as received. Deionized water (18.2 MΩ·cm at 25ºC) was used to prepare all fluids.

Table 4—Mineral composition for sandstone cores

Mineral, wt%	Berea	Bandera	Boise
Quartz	86	57	63
Dolomite	1	16	–
Calcite	2	–	1
Feldspar	3	12	25
Kaolinite	5	3	5
Illite	1	10	4
Chlorite	2	1	2

Core plugs were cut from Berea, Bandera, and Boise sandstone blocks, or high-permeability Indiana limestone with a 6-in. length and 1.5-in. diameter. The mineralogy of the sandstone cores are shown in **Table 4**. The chemical composition of Indiana limestone core includes $CaCO_3$ 97.3%, $MgCO_3$ 0.4%, Al_2O_3 0.5%, and SiO_2 1.7%. The porosity and initial permeability measured with 5 wt% KCl or deionized water was shown in **Table 6**, **Table 7**, **Table 8**, and **Table 9**.

4.2.2. Fluid systems

The formulations of all fluids are given in **Table 5**. An overhead mixer was used for all fluids. NFC-based fluids (8.3 or 40 lb/1000gal) were prepared by mixing each NFC slurry and deionized water. KCl (5 wt%) was added when necessary. The concentration of NFC fluids (40 lb/1000gal) was calculated as active NFC loading. Guar/HPG fluids were prepared by adding guar/HPG solid into deionized water slowly when the fluid was stirring. Hydration time was 30 min. KCl (5 wt%) was added to the polymer fluids if necessary. The concentration of guar/HPG fluids (40 lb/1000gal) was calculated as the active guar or HPG polymer loading. The VES fluid was made by mixing VES liquid with 5 wt% KCl solution. Air bubbles trapped in the fluids were removed by centrifuge at 2500 rpm for 30 minutes. The concentration of VES fluid (40 gal/1000gal) was calculated as the VES liquid (a mixture liquid as received) loading.

Table 5—Formulation of hydraulic fracturing fluids based on 1000 gal

	Viscosifier Concentration	Water, gal	Viscosifier
ENZ-NFC Fluid	40 ppt[a]	490	510 gal
ENZ-NFC Fluid	8.3 ppt	894	106 gal
ME-NFC Fluid	40 ppt	473	527 gal
ME-NFC Fluid	8.3 ppt	890	110 gal
TEMPO-NFC Fluid	40 ppt	510	490 gal
TEMPO-NFC Fluid	8.3 ppt	898	102 gal
KS-NFC Fluid	40 ppt	771	229 gal
KS-NFC Fluid	8.3 ppt	952	48 gal
Guar Fluid	40 ppt	1000	40 lb
Guar Fluid	67 ppt	1000	67 lb
HPG Fluid	40 ppt	1000	40 lb
VES Fluid	40 gpt[b]	960	40 gal

b. ppt: lb/1000gal; b. gpt: gal/1000gal

4.2.3. Coreflood Setup and Procedures

a. The core was dried at 250ºF for 4 hours and weighed to obtain its dry weight. Then the core was saturated with brine solution (5 wt% KCl in deionized water, for sandstone cores) or deionized water (for carbonate cores) for 6 hours under vacuum and its wet weight was measured. The pore volume was calculated using these measurements and the density of the brine solution or water (density = 1.03 g/cm^3 at 70ºF for 5% wt KCl and 1 g/cm^3 for water).

b. The coreflood setup was shown in **Fig. 54**. The core was placed inside the core holder. The brine (5 wt% KCl, for sandstone) or deionized water (carbonate) was pumped through the core in the production direction. If elevated temperature was required, the temperature was raised to the target value (250ºF) and kept constant in the whole process. The pressure drop across the core was monitored and recorded until it was stabilized. The initial permeability was calculated.

c. The treatment fluid (NFC fluids, guar, HPG, or VES fluid) was pumped, in the injection direction (reversed to production direction), at the back pressure of 1100 psi. The pressure drop across the core was recorded.

d. The direction of flow was then reversed to the production direction and the brine (5 wt% KCl, for sandstone) or deionized water (for carbonate) was injected into the core until the pressure drop across the core was stabilized. The regained permeability after fluid treatment was calculated.

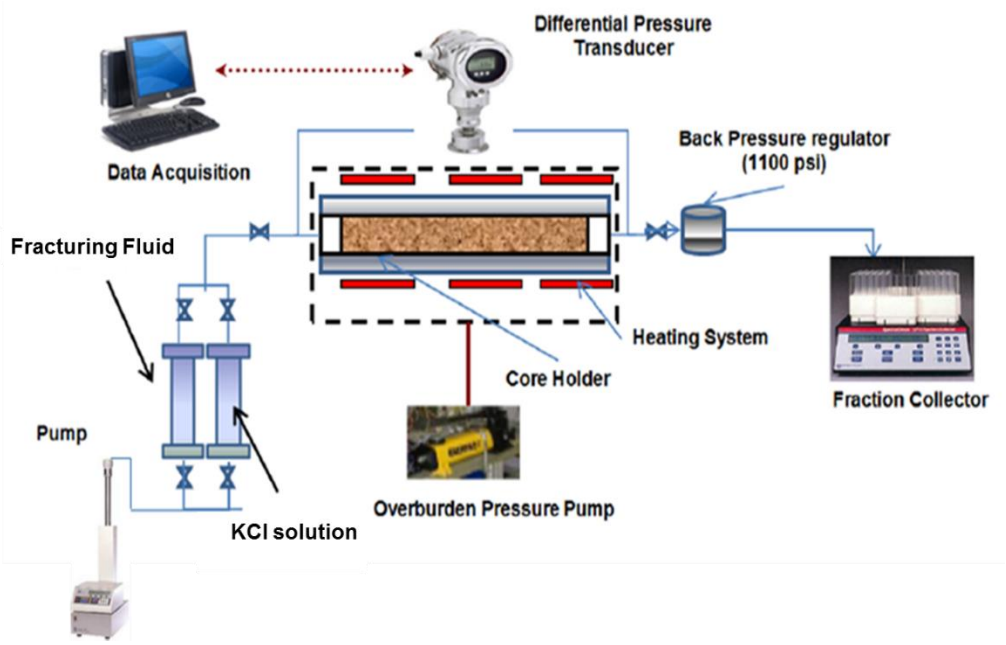

Fig. 54—The setup of the coreflood test.

4.3. Formation damage evaluation of ENZ-NFC, guar, HPG, ang VES fluids

4.3.1. Formation damage evaluation in low/moderate-permeability cores

Six coreflood tests were performed using ENZ-NFC-based fluids. The pressure drop across the core and permeability of these cores are given in **Table 6**. During the coreflood test, as shown in **Fig. 55**, 5 wt% KCl was injected in the injection direction, and the fiber fluid was injected in the production direction. The initial pressure drop was measured by injecting 5 wt% KCl solution before ENZ-NFC fluid treatment, and the final pressure drop was obtained after ENZ-NFC fluid treatment. The initial and final permeability were calculated by Darcy's law. The regained permeability percentage was calculated by dividing the final permeability by the initial permeability of the core. The formation damage was evaluated based on this percentage. A high percentage value

indicated a low formation damage degree. The effects of temperature, viscosifier concentration, and formation type were studied. In Test 1 and Test 2, Berea cores were used at 75 and 250ºF. The regained permeability percentages were 89% at 75ºF and 88% at 250ºF, which suggested that the temperature did not affect the formation damage.

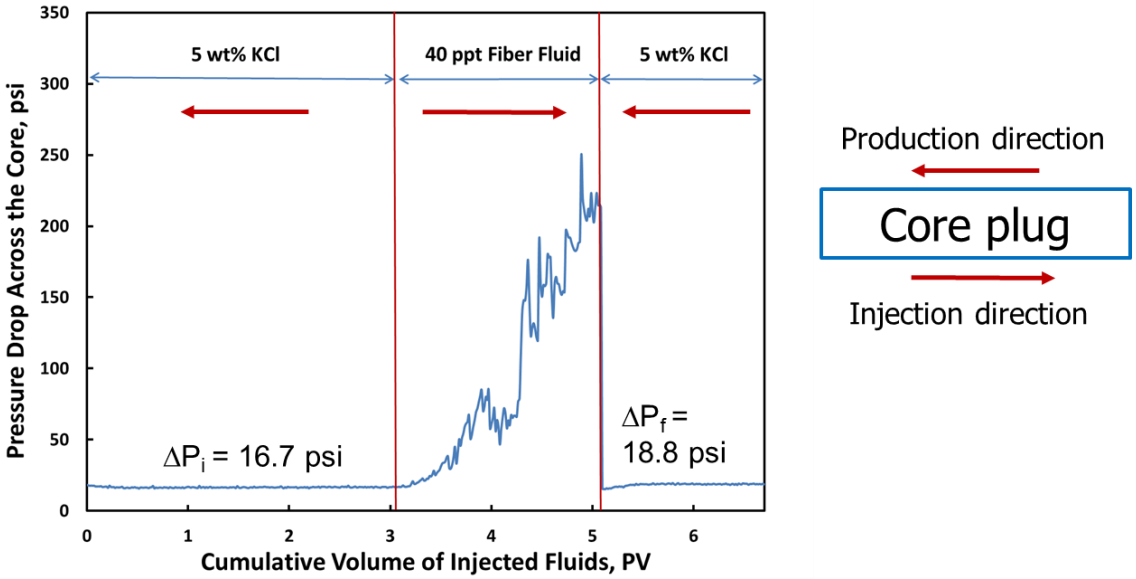

Fig. 55—Test 1: Pressure drop across the core with 40 lb/1000gal ENZ-NFC fluid and Berea core at 75ºF.

Table 6—Coreflood tests using ENZ-NFC fluids in low/moderate-permeability cores						
Coreflood No.	Test 1[a]	Test 2[a]	Test 3[a]	Test 4[a]	Test 5[a]	Test 6[b]
Core Type	Berea	Berea	Berea	Bandera	Bandera	Berea
Porosity, vol%	17.3	18.0	17.5	20.5	21.1	17.7%
Temperature, ºF	75	250	250	250	250	75
ENZ-NFC Concentration, ppt[c]	40	40	67	40	67	40
Initial Permeability, md	98.1	90.5	79.1	19.8	17.8	65.5
Final Permeability, md	87.1	79.9	78.4	19.2	17.5	46.8
Percentage	89%	88%	99%	97%	98%	71%

a. The brine solution was injected immediately after ENZ-NFC treatment.
b. The brine solution was injected after 3 days after ENZ-NFC treatment.
c. ppt: lb/1000gal

Different viscosifier concentrations were used in Test 2 (40 lb/1000gal) and Test 3 (67 lb/1000gal) under the same conditions. When a higher concentration of ENZ-NFC (67 lb/1000gal) was used in Test 3, the regained permeability was very close to the initial permeability, with a regained permeability percentage of 99%, which was higher than Test 2. This result has shown that less formation damage was caused in Test 3 than in Test 2. This may be because filter cake formed quickly with a high concentration of ENZ-NFC fluid (67 lb/1000gal) and thus it could prevent the fluid from invading the core. In Test 3, the pressure drop across the core decreased very quickly after about 1 pore volume was injected (**Fig. 56**), because the coreflood system was blocked due to the formation of filter cake on the injection face of the core (**Fig. 57**). In this case, the flow rate of the fluid that

flew out of the core reduced until no fluid was flowing inside the core, as indicated by the observation that no fluid came out from the outlet tube. The pumping pressure increased to the maximum pressure 2000 psi where the injection stopped. The filter cake was removed mechanically when brine solution was injected in the production direction. The regained permeability was very similar to the initial permeability of the core. For Berea sandstone with permeability higher than 50 md, a concentration of 67 lb/1000gal ENZ-NFC fluid caused less damage than a concentration of 40 lb/1000gal.

In Test 6, the aging effect of the filter cake was studied. After ENZ-NFC fluid was injected, the coreflood system was closed and kept for three days. The final permeability was then measured by injecting 5 wt% KCl solution. Other conditions were the same as in Test 5. However, the regained permeability percentage was 71%, which was lower than that in Test 5. These results have shown that aging filter cake caused a more severe damage to the core.

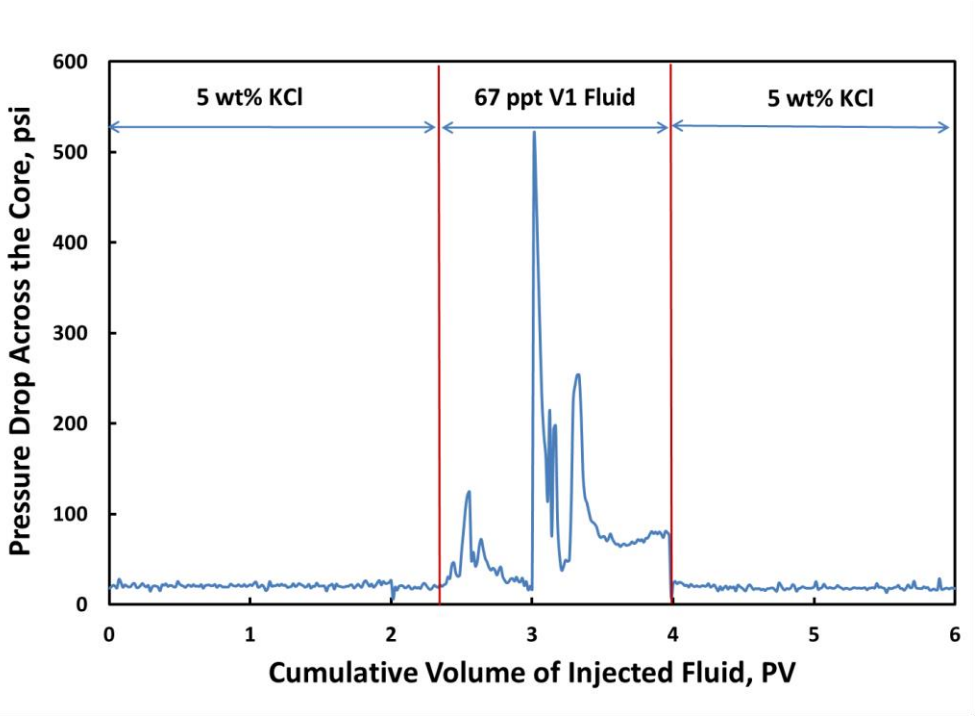

Fig. 56—Test 3: Pressure drop across the core with 67 lb/1000gal ENZ-NFC (V1) fluid and Berea core at 250ºF.

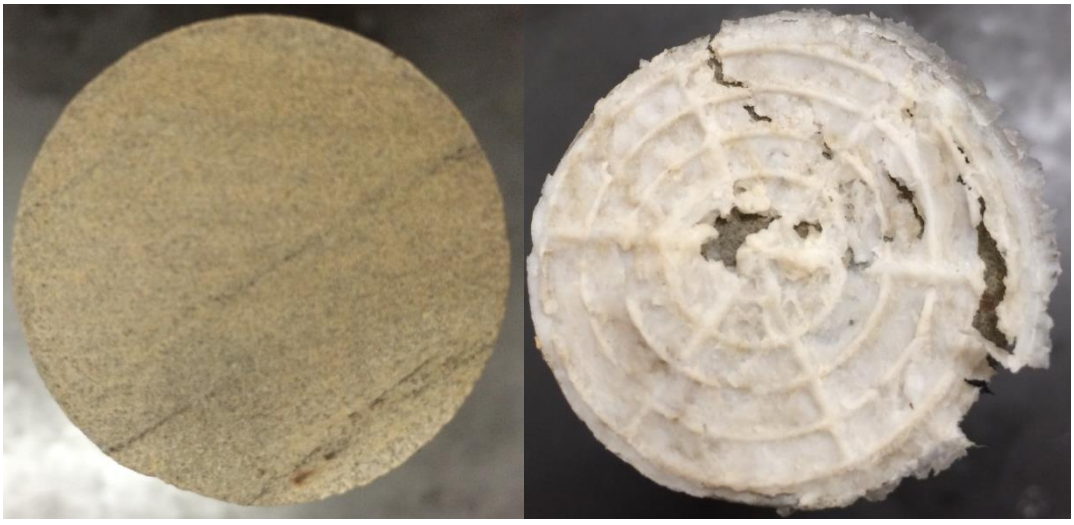

Fig. 57—Injection face of the core before (left) and after (right) ENZ-NFC (V1) (67 lb/1000gal) fluid injection.

When Bandera sandstone was used in Test 4 and Test 5, different concentrations of viscosifier (40 or 67 lb/1000gal) were used. The regained permeability was very close to the initial permeability for both tests. Comparing Test 2 and Test 4, a regained permeability percentage of 97% was obtained with Bandera sandstone, which was higher than Test 2 with Berea sandstone (88%). The initial permeability of Bandera core was 19.8 md in Test 4, which was much lower than that of Berea core (90.5 md) in Test 2. Therefore, ENZ-NFC -based fluid is less damaging in Bandera sandstone than Berea sandstone. This result is different from studies on the formation damage of guar-based fracturing fluids, which caused severe formation damage in Bandera formations as shown in the following work in this paper. In Bandera sandstone formation, the pore throat is small. Therefore, the filter cake builds up very quickly, which makes it difficult for ENZ-NFC fluid invasion. The formation of filter cake did not cause damage, because it can be removed very easily when brine was injected in the core in the production direction.

In Test 5, the regained permeability percentage was 98% when 67 lb/1000gal ENZ-NFC fluid was used, which was very close to Test 4 with 40 lb/1000gal ENZ-NFC fluid. The pressure drop across the core started to decrease quickly after about 1 pore volume of ENZ-NFC fluid was injected, which was similar to Test 3, due to the formation of filter cake.

Table 7—Coreflood tests using guar fluids					
Coreflood No.	Test 7	Test 8	Test 9	Test 10	Test 11
Core Type	Berea	Berea	Berea	Bandera	Bandera
Porosity, vol%	17.8	18.4	18.9	20.3	20.8
Temperature, ºF	75	250	250	250	250
Guar Concentration, lb/1000gal	40	40	67	40	67
Initial Permeability, md	142.2	65.0	74.4	12.7	13.4
Final Permeability, md	46.7	39.5	15.8	2.9	3.1
Percentage	33%	61%	21%	23%	23%

Table 8—Coreflood tests using HPG fluids		
Coreflood No.	Test 12	Test 13
Core Type	Berea	Bandera
Porosity, vol%	17.9	19.7
Temperature, ºF	250	250
HPG Concentration, lb/1000gal	40	40
Initial Permeability, md	83.1	22.7
Final Permeability, md	49.9	5.4
Percentage	60%	24%

Guar and HPG fluids caused severe formation damage in the coreflood tests (**Table 7** and **Table 8**). The effects of temperature, viscosifier concentration, and formation type were studied in order to compare with ENZ-NFC-based fluid. When Berea core was used in Tests 7 and 8, different temperatures were tested (75 and 250ºF). The regained permeability percentage was higher at 250ºF (61%) than that at 75ºF (33%). For Tests 8 and 9, different concentrations of guar (40 and 67 lb/1000gal) were used. In Test 8, the regained permeability percentage was 61%, while in Test 9 the regained permeability percentage was only 21%. In Test 9, the pressure drop across the core decreased slowly at the beginning of brine injection after the fiber treatment (**Fig. 58**), indicating that partial guar polymers were flushed out. However, the final pressure drop was still very high when it was stable. These results have shown that a higher concentration of guar (67 lb/1000gal) resulted in a more severe damage than a lower concentration of guar (40 lb/1000gal). Similar results of the effect of polymer concentration on formation damage were reported previously (Sarwar et al. 2011). However, the conclusion was not supported when Bandera cores were used in Tests 10 and 11. With 67 lb/1000gal of guar fluid in Test 11, the regained permeability percentage was similar to that in Test 10 with 40 lb/1000gal guar fluid. The regained permeability of Bandera in Test 11 was 3.1 md, which was quite low and may have prevented further invasion of guar polymers. Moreover, less than 2 pore volume of guar fluid was injected, because the pumping pressure increased to the maximum pressure 2000 psi where the injection stopped automatically (**Fig. 59**).

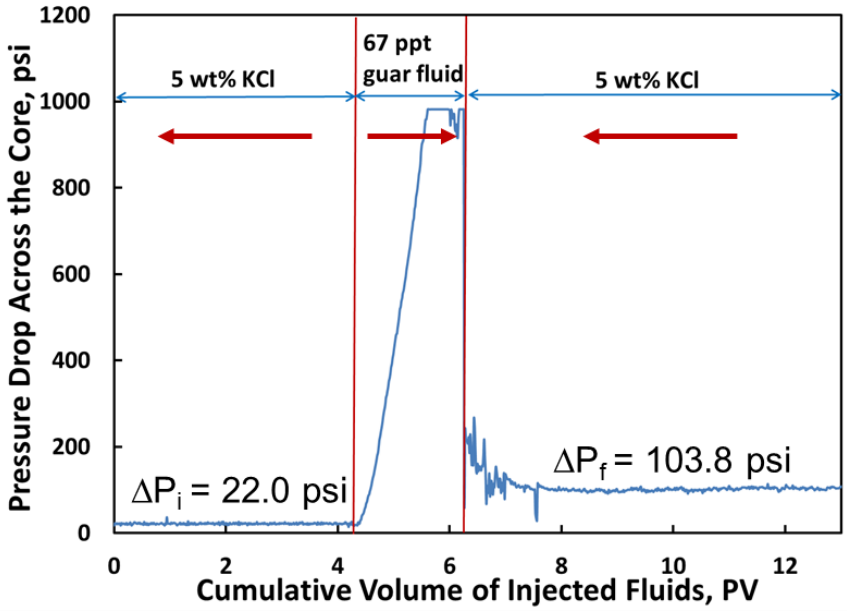

Fig. 58—Test 9: Pressure drop across the core with 67 lb/1000gal guar fluid and Berea core at 250°F.

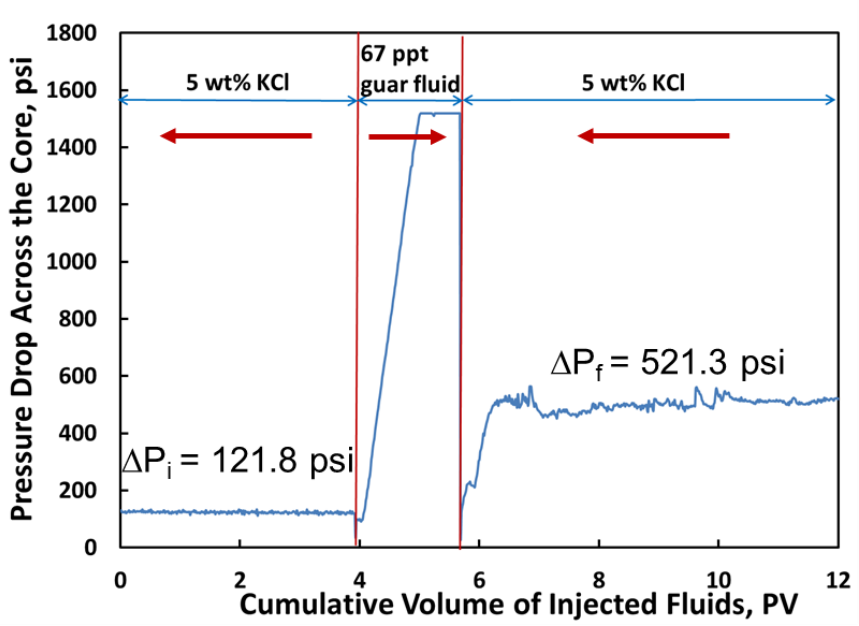

Fig. 59—Test 11: Pressure drop across the core with 67 lb/1000gal guar fluid and Bandera core at 250°F.

The formation type also affected the damage degree. In Tests 8 and 10, the core mineralogy and permeability were different. Berea core with the permeability of 65 md was used in Test 8, while Bandera core with 12.7 md in Test 10. Moreover, Bandera has more clay minerals than Berea. A higher regained permeability percentage was obtained in Test 8 (61%) than Test 10 (23%). Comparison of Tests 12 and 13 provided similar results that Test 12 with Berea core afforded a higher regained permeability percentage. These results have shown that the damage to Bandera was more severe than Berea under same conditions for both guar and HPG, which were completely different from ENZ-NFC-based fluid. For tests with guar or HPG fluids, no filter cake was formed, and the damaged was caused due to the fluid invasion and pore throat plugging. Therefore, the differences in permeability and mineralogy between Berea and Bandera have caused the different regained permeabilities of the cores.

The formation damage was similar when guar or HPG was used as the viscosifier. In Tests 8 and 12, polymer concentration, formation type, and temperature were same, and the only difference lied in the polymer type. Guar was used in Test 8 while HPG was added in Test 12. However, both tests resulted in similar regained permeability percentages (61% for Test 8 and 60% for Test 12). Tests 10 and 13 have shown the same results when Bandera cores were used (23% for Test 10 and 24% for Test 13). Therefore, guar and HPG caused similar damage under the same conditions, as seen in Tests 8 and 12, or Tests 10 and 13.

Table 9—Coreflood tests using VES fluids		
Coreflood No.	Test 14	Test 15
Core Type	Berea	Bandera
Porosity, vol%	18.1	20.2
Temperature, ºF	250	250
VES Concentration, gal/1000gal	40	40
Initial Permeability, md	81.5	15.9
Final Permeability, md	78.7	14.5
Percentage	97%	91%

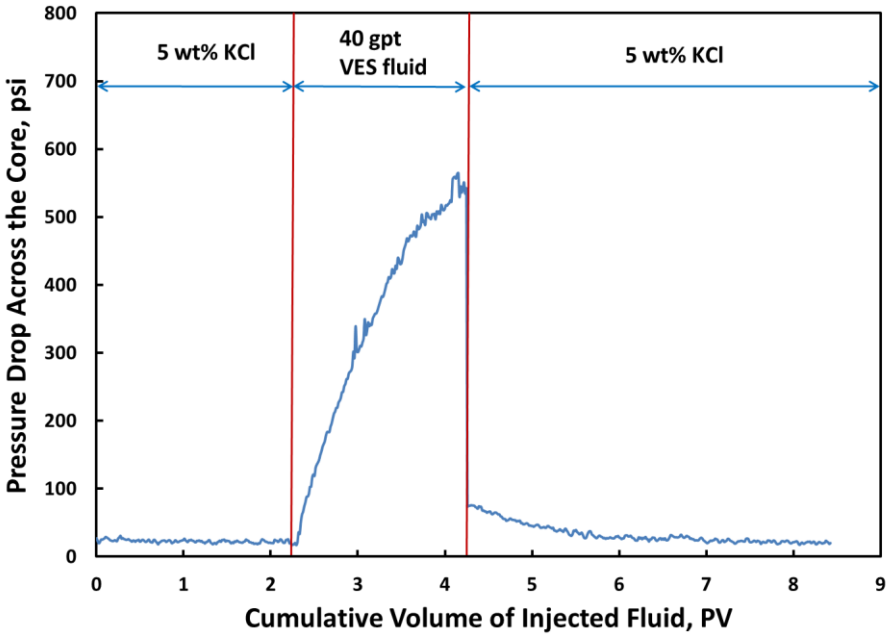

Fig. 60—Test 14: Pressure drop across the core with 40 gal/1000gal VES fluid and Berea core at 250ºF.

VES-based fluid was also studied, which showed similar results to the ENZ-NFC-based fluid in the degree of formation damage (**Table 9**). No filter cake was observed on the injection face of the cores. Therefore, the VES-based fluid used in this work is considered non-damaging under the tested conditions shown in **Table 9**. However, this may be due to the thermal degradation of VES, which led to a significant drop in the viscosity and thus an easy flush of the degraded molecules (Li et al. 2011). As shown in **Fig. 60**, the pressure drop decreased slowly when brine was injected after VES treatment, which suggested that the damaging chemicals was being flushed out by brine injection.

Another difference among the three types of fluids lied in that the external filter cake was formed when ENZ-NFC-based fluids were injected; however, no external filter cake was found for guar, HPG, or VES. As shown in **Fig. 61**, the lengths of many fibers are more than 50 μm, which is larger than the pore throats of the sandstone cores (Titov et al. 2010), leading to the formation of filter cake on the injection face of the core. However, when brine solution was pumped in the production direction in the coreflood tests, the filter cake was removed easily and did not cause damage. This was confirmed by the pressure drop across the core when brine was pumped after the injection of ENZ-NFC fluid in coreflood tests. The guar and HPG polymers could enter the core to block the pore throat, which have been studied by SEM and elemental analyses in others' work (Parker et al. 1994; Vitthal et al. 1996; DeVine et al. 1998). VES could also enter the core, but VES molecules would have been flushed out when the brine was injected to measure the regained permeability (Centurion et al. 2006).

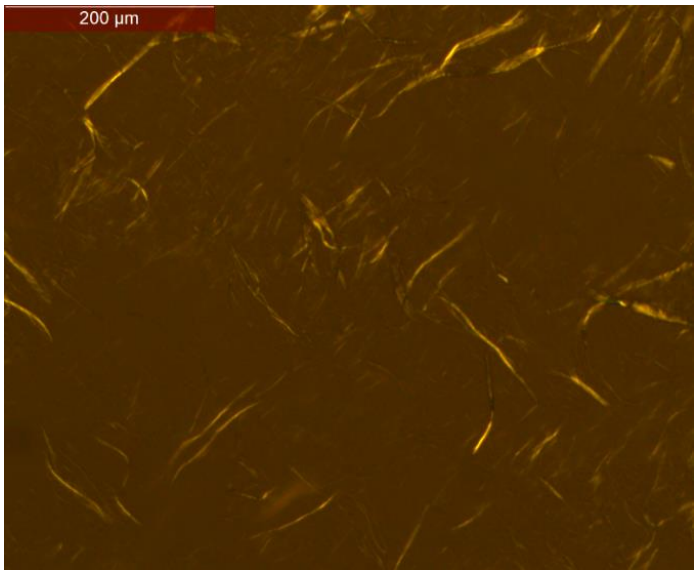

Fig. 61—The picture of ENZ-NFC fluid (67 lb/1000gal) under microscope.

4.3.2. Formation damage evaluation in high-permeability cores

When the permeability of the cores was lower than 150 md, ENZ-NFC fluid caused slight or no damage. The reason lies in that the ENZ-NFC fiber chain is much larger than the pore throat of the core. The filter cake was built up very quickly in the injection face of the core during the coreflood tests. In this part, three coreflood tests were performed using high-permeability cores: high-permeability Indiana limestone, and Boise sandstone (**Table 10**). Moreover, the concentration of ENZ-NFC was reduced to 8.3 lb/1000gal to prevent the quick buildup of filter cake in the injection face of the core in the coreflood test. In order to compare, guar-based fluid was used to run the same coreflood tests.

In Test 16, Indiana limestone was treated with 3 pore volume of ENZ-NFC fluid (8.3 lb/1000gal). The initial permeability was 348.4 md, much higher than Berea and Bandera cores. When ENZ-NFC fluid was being injected, the pressure drop increased

slowly at the beginning. However, at the end of ENZ-NFC fluid injection, the pressure drop increased in a much faster fashion, indicating the formation of filter cake (**Fig. 62**). The regained permeability percentage was 66%, which was lower than those in the coreflood tests using Berea and Bandera cores. This is probably because that the NFC fiber invaded into the core due to the increased pore throat of the core. But most of NFC fiber stayed on the injection face of the core to form filter cake (**Fig. 63**). However, in Test 18, when guar fluid was injected into Indiana limestone core, the final permeability was 85% of the initial permeability, which was higher than that of ENZ-NFC fluid. Guar polymer, which was much smaller than ENZ-NFC fiber, flew through the limestone core, and did not cause much damage. No external filter cake was found in Test 18.

In Test 17, when Boise sandstone core was treated with ENZ-NFC fluid, the final permeability was 88% of the initial value, indicating that ENZ-NFC fluid did not cause severe damage to Boise core. This is probably because Boise sandstone core has more homogeneous pore structure than limestone, and most fiber was blocked out and formed external filter cake. When guar fluid was used in Test 19, the percentage of final permeability and initial permeability was 71%, which was lower than that of ENZ-NFC fluid.

Table 10—Coreflood tests using ENZ-NFC and guar fluids in high-permeability cores				
Coreflood No.	Test 16	Test 17	Test 18	Test 19
Viscosifier	ENZ-NFC		Guar	
Core Type	Limestone	Boise sandstone	Limestone	Boise sandstone
Porosity, vol%	12.1	25.5	13.3	27.8
Temperature, ºF	75	75	75	75
ENZ-NFC Concentration, lb/1000gal	8.3	8.3	8.3	8.3
Initial Permeability, md	348.4	937	420	1024
Final Permeability, md	230.7	819	355	728
Percentage, %	66	88	85	71

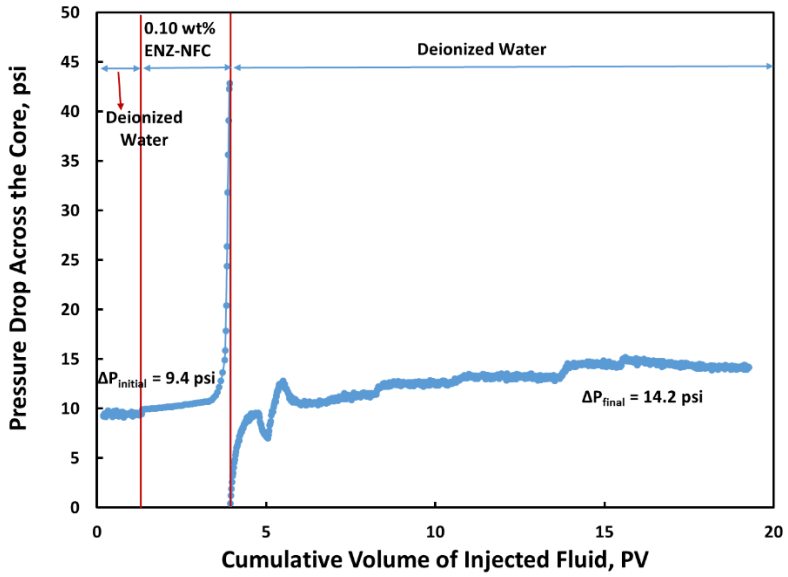

Fig. 62—Test 16: Pressure drop in using ENZ-NFC fluid (8.3 lb/1000gal) and Indiana limestone core at 75°F.

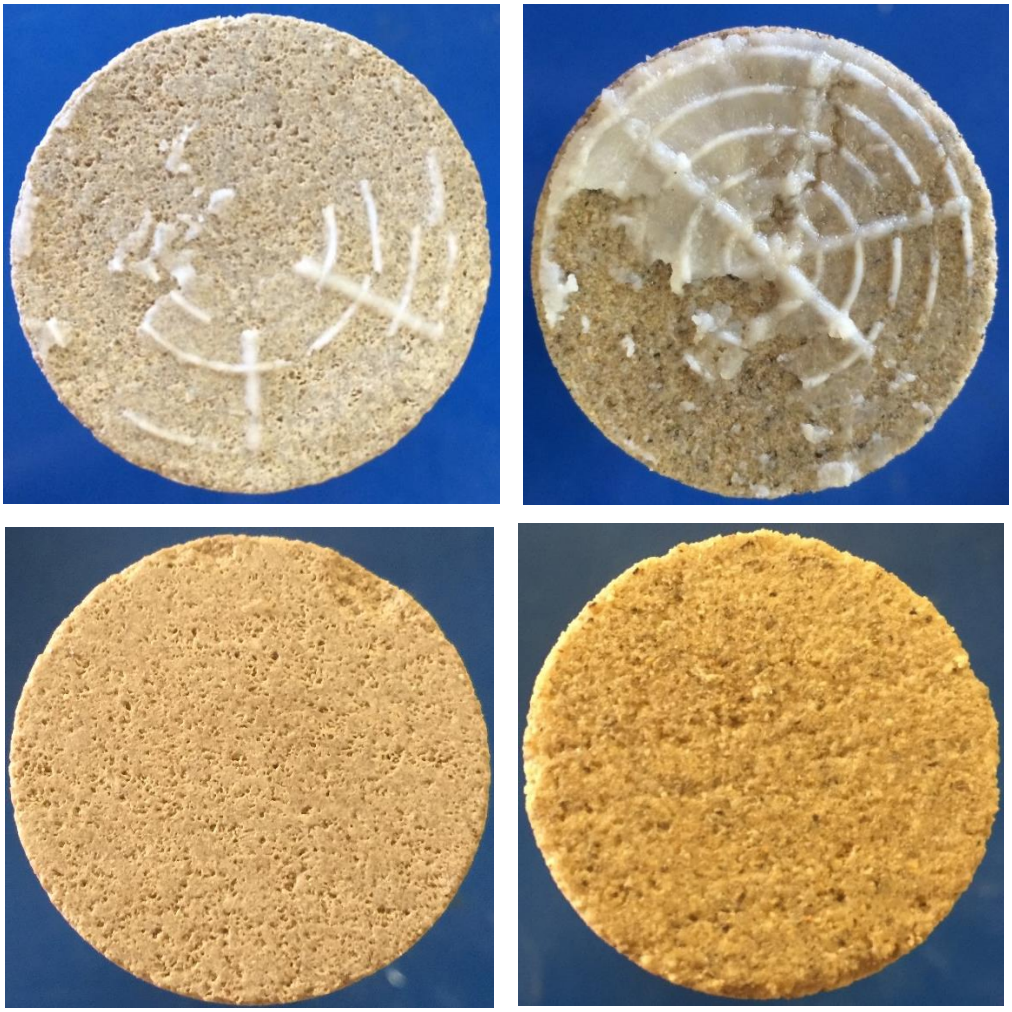

Fig. 63—The injection face of the core in Test 16 (top left), Test 17 (top right), Test 18 (bottom left), and Test 19 (bottom right).

4.4. Formation damage evaluation of different NFC-based fluids

4.4.1. Formation damage evaluation of ME-NFC fluid

Four coreflood tests were run using ME-NFC fluids (**Table 11**) in the same method as ENZ-NFC fluids. Berea and Bandera cores were used as low/moderate-permeability cores. The regained permeability percentage for all tests were 88% or higher, indicating that ME-NFC-based fluids was also non-damaging fluids to Berea and Bandera cores.

Table 11—Coreflood tests using ME-NFC fluids in low-permeability cores

Coreflood No.	Test 20	Test 21	Test 22	Test 23
Core Type	Berea	Berea	Bandera	Bandera
Porosity, vol%	18.2	18.9	20.2	20.7
Temperature, ºF	75	250	250	250
ME-NFC Concentration, lb/1000gal	40	67	40	67
Initial Permeability, md	61.3	75.8	20.1	17.1
Final Permeability, md	56.1	68.2	17.6	15.1
Percentage	92%	90%	88%	88%

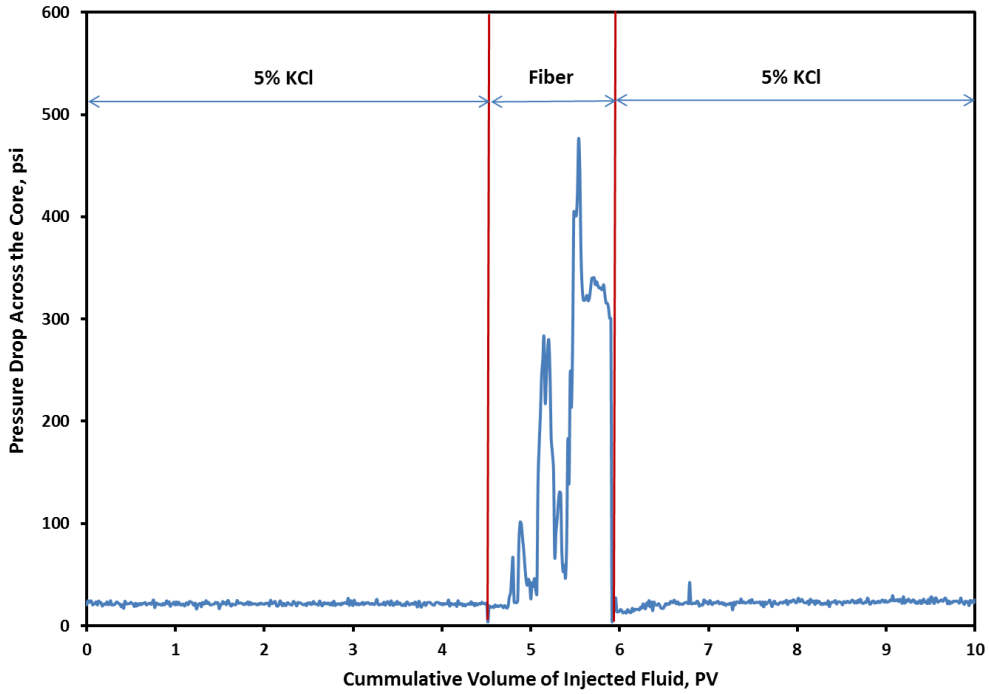

Fig. 64—Test 21: Pressure drop across the core with ME-MFC fluid (67 lb/1000gal) at 250ºF.

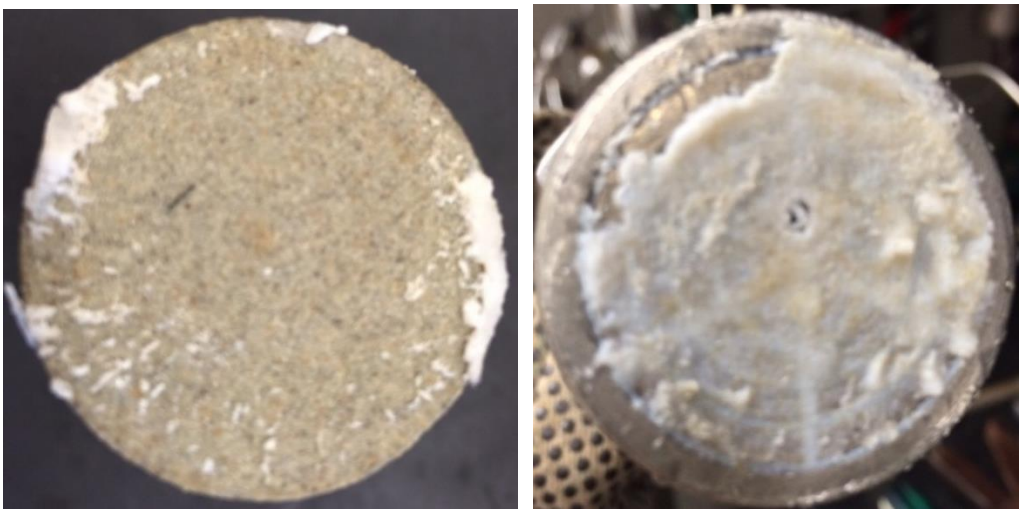

Fig. 65—Test 21: Injection face of the core after fiber injection (right) and the injection face of the injection tubing head (left, most of the filter cake was left on the injection tubing head).

In Test 21, only 1.4 pore volume of ME-NFC fluid was injected. Because the space between the injection tubing head and the core is very limited, the injection tube was blocked as the thickness of filter cake grew. Therefore, the flow rate was dropped down greatly and the pressure drop decreased significantly (**Fig. 64**). When the injection pressure of the pump reached the maximum pressure 2000 psi, the fluid injection stopped automatically.

Two coreflood tests were run at 250ºF using Bandera sandstone cores and ME-NFC fluid. In Test 22, two pore volume of fiber fluid was injected (**Fig. 66**). However, in Test 23, only 1.2 pore volume of fiber fluid was injected, because the formation of the filter cake blocked the further injection of the fluid (**Fig. 67**). In both tests, the regained permeability was 88% of the initial permeability. These tests showed that ME-NFC under different concentrations caused damage to the Bandera core, but the damage was not severe.

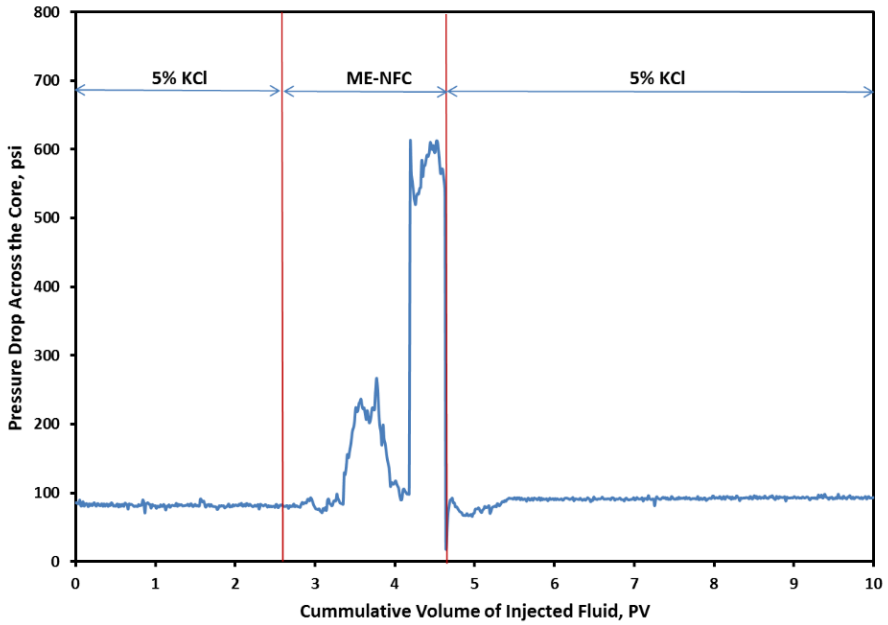

Fig. 66—Test 22: Pressure drop across the core with ME-MFC fluid (40 lb/1000gal) and Bandera core at 250ºF.

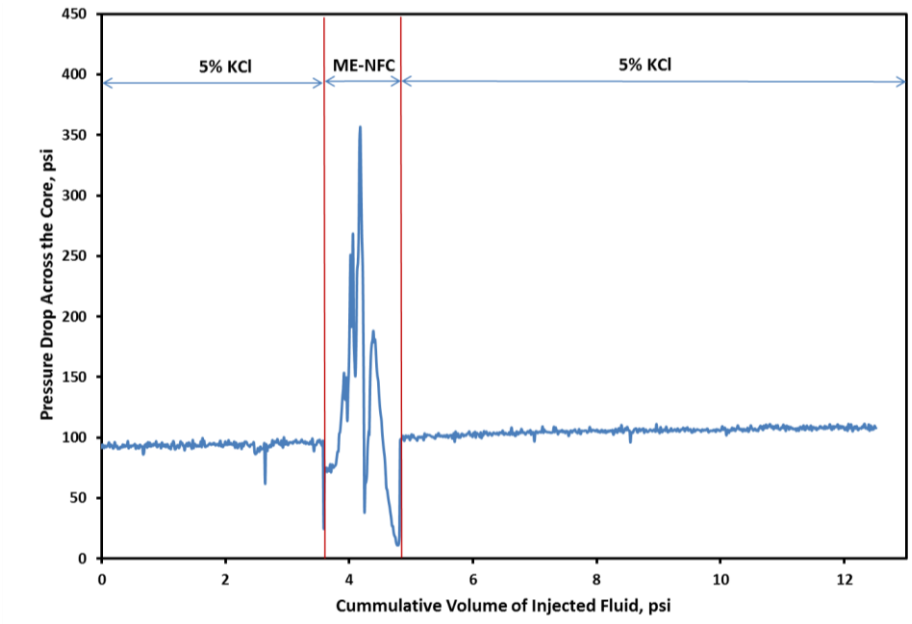

Fig. 67—Test 23: Pressure drop across the core with ME-MFC fluid (67 lb/1000gal) and Bandera core at 250ºF.

Test 20, Test 21, Test 22, and Test 23 have shown that ME-NFC fluid did not cause much damage to Berea and Bandera cores, which were similar to ENZ-NFC fluid under the same conditions. Berea and Bandera cores have relatively low/moderate permeability. In **Table 12**, high-permeability cores were tested to study if ME-NFC could cause damage in these formations. Two types of cores were used, Indiana limestone carbonate and Boise sandstone. The initial permeability was in a range of from 380 to 1100 md.

Table 12—Coreflood tests using ME-NFC fluids in high-permeability cores

Coreflood No.	Test 24	Test 25	Test 26
Core Type	Limestone	Limestone	Boise
Porosity, vol%	9.9	11.8	27.6
Temperature, ºF	75	75	75
ME-NFC Concentration, lb/1000gal	12.5	8.3	8.3
Initial Permeability, md	409	381	1040
Final Permeability, md	215	246	905
Percentage	53%	65%	87%

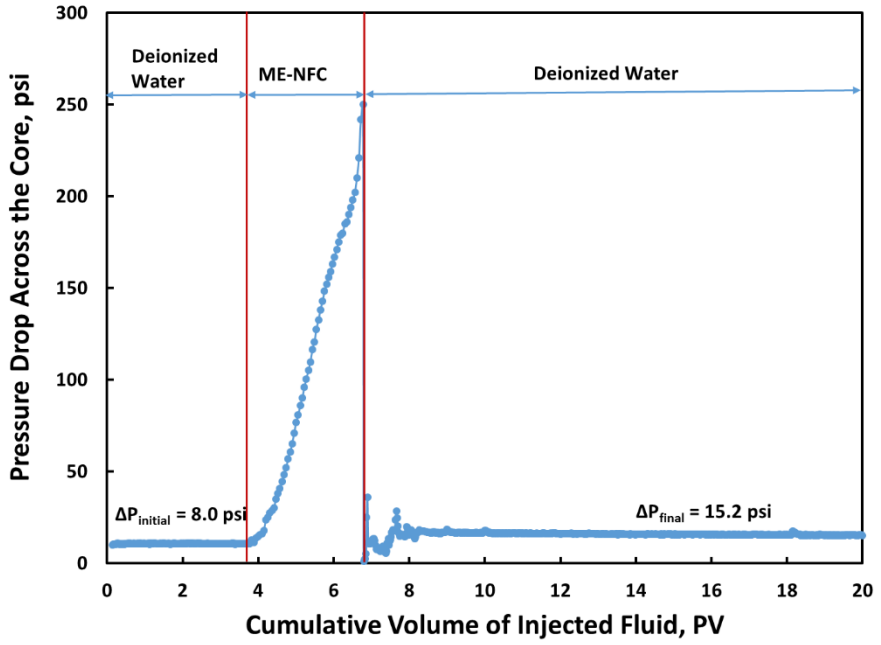

Fig. 68—Test 24: Pressure drop across the core using ME-NFC fluid (12.5 lb/1000gal) and limestone core.

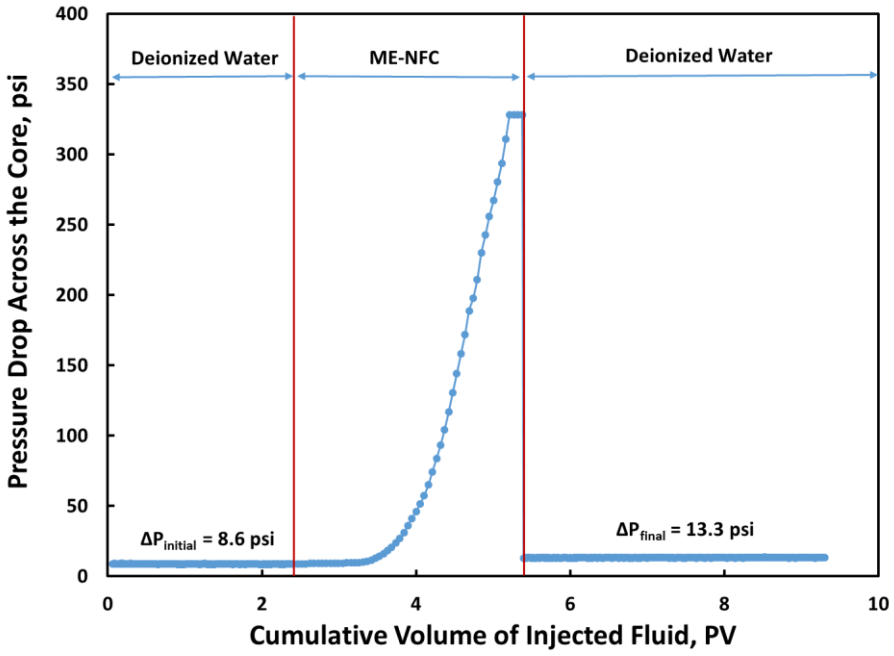

Fig. 69—Test 25: Pressure drop across the core using ME-NFC fluid (8.3 lb/1000gal) and Indiana limestone core.

In Test 24 and Test 25, Indiana limestone carbonate cores were used with the permeability of about 400 md. For both tests, the pressure drop increased significantly when ME-NFC fluid was injected (**Fig. 68** and **Fig. 69**). The final permeability was 53% of the initial permeability when 3 pore volume of ME-NFC (12.5 lb/1000gal) fluid was injected into the core, which indicated a severe damage existed. This was probably due to the invasion of the fibers into the core and the external filter cake on the injection face of the core. When the fiber concentration was reduced to 8.3 lb/1000gal, the final permeability was 63% of the initial value, which was a little higher than that in Test 24. Therefore, a reduction in the fiber concentration led to less damage under these conditions in Test 24 and Test 25. For both tests, fiber solid was observed on the injection face of the core (**Fig. 70**). This is because the fiber solid could not enter the core and therefore formed external filter cake on the injection face of the core.

Fig. 70—Injection face of the core after ME-NFC injection (left for Test 24 and right for Test 25).

High-permeability sandstone core, Boise, was also tested using ME-NFC fluid. In Test 26, Boise sandstone core with an initial permeability of 1040 md was treated with 3 pore volume ME-NFC (8.3 lb/1000gal) fluid at room temperature (**Fig. 71**). The pressure drop started to increase after 2 pore volume ME-NFC fluid was injected. The pressure drop built up very quickly to around 300 psi when the third pore volume fluid was injected. This was mainly resulted from the formation of external filter cake on the injection face of the core. The final permeability was 87% of the initial permeability. These results indicated that the damage of ME-NFC to Boise sandstone core was small. Most fiber solid was left on the injection face of the core. The fluid that came out after flowing through the core did not contain any fiber solid.

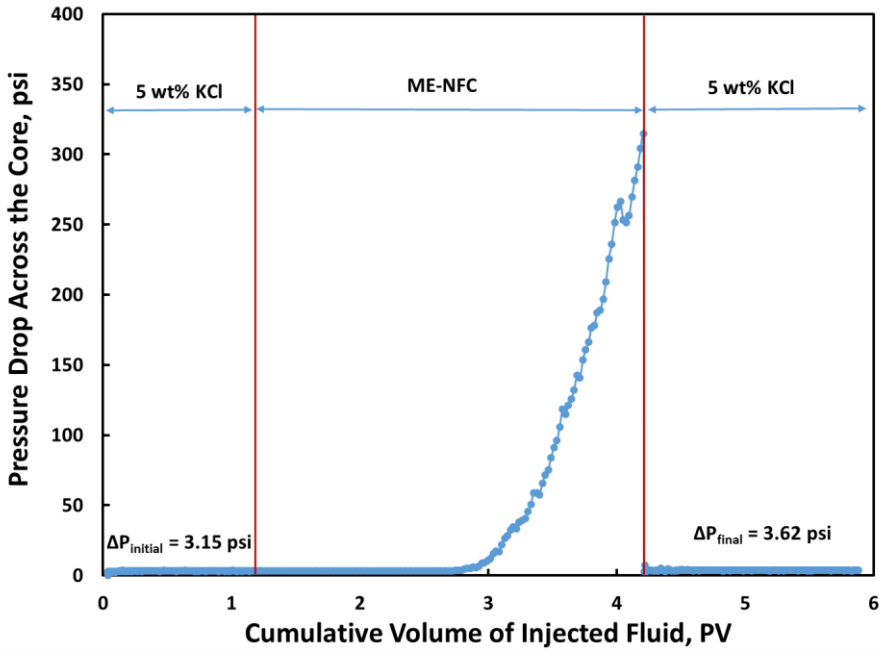

Fig. 71—Test 26: Pressure drop across the core using ME-NFC fluid (8.3 lb/1000gal) and Boise sandstone core.

4.4.2. Formation damage evaluation of KS-NFC and TEMPO-NFC fluids

Three tests have been performed to evaluate the formation damage of KS-NFC fluid (**Table 13**). Three types of cores were used, Berea sandstone, Indiana limestone, and Boise sandstone, which had different permeability and mineralogy. In Test 27, Berea core with an initial permeability of 47 md was used and 2 pore volume KS-NFC (40 lb/1000gal) fluid was injected into the core. The finial permeability, 41 md, was 87% of the initial value, suggesting that KS-NFC fluid did not cause much damage to Berea core under the tested conditions. As shown in **Fig. 72**, the pressure drop across the core increased significantly to about 1400 psi after 2 pore volume of KS-NFC fluid was injected. This is because the external filter cake was formed on the injection face of the core. However, the filter cake did not reduce the final permeability significantly when 5% KCl was injected in the production direction. The filter cake was removed by flowing KCl solution.

In Test 28, high-permeability Indiana limestone was treated with 3 pore volume KS-NFC (8.3 lb/1000gal) fluid (**Fig. 73**). The permeability dropped from 420 to 76 md after the treatment of KS-NFC fluid, which indicated that a very severe damage was caused by KS-NFC. KS-NFC is smaller than ENZ-NFC and ME-NFC in diameter and length. Therefore, more KS-NFC fibers could invade the core to block the pore throats and reduced the permeability. In Test 29, Boise sandstone core was used and the permeability decreased from 1100 to 398 md after injecting 3 pore volume of KS-NFC (8.3 lb/1000gal) fluid (**Fig. 74**). The damage was also severe. The pressure drop became flat at around 320 psi for both tests, because it reached the maximum reading of the transducer.

Table 13—Coreflood tests using KS-NFC fluids in different cores			
Coreflood No.	Test 27	Test 28	Test 29
Core Type	Berea	Limestone	Boise
Porosity, vol%	18.9	11.0	26.7
Temperature, ºF	75	75	75
KS-NFC Concentration, lb/1000gal	40	8.3	8.3
Initial Permeability, md	47	420	1110
Final Permeability, md	41	76	398
Percentage	87%	18%	36%

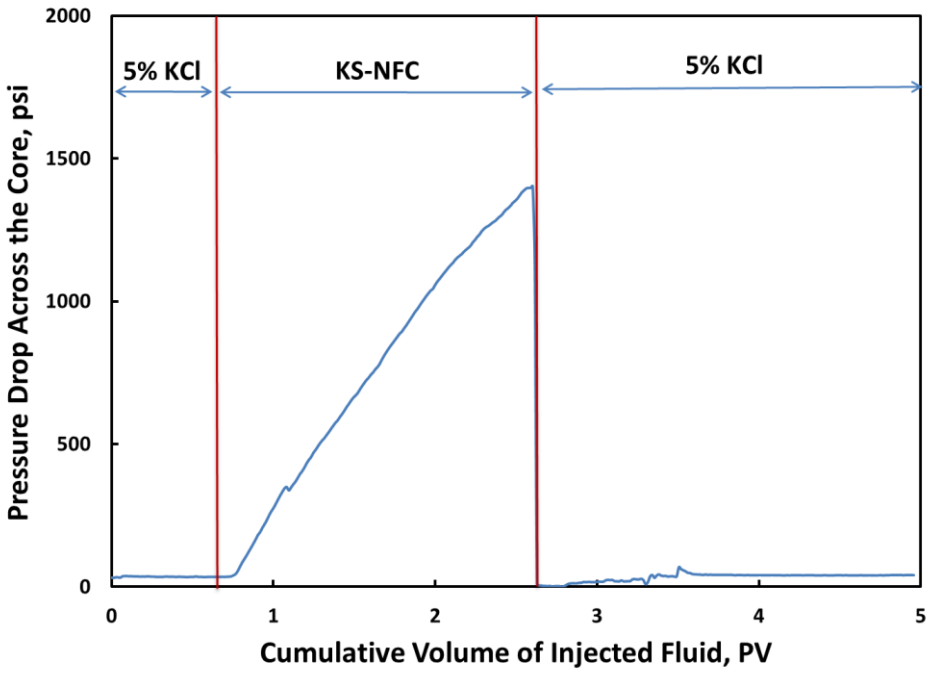

Fig. 72—Test 27: Pressure drop across the core using KS-NFC fluid (40 lb/1000gal) and Berea sandstone core.

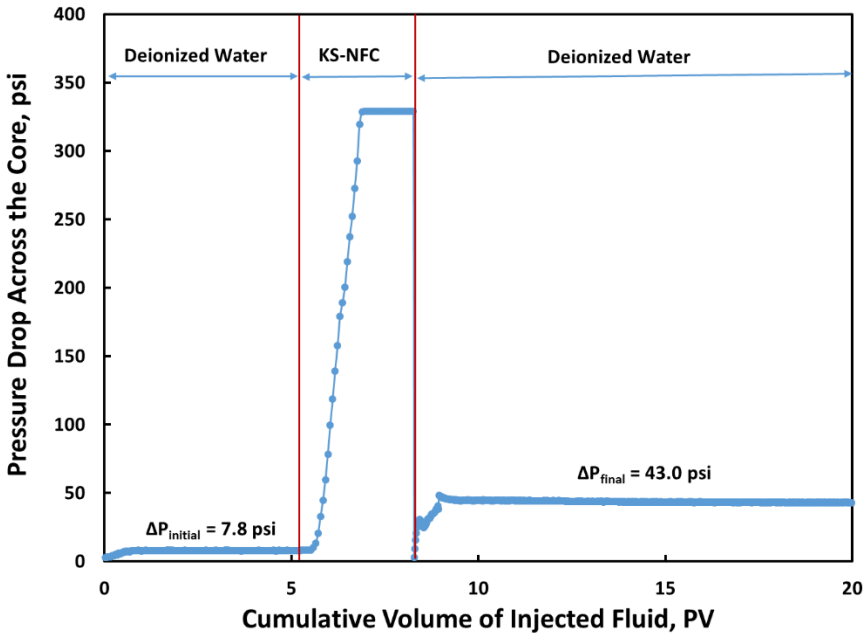

Fig. 73—Test 28: Pressure drop across the core using KS-NFC fluid (8.3 lb/1000gal) and Indiana limestone core.

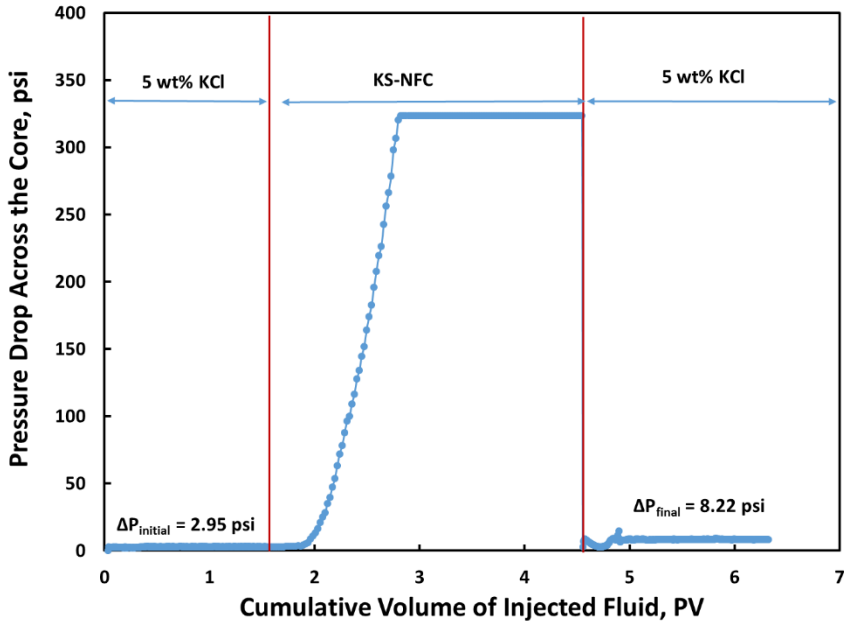

Fig. 74—Test 29: Pressure drop across the core using KS-NFC fluid (8.3 lb/1000gal) and Boise sandstone core.

Three coreflood tests were performed by using TEMPO-NFC fluids (**Table 14**). Two types of cores were used, Berea sandstone and Indiana limestone. When Berea sandstone core was used in Test 30, 2 pore volume TEMPO-NFC (40 lb/1000gal) fluid was injected (**Fig. 75**). The final permeability of the core was very close to the initial permeability. The results were similar to those using KS-NFC fluid in Test 27. When the fiber concentration was reduced to 8.3 lb/1000gal, there was still no damage as in Test 31 (**Fig. 76**). However, when high-permeability Indianan limestone was treated with 3 pore volume TEMPO-NFC fluid (8.3 lb/1000gal), the final permeability was reduced significantly, only 13% of the initial permeability (**Fig. 77**). These results have shown that a very severe damage was caused. This was similar to Test 28 with KS-NFC (8.3 lb/1000gal) fluid. In both tests using limestone cores, fibers could invade the core and blocked the pore throats. But when Berea cores were used, most fibers stayed on the injection face of the core and formed external filter cake. When 5% KCl was injected in the reverse direction, the external filter cake was removed and did not affect the final permeability.

Table 14—Coreflood tests using TEMPO-NFC fluids in different cores			
Coreflood No.	Test 30	Test 31	Test 32
Core Type	Berea	Berea	Limestone
Porosity, vol%	17.6	17.8	10.2
Temperature, ºF	75	250	75
TEMPO-NFC Concentration, lb/1000gal	40	8.3	8.3
Initial Permeability, md	90	49	376
Final Permeability, md	87	47	47
Percentage	97%	96%	13%

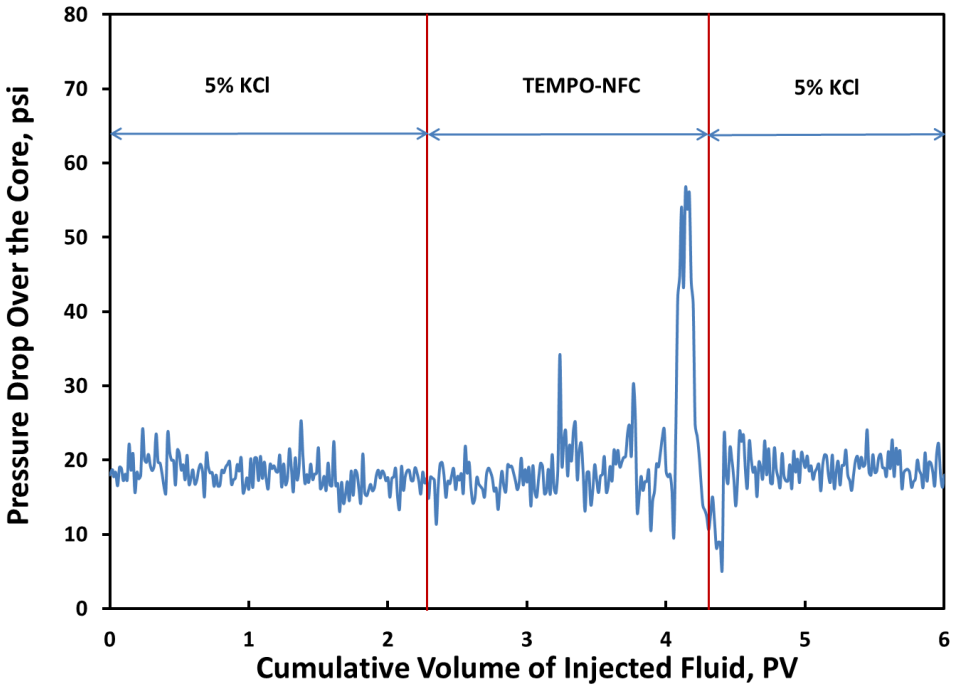

Fig. 75—Test 30: Pressure drop across the core using TEMPO-NFC fluid (40 lb/1000gal) and Berea sandstone core.

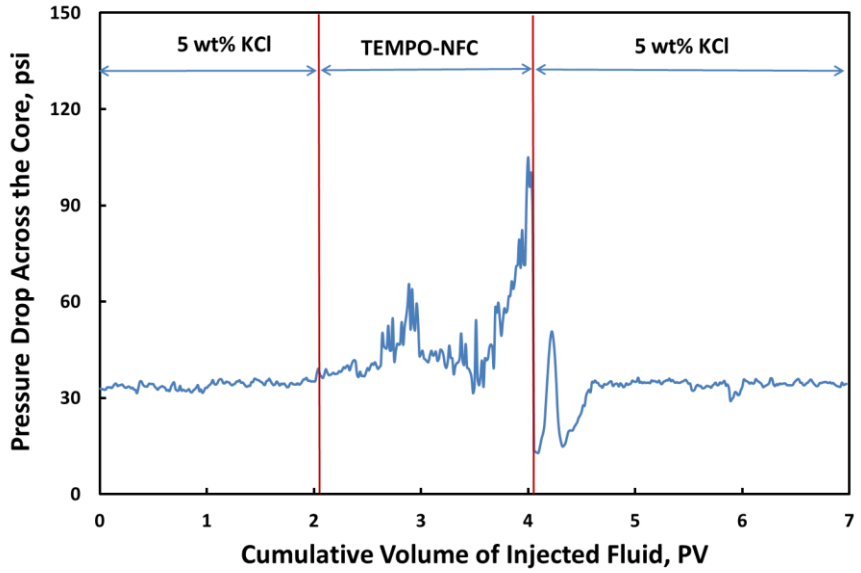

Fig. 76—Test 31: Pressure drop across the core using TEMPO-NFC fluid (8.3 lb/1000gal) and Berea sandstone core.

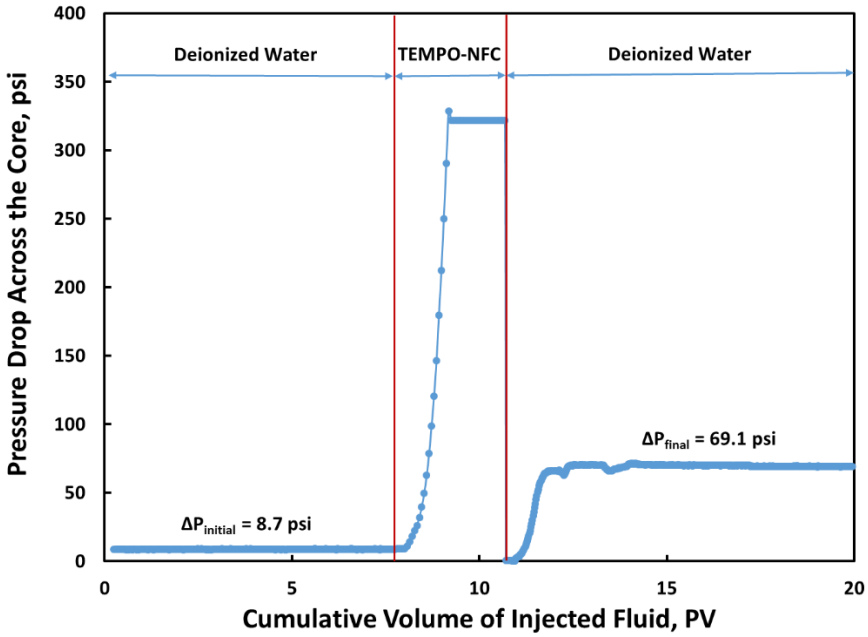

Fig. 77—Test 32: Pressure drop across the core using TEMPO-NFC fluid (8.3 lb/1000gal) and Indiana limestone core.

4.5. Conclusion

The formation damage of four types of nanofibrillated cellulose fibers have been evaluated using different types of cores. The fiber fluids were injected into the cores. The final permeability of the core, expressed as a percentage of the initial permeability, was used to quantify the damage caused by the fiber fluid treatment. Generally, when low/moderate-permeability sandstone cores (Bandera and Berea) were treated with the cellulose fiber fluids, the damage was very small. However, guar-based fluids caused severe damage under the same conditions.

When high-permeability cores (Indiana and Boise) were treated with the fiber fluids, the final permeability was reduced, especially for KS-NFC and TEMPO-NFC. KS-NFC and TEMPO-NFC fibers were smaller than ENZ-NFC and ME-NFC in fiber diameter and length. Therefore, KS-NFC and TEMPO-NFC fibers could invade the core more easily and blocked the pore throats.

Since severe damage may exist when the fiber fluids are used, it is necessary to remove the damage. Therefore, the degradation of fiber fluids will be investigated in the next section.

5. DEGRADATION STUDIES OF NFC-BASED FLUIDS

5.1. Introduction

Polymers can cause damage by blocking or reducing the flow path of reservoir fluids (DeVine et al., 1998). Therefore, polymers must be removed to avoid or minimize damage. Breakers are used to degrade polymers by cleaving the polymers into small fragments, and thus to remove the damage of polymers. In this section, different breakers, including acid, oxidative breakers, and enzyme breaker, have been used to degrade the fiber fluids. The successful degradation of fiber fluids can be indicated by the significant decrease of the fluid viscosity. The effects of breaker type, breaker concentration, break time, and temperature will be investigated. The degraded products will be analyzed by High Performance Liquid Chromatography (HPLC). Coreflood tests will be performed to show that the damage of fiber fluids can be removed efficiently.

5.2. Experimental methods

Viscosity measurements are the most common methods to evaluate the efficiency of breakers. A viscosity reduction of the polymer fluid is commonly considered to be an indicator of polymer degradation. Viscosity measurements have been conducted before and after degradation. Different breakers, including strong acids, oxidative breakers, and enzymes, were tested. The effects of breaker type, breaker concentration, and temperature were also studied.

5.2.1. Materials

Breaker (hemicellulose enzyme concentrate, 60-100%, GBW-26C) were obtained from Baker Hughes. This enzyme breaker can be used at temperatures up to 200ºF. Sodium persulfate, sodium bromate, and hydrochloric acid were purchased from Sigma Aldrich. All chemicals were used as received.

5.2.2. Degradation studies by viscosity measurement

A series of degradation reactions were run at different temperatures. The viscosity of the polymer fluids was measured after the reactions. If the viscosity decreases significantly, the new polymer can be degraded by the breaker under the tested conditions. Otherwise, the breaker cannot break the polymer. The effects of polymer concentration, breaker type, breaker concentration, and temperature have been studied. These studies have provided the optimum breakers and conditions for a complete degradation of the polymer.

5.2.2.1. Degradation reaction procedures

a. The polymer fluid mixed with one breaker was put into a Teflon liner of a steel-aging cell. A 300psi pressure was applied using nitrogen. Then the steel aging cell was put into an oven which was preheated to the target temperature.
b. The cell was kept closed for a period of time (8, 16, 24 or 48 h) in the oven.
c. Cell was taken out of the oven, and cooled down to room temperature. The pressure was released. The viscosity of the fluid inside was measured at room

temperature and atmospheric pressure and compared to that of the fluid before heating.

5.2.2.2. Viscosity measurement

A rotational rheometer, Grace M5600, was used to measure the apparent viscosity of polymer fluids at room temperature and atmospheric pressure. The viscosity was measured as a function of shear rate (from 0.1 to 935 s^{-1}). A B5 bob was used to measure viscosity in this work, which required a sample volume of 52 cm^3.

5.2.3. Analysis of degraded solution by HPLC

The degraded fluids were filtered, and the filtrate was analyzed by HPLC (Agilent 1100 series). Mobile phase is deionized water with a flow rate at 0.3 ml/min. The temperature of the column was set at 60ºC, and the temperature for Refractive Index Detector (RID) was 40ºC. The calibration curve of glucose was established and used to identify and quantify the concentration.

5.2.4. Residue after break (RAB) tests and analysis of solid residue by SEM

The fluids after degradation were filtered, and the solid was dried under vacuum overnight. The weight of the solid was recorded and compared.

Small pieces of solid residues were coated with gold using MSC-1000 Mini-Sputter Coater. Evex Mini Scanning Electron Microscope (SEM) was used to analyze the solid residues (**Fig. 78**).

Fig. 78—The setup of HPLC (top) and Evex Mini Scanning Electron Microscope (SEM) and energy-dispersive X-ray spectroscopy (EDS) (bottom).

5.2.5. Coreflood setup and procedures

a. Each fiber fluid was mixed with 0.2% enzyme, and added in the aging cell. The aging cell was pressurized with nitrogen at 300 psi and kept in the oven at 150ºF for 24 h. Then the fiber fluid was cooled down to room temperature. This degraded fluid was used to treat the core in the following step.

b. The core was dried at 250ºF for 4 hours and weighed to obtain its dry weight. Then the core was saturated with brine solution (5 wt% KCl in deionized water, for

sandstone cores) or deionized water (for carbonate cores) for 6 hours under vacuum and its wet weight was measured. The pore volume was calculated using these measurements and the density of the brine solution or water (density = 1.03 g/cm^3 at 70ºF for 5% wt KCl and 1.0 g/cm^3 for deionized water).

c. The coreflood setup was shown in **Fig. 54**. The core was placed inside the core holder. The brine (5 wt% KCl, for sandstone) or deionized water (carbonate) was pumped through the core in the production direction. If elevated temperature was required, the temperature was raised to the target value (250ºF) and kept constant in the whole process. The pressure drop across the core was monitored and recorded until it was stabilized. The initial permeability was calculated.

d. The treatment fiber fluid was pumped, in the injection direction (reversed to production direction), at the back pressure of 1100 psi. The pressure drop across the core was recorded.

e. The direction of flow was then reversed to the production direction and the brine (5 wt% KCl, for sandstone) or deionized water (for carbonate) was injected into the core until the pressure drop across the core was stabilized. The regained permeability after fluid treatment was calculated.

5.3. Degradation studies of ENZ-NFC fluids with different breakers

5.3.1. Degradation studies of ENZ-NFC fluids with enzyme

Ten degradation tests were run using ENZ-NFC and enzyme, GBW-26C. The effects of temperature, enzyme concentration, and presence of KCl were studied. A

concentration of 40 lb/1000gal for the viscosifier, ENZ-NFC, was used in all tests. Tests 1-7 were run at 200ºF, and Tests 8-10 were run at 150ºF (**Table 15**). Viscosity was measured after degradation and compared with the viscosity before degradation. Filtration was used to separate the solid and solution after degradation. HPLC was used to analyze the degraded products which were soluble in water. The solid residue was analyzed by SEM.

First of all, the stability of ENZ-NFC-based fluid at high temperature was tested before degradation studies. In Test 1, the fluid was kept at 200ºF for 24 hours. As shown in **Fig. 79**, the viscosity was very close to that of fluid before heating, indicating that ENZ-NFC-based fluid did not go through thermal degradation at 200ºF for 24 hours. When 5 wt% KCl was added in Test 2, the viscosity did not decrease after 24 hours at 200ºF, therefore, KCl did not affect the stability of ENZ-NFC-based fluid at 200ºF. These results have shown that ENZ-NFC-based fluid was very stable after heating at 200ºF for 24 hours, and the addition of salts would not affect the viscosity stability. This will be useful to the treatments when salts are present in the fluids.

Table 15—Degradation tests of ENZ-NFC-based fluids using enzyme

Test No.	Enzyme Concentration	Break Time, hrs	Temperature, ºF	KCl Concentration
1	0	24	200	0
2	0	24	200	5%
3	0.05%	24	200	0
4	0.2%	24	200	0
5	0.2%	24	200	5%
6	0.2%	48	200	0
7	0.5%	24	200	0
8	0.05%	24	150	0
9	0.2%	24	150	0
10	0.5%	24	150	0

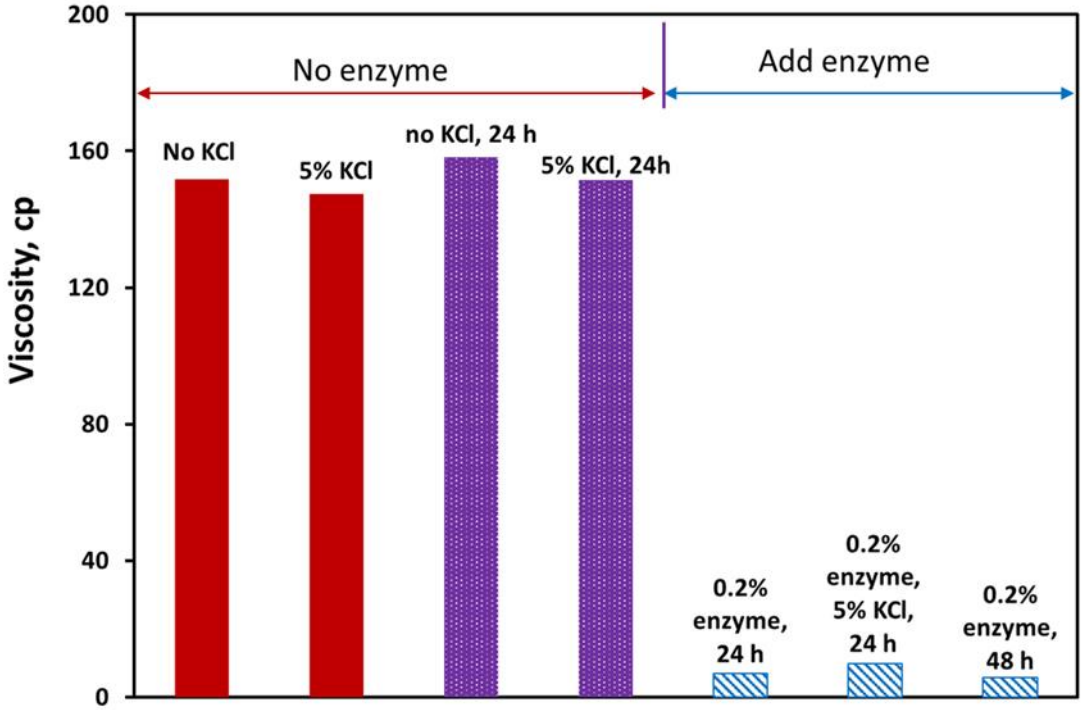

Fig. 79—The viscosity of ENZ-NFC (40 lb/1000gal) fluid at a shear rate of 10 s^{-1} in Tests 1, 2, 4, 5, and 6 at 200ºF.

In the following tests, the enzyme breaker, GBW-26C, was added to decrease the viscosity of ENZ-NFC fluid (40 lb/1000gal). ENZ-NFC-based fluid was degraded by this enzyme, indicated by the decrease of the fluid viscosity. In Test 4 and 5, 0.2 vol.% enzyme was added, and the fluid was kept at 200ºF for 24 hours (**Fig. 79**). The difference lied in that 5 wt% KCl was used in Test 5. The final viscosity of the fluids from Tests 4 and 5 decreased significantly after 24 hours compared to the fluid without enzyme in Test 1. The final viscosity in Test 4 was close to that in Test 5, indicating that the presence of KCl did not affect the activity of the enzyme. In Test 6, with the same concentration of enzyme (0.2 vol.%), a longer break time (48 hours) was tested. The viscosity was very close to the

viscosity in Test 4, which has shown that the extended time beyond 24 hours did not reduce the viscosity further.

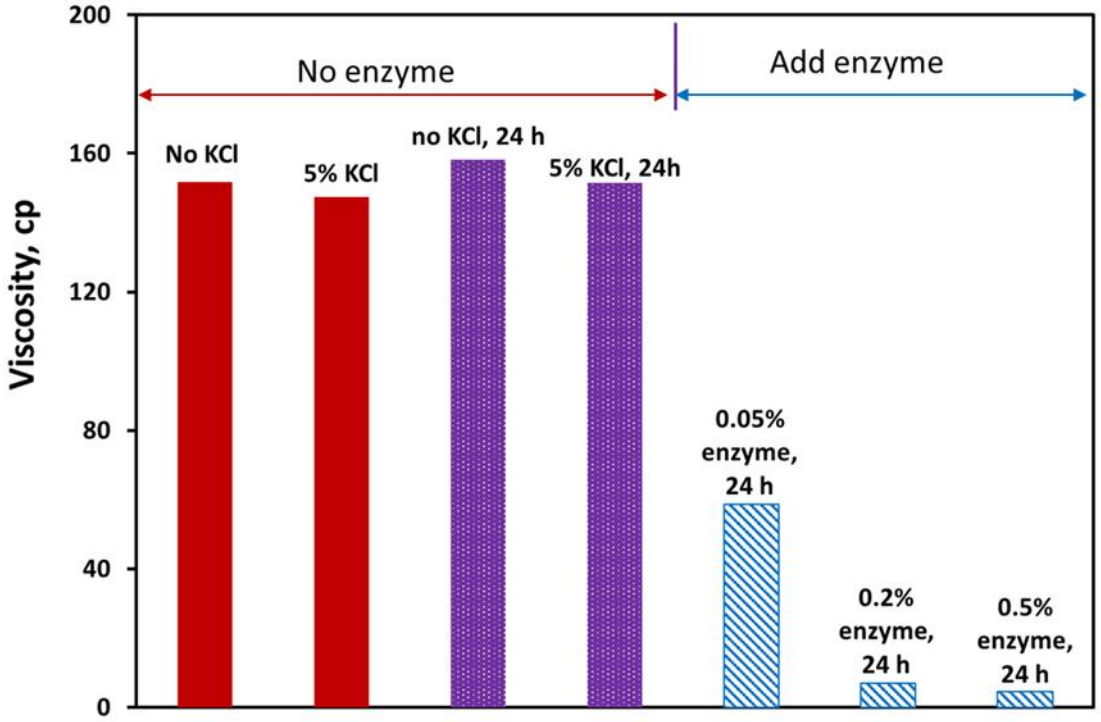

Fig. 80—The viscosity of ENZ-NFC (40 lb/1000gal) fluids at a shear rate of 10 s^{-1} in degradation tests 3, 4 and 7 with different enzyme concentrations at 200ºF.

The effect of enzyme concentration was studied when we compared Tests 3, 4, and 7, in which different concentrations of the enzyme breaker were used under same conditions. As shown in **Fig. 80**, when 0.05 vol.% enzyme was used, the viscosity was 59 cp at 10 s^{-1}, which was close to the initial viscosity. Therefore, 0.05 vol.% enzyme was not adequate to degrade ENZ-NFC-based fluid completely under the tested conditions. In contrast, 0.2 vol.% enzyme afforded the viscosity 6 cp at 10 s^{-1}. In test 7, a further higher

concentration of enzyme (0.5 vol.%) was used, but the final viscosity was close to that in test 4. There results have shown that 0.2 vol.% enzyme afforded a lower viscosity (6 cp) than 0.05 vol.% enzyme (59 cp), which has suggested that a more complete degradation was achieved by an enzyme concentration of 0.2 vol%. However, 0.5 vol.% enzyme at 200ºF did not improve the degradation compared to 0.2 vol.% enzyme.

The temperature also affected the degradation process. Comparing Tests 4 and 9, or Tests 7 and 10, temperatures were different (**Fig. 81**). The viscosity was around 10 cp at 10 s^{-1} for Tests 4 and 7 at 200ºF. However, the viscosity was close to 1 cp at 10 s^{-1} for Tests 9 and 10 at 150ºF. This is because the enzyme has a higher activity at 150ºF. At 200ºF, an increase enzyme concentration from 0.2 vol.% to 0.5 vol% did not decrease the viscosity. However, a decrease temperature from 200 to 150ºF with a same enzyme concentration (0.2 vol.% or 0.5% vol.%) reduced the viscosity from 10 cp to 1-2 cp at 10 s^{-1}. Therefore, the temperature has a significant effect on ENZ-NFC degradation. As shown in Test 10, the viscosity was very low (1 cp at 10 s^{-1}) after 24 hours at 150ºF when 0.5 vol.% enzyme was used, and the final fluid was water-like consistency. However, this enzyme only works up to 200ºF. Other enzymes that can work at very high temperatures may be tested in the future.

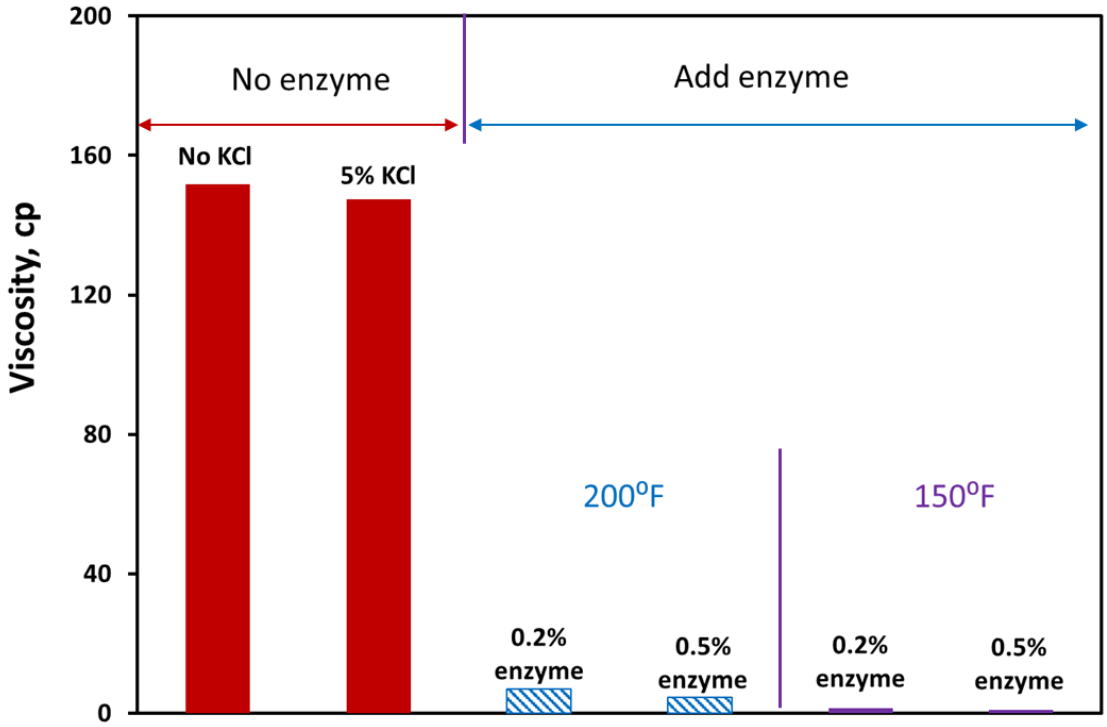

Fig. 81—The viscosity of ENZ-NFC (40 lb/1000gal) fluids at a shear rate of 10 s^{-1} in degradation tests at 200 or 150°F.

5.3.2. HPLC analyses of ENZ-NFC solutions after enzyme degradation

HPLC was used to analyze the soluble products of degradation reactions between ENZ-NFC and enzyme (**Fig. 82**). 100 ml of 0.48% ENZ-NFC-based fluid was used, therefore the theoretical total weight of ENZ-NFC was 0.48 g for all degradation tests. After degradation, the fluid was filtered for Tests 1, 3, 7, 8, and 10. The filtered solutions were analyzed by HPLC. The unit of the viscosifier ENZ-NFC was glucose, so HPLC was used to identify the concentration of glucose. The percentage of glucose in the total weight of ENZ-NFC (0.48 g) was calculated, which was to evaluate the degradation degree. As shown in **Fig. 82**, in Test 1 when enzyme was not added, the solution did not contain any

soluble saccharide molecules. For test 10 (0.5% enzyme, 24 h, 150ºF), glucose was identified, and the total weight was 0.374g, accounting for 78% of total viscosifier weight (0.48g). Soluble oligomers/polymers were also present in the solution. These analyses have shown that the insoluble ENZ-NFC can be mostly degraded into soluble products with low viscosity, which can be flowed back easily.

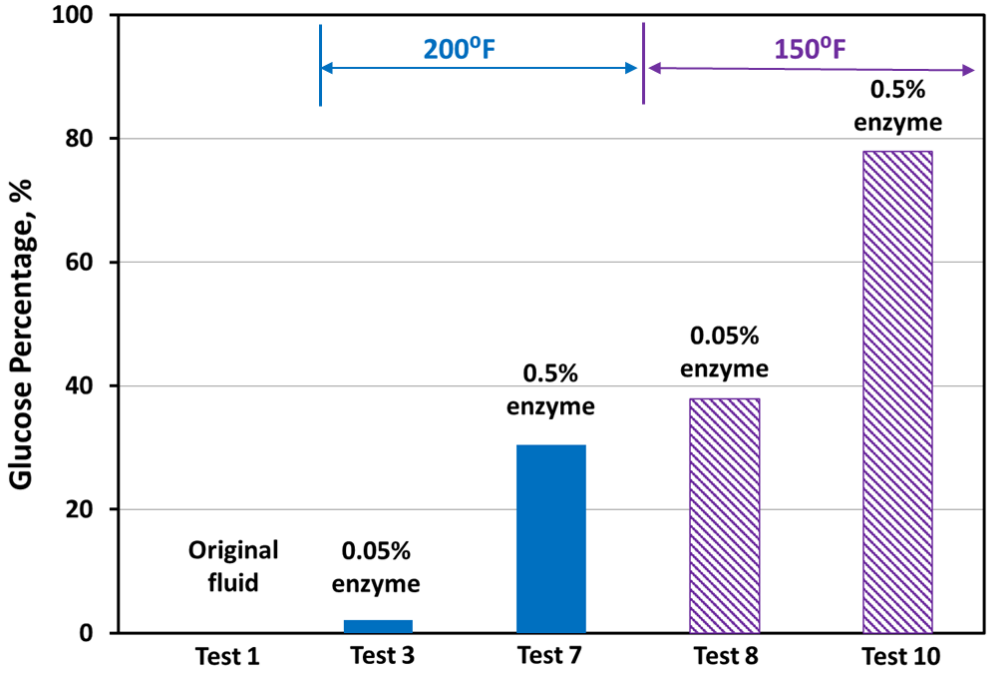

Fig. 82—The glucose percentage identified by HPLC in ENZ-NFC (40 lb/1000gal) fluids in degradation tests.

In test 3, the addition of 0.05% enzyme at 200ºF produced a small amount of glucose, only 0.01 g. However, in Test 8, same concentration of enzyme was used but at a different temperature of 150ºF. In this test, a total weight of 0.18 g glucose was produced, which accounted for 38% of total viscosifier weight. When Test 7 was compared to Test

10, same amount of enzyme was added in both tests, but different temperature were tested. Test 10 produced 0.37 g glucose while only 0.15 g glucose was obtained in Test 7. These results have confirmed that the temperature has a significant effect on the degradation reactions, which supported the results of viscosity measurements. For example, in Test 10, the viscosity was the lowest after degradation in all these tests. In corresponding to this result, the amount of glucose in Test 10 was the highest, which indicated a most complete degradation.

When different concentrations of enzyme was used at same temperatures, as shown in Test 3 and 7 at 200ºF, or Test 8 and 10 at 150ºF, the amounts of glucose were various. Larger amounts of glucose (0.01 g in Test 3 vs. 0.15 g in Test 7; 0.18 g in Test 8 vs. 0.37 g in Test 10) were obtained when a higher concentration of enzyme was used. These results were also consistent with the viscosity results of degraded fluids. At 200ºF, an increase of the enzyme concentration from 0.05 vol.% to 0.5 vol.% reduced the viscosity from 59 to 10 cp at 10 s^{-1}. In consistent to this result, the glucose amount increased from 0.01 to 0.15 g.

5.3.3. Residue after break (RAB) tests and SEM analysis of the solid residue

After degradation, the fluid was filtered for Tests 1, 3, 7, 8, and 10, and the solids were dried under vacuum and weighed (**Fig. 83**). SEM was used to analyze the solid from Tests 1, 8, and10. In Test 1, enzyme was not added, therefore, most of the viscosifier, ENZ-NFC (0.473 g) was recovered as solid, which also suggested that ENZ-NFC was not

thermal degradable at 200ºF. However, in Test 10, only 0.060 g insoluble solid was obtained, and most of ENZ-NFC was degraded into soluble products in solution.

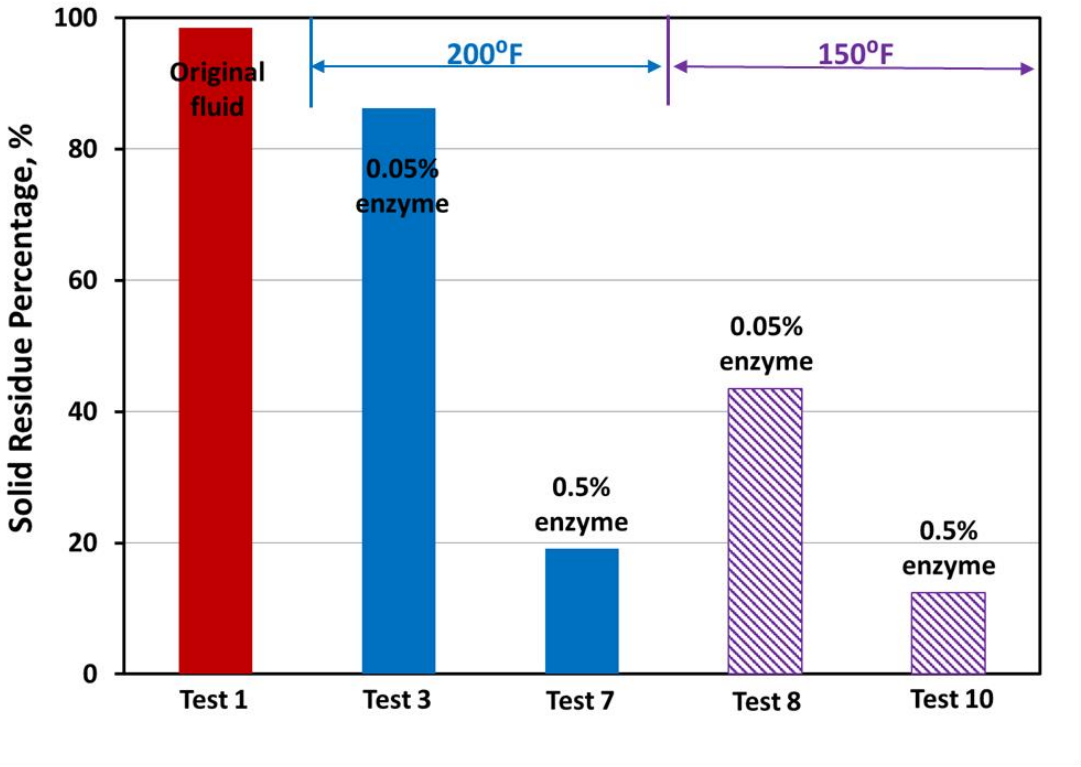

Fig. 83—The solid residue percentage from RAB tests for ENZ-NFC (40 lb/1000gal) fluids in degradation tests.

The effects of temperature and enzyme concentration were also confirmed by RAB tests. In Tests 3 and 8, same concentration of enzyme (0.05 vol.%) was used at different temperatures, 200 and 150ºF, respectively. 0.414 g insoluble solid was obtained in Test 3, indicating that most of ENZ-NFC was not degraded. This was consistent with the high viscosity of the fluid as well as the low concentration of glucose in the filtered solution by HPLC analysis. In test 8, a smaller amount of solid (0.209 g) was produced, because more

ENZ-NFC was degraded into soluble products at 150ºF. Comparison of Tests 7 with 10 has shown similar results that 0.06 g and 0.09 g solid residue was obtained at 150 and 200ºF, respectively.

At same temperature, an increase in the enzyme concentration afforded a more complete degradation, therefore, the amount of solid decreased, such as in Tests 3 and 7 at 200ºF, or in Tests 8 and 10 at 150ºF. 0.05 and 0.5 vol.% were used in Tests 3 and 7, respectively. Only 0.092 g solid was obtained in Test 7, while 0.414 g solid was from Test 3. These results were also supportive to the conclusions from the viscosity measurements as well as HPLC results.

In Test 7, a small amount of solid was obtained (19.1%), but the amount of glucose in filtered solution only accounted for 30.4% of the total weight of the viscosifier. The total weight of solid residue and glucose was about 49.5% of the weight of the original viscosifier. Other soluble products were present in the filtered solution, which may be di-, or tri-saccharide, or oligomers. However, we did not identify these products in this study. For other tests, major product after degradation was glucose and insoluble residue, with a total amount higher than 80% of the total viscosifier weight.

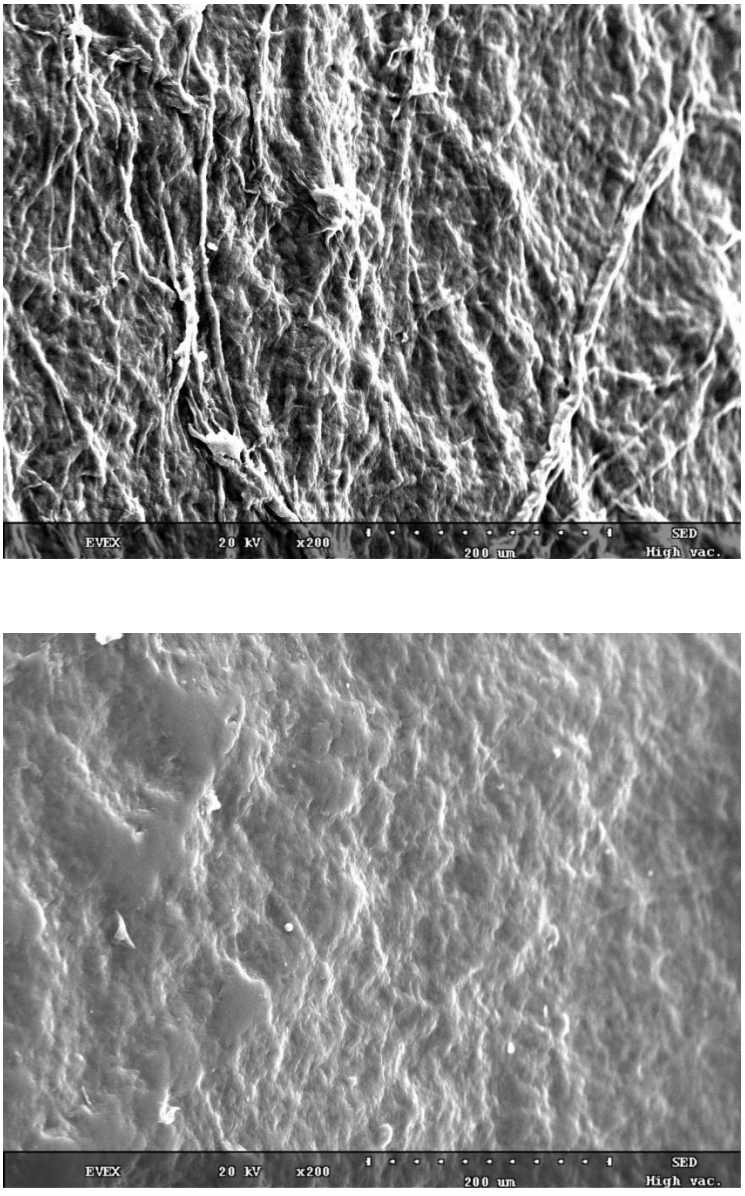

Fig. 84—The SEM of solid residue in Tests 1 (top) and 10 (bottom).

The solid residue samples were analyzed using SEM (**Fig. 84**). Without enzyme treatment, many long and thin filaments were present (Test 1). When the fluid was degraded by enzyme as in Test 10, the solid residue did not contain long thin filaments

shown in **Fig. 84**. These results indicated that the viscosifier was degraded successfully by enzyme.

5.3.4. Degradation studies of ENZ-NFC fluids with acid and oxidative breakers

The degradation of ENZ-MFC with acid at 200 and 250ºF has been studied using viscosity measurements. 5 wt% HCl was used as the breaker. At room temperature, the addition of 5 wt% HCl did not decrease the viscosity of ENZ-NFC fluid (40 lb/1000gal). In the following tests, extended break time and elevated temperatures were applied. In order to evaluate the break time, the fiber fluid, ENZ-MFC (40 lb/1000gal) in 5 wt% KCl mixed with 5 wt% HCl, was heated for 1, 2, 4, or 8 hours at 200ºF. The viscosity has been measured after the test time and compared to the original viscosity before heating (**Fig. 85**). The viscosity of the fluids with acid did not decrease significantly after heating for 1 hour, indicating that the fiber did not break completely. But a longer heating time can decrease the viscosity further. After 8 hours, the viscosity was quite low. At 250ºF, the addition of 5 wt% HCl provided a lower viscosity than that at 200ºF when both tests were kept for 2 h (**Fig. 86**). Therefore, higher temperature could help acid degrade the fiber more efficiently. However, HCl could not be used at very high temperatures since it is corrosive.

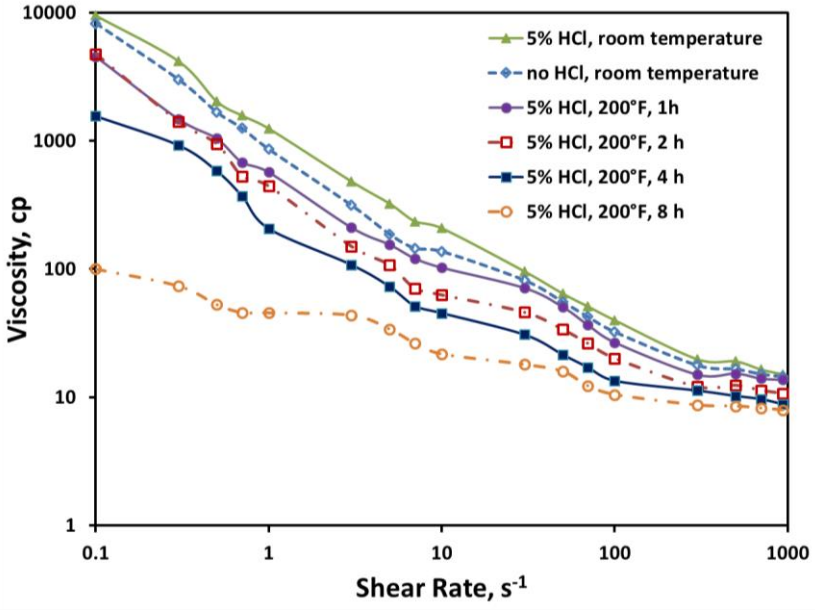

Fig. 85—The viscosity of ENZ-NFC fluids in the degradation tests with 5 wt% HCl at 200ºF.

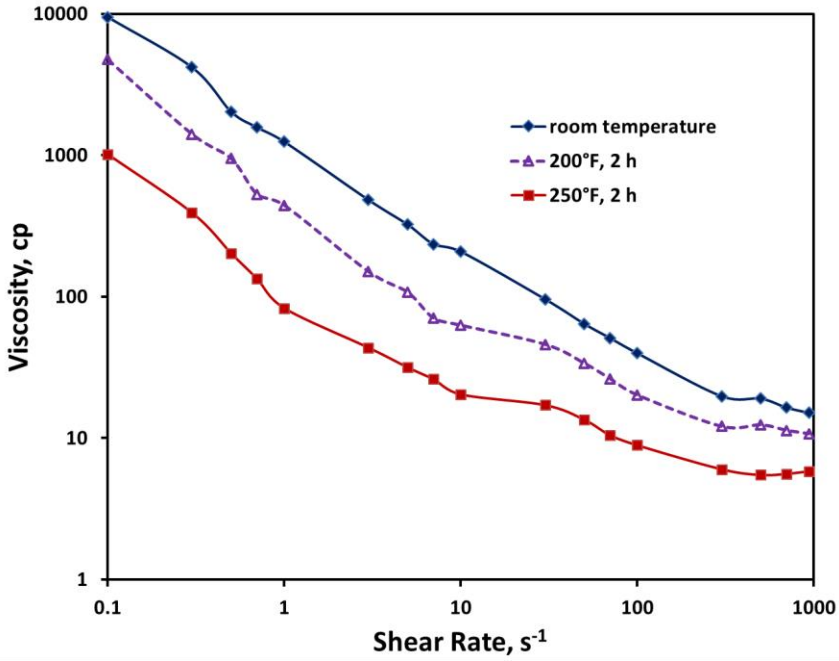

Fig. 86—The viscosity of ENZ-NFC fluids in the degradation tests with 5 wt% HCl at 200 and 250ºF for 2 h.

The fiber, ENZ-NFC, has been degraded successfully by two oxidative breakers, sodium persulfate and sodium bromate, at elevated temperatures. Two degradation tests were run using fiber, ENZ-NFC, and two oxidative breakers. All tests were run at 200ºF or 300ºF. Persulfate breaker was recommended to be used between 125 and 225ºF, and sodium bromate was more effective above 250ºF (Sarwar et al. 2011). Therefore, the test using ENZ-NFC fluid with sodium persulfate was run at 200ºF, and the test using sodium bromate was at 300ºF. The fluids in both tests were heated for 24 hours. Viscosity was measured after degradation and compared with the viscosity before degradation. As shown in **Fig. 87**, the viscosity was reduced significantly for the test with persulfate. The solid residue was 20.3% of the total fiber weight added in the original fluid. 79.7% of fibers were degraded and dissolved in the aqueous phase. Similar results were obtained when sodium bromate was used to break ENZ-NFC fluid at 300ºF. But the viscosity was even lower than that of the test using persulfate. The solid residue after break was 15.4% of the total fiber weight, which was also lower than that with persulfate. These results have shown that ENZ-NFC fiber fluid were degraded with the two oxidative breakers. However, the amounts of the solid residue after break were relatively high compared to the tests with enzyme breaker.

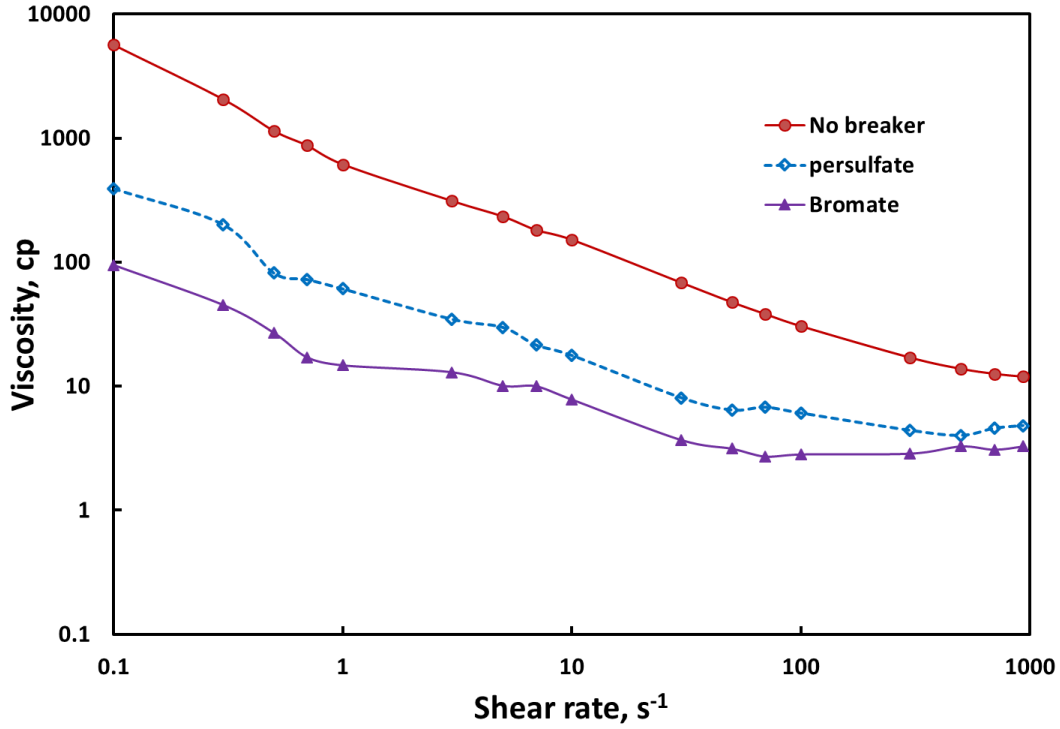

Fig. 87—The viscosity of ENZ-NFC fluids in the degradation tests with sodium persulfate at 200ºF and sodium bromate at 300ºF.

5.4. Degradation studies of other NFC fluids

5.4.1. Degradation studies of ME-NFC fluid

The fiber, ME-NFC, has been degraded successfully by two oxidative breakers, sodium persulfate and sodium bromate, at elevated temperatures. Nine degradation tests were run with the fiber fluid, ME-NFC, and two oxidative breakers. All tests were run at 200ºF or 300ºF. Persulfate breaker was recommended to be used between 125 and 225ºF, and sodium bromate was more effective above 250ºF (Sarwar et al. 2011). Viscosity was measured after degradation and compared with the viscosity before degradation. The effect of break time was investigated.

Five tests using persulfate to break ME-NFC fluid (40 lb/1000gal) were run at 200ºF (**Table 16**). In Test 1, when 0.5% sodium persulfate was used for 24 h, the viscosity decreased significantly. Addition of 1% sodium persulfate provided a more reduced viscosity profile, especially at low shear rates. When 1% sodium persulfate was used, four tests were performed to evaluate the effect of break time. After 8 h, the viscosity was still relatively high. But after heating for 16 h, the viscosity was quite low. Extended time beyond 18 h did not reduce the viscosity further significantly.

Table 16—Degradation tests of ME-NFC-based fluids using persulfate

	Test 1	Test 2	Test 3	Test 4	Test 5
Temperature, ºF	200	200	200	200	200
Breaker Concentration, wt%	0.5	1	1	1	1
Break Time, h	24	8	16	24	48

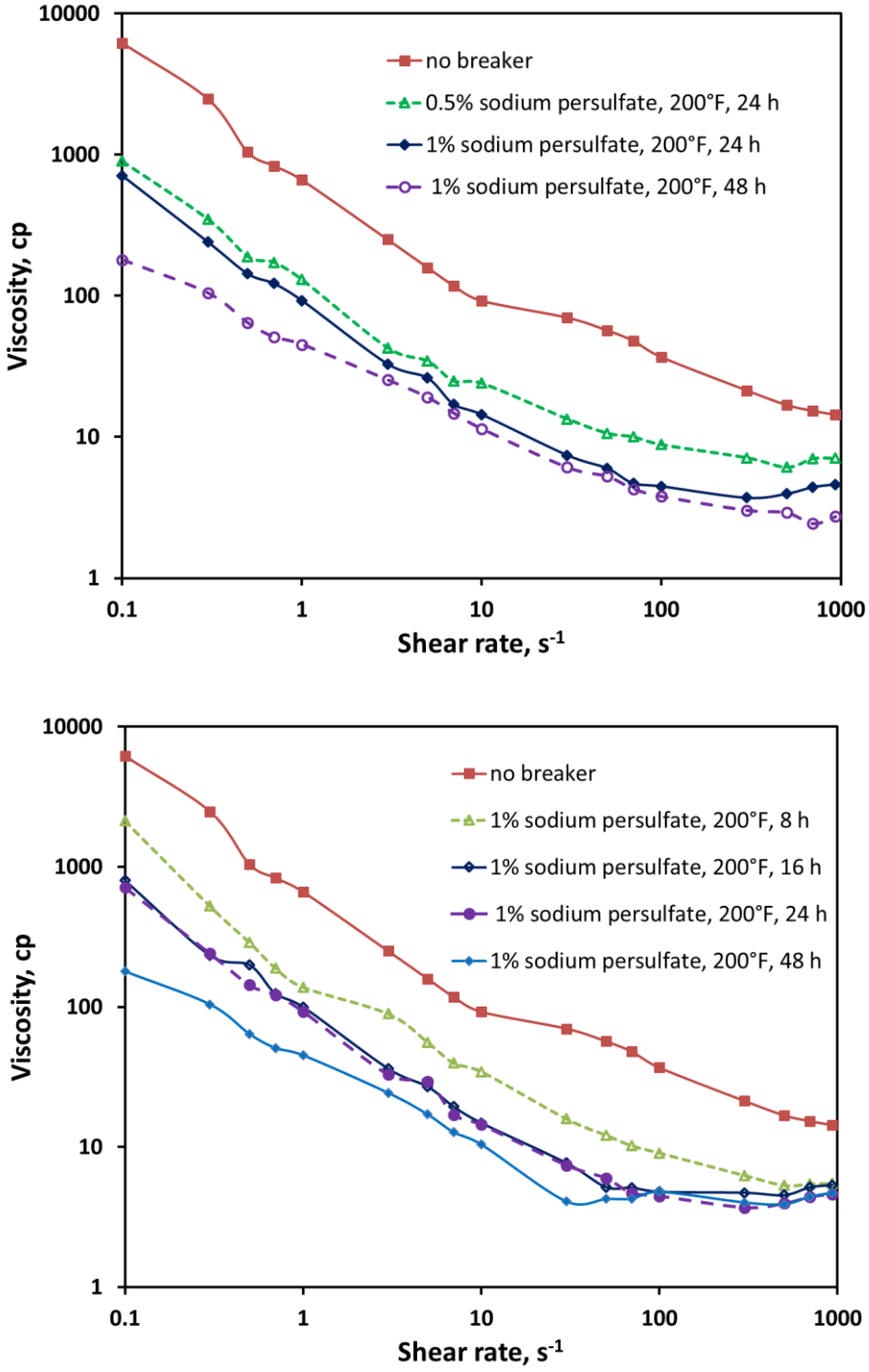

Fig. 88—The viscosity of ME-NFC fluids in the degradation tests with sodium persulfate at 200°F.

Sodium bromate was also used to break ME-NFC fluid (40 lb/1000gal) (**Table 17**). When no sodium bromate was added in Test 7, ME-NFC fluid was heated at 300ºF for 24 h. The viscosity decreased to some degree, but was still very high. This indicated that ME-NFC has a good stability at high temperatures, and the viscosity decrease in other tests was due to the break not the temperature effect. In Test 6, when 0.5% sodium bromate was mixed with the fiber at 200ºF for 24 h, the viscosity was still high, similar to the result of Test 7. This result indicated that this bromate breaker was less effective than sodium persulfate at 200ºF. When 1% bromate was used at 300ºF for 24 h in Test 10, the viscosity was reduced to low values (**Fig. 89**). Then the effect of break time was examined. After 8 h in Test 8, the viscosity was high. However, after 16 h, the viscosity decreased to very low values, suggesting that the fiber were successfully degraded under such conditions. Extended heating time beyond 16 h did not help reducing the viscosity further.

Table 17—Degradation tests of ME-NFC-based fluids using bromate

	Test 6	Test 7	Test 8	Test 9	Test 10
Temperature, ºF	200	300	300	300	300
Breaker Concentration, wt%	0.5	0	1	1	1
Break Time, h	24	24	8	16	24

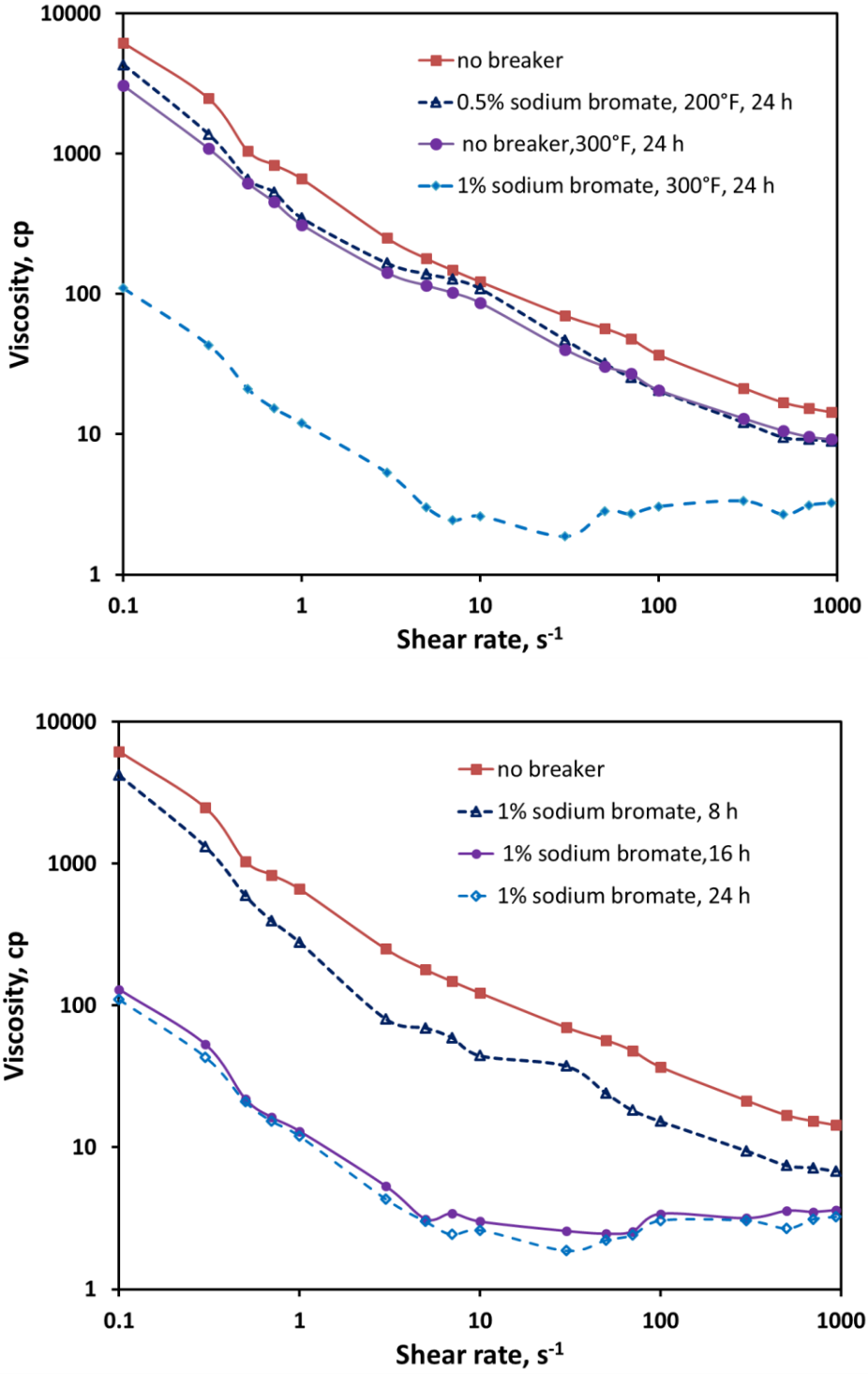

Fig. 89—The viscosity of ME-NFC fluids in the degradation tests with sodium bromate at 200 and 300°F.

ME-NFC fluid can also be degraded by enzyme, GBW-26C. Six tests were performed for ME-NFC fluid (40 lb/1000gal) at 150 and 200ºF (**Table 18**). The effects of breaker concentration and temperature have been examined. Three tests were run at 200ºF with different concentration of enzyme (**Fig. 90**). When ME-NFC fluid was heated for 24 h at 200ºF without the presence of enzyme, the viscosity after heating was very close to that of ME-NFC fluid before heating. This test has shown that the fiber fluid was very stable if no breaker was added at 200ºF. When 0.05% enzyme was added in Test 2, the viscosity decreased. Increasing the enzyme concentration to 0.5% reduced the viscosity significantly, indicating a more complete degradation.

Three tests were performed at 150ºF with ME-NFC fluid and different concentrations of enzyme (**Fig. 91**). When ME-NFC fluid and 0.05% enzyme were heated for 24 h at 150ºF, the viscosity decreased. In Test 5, 0.2% enzyme was used under the same conditions, the viscosity was reduced further to very low value. In Test 6, 0.5% enzyme provided similar viscosity to Test 5. Therefore, 0.2% enzyme was good enough to degrade ME-NFC fluid at 150ºF for 24 h.

As for the temperature effect, when 0.05% enzyme was added in Tests 2 and 4, the viscosity was lower at 150 than 200ºF (**Fig. 92**). This is because that enzyme has a higher activity at 150 than 200ºF. These results are very similar to those of tests with ENZ-NFC fluid, where the enzyme degraded ENZ-NFC more complete at 150 than 200F with the same enzyme concentration.

Table 18—Degradation tests of ME-NFC-based fluids using enzyme			
Test No.	Enzyme Concentration	Break Time, h	Temperature, °F
1	0	24	200
2	0.05%	24	200
3	0.5%	24	200
4	0.05%	24	150
5	0.2%	24	150
6	0.5%	24	150

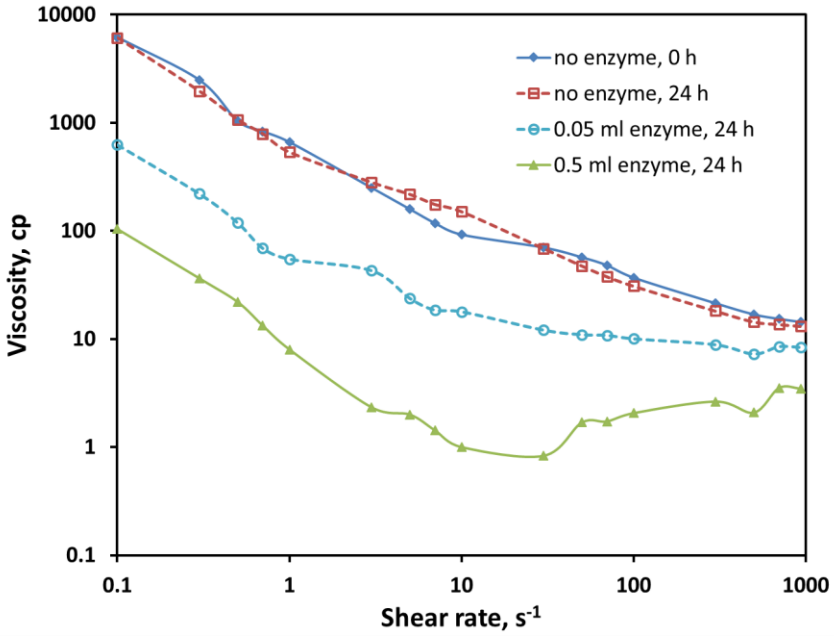

Fig. 90—The viscosity of ME-NFC fluids in the degradation tests with enzyme at 200°F.

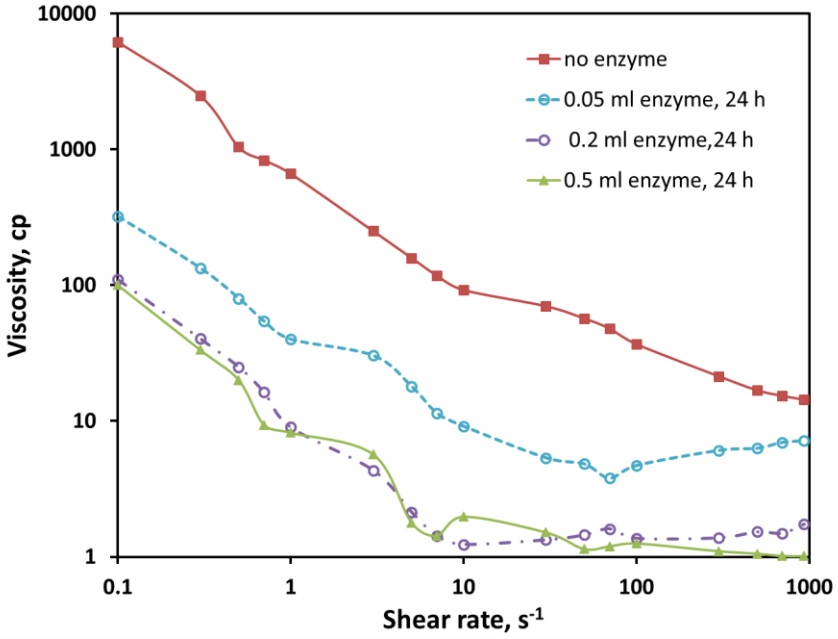

Fig. 91—The viscosity of ME-NFC fluids in the degradation tests with enzyme at 150ºF.

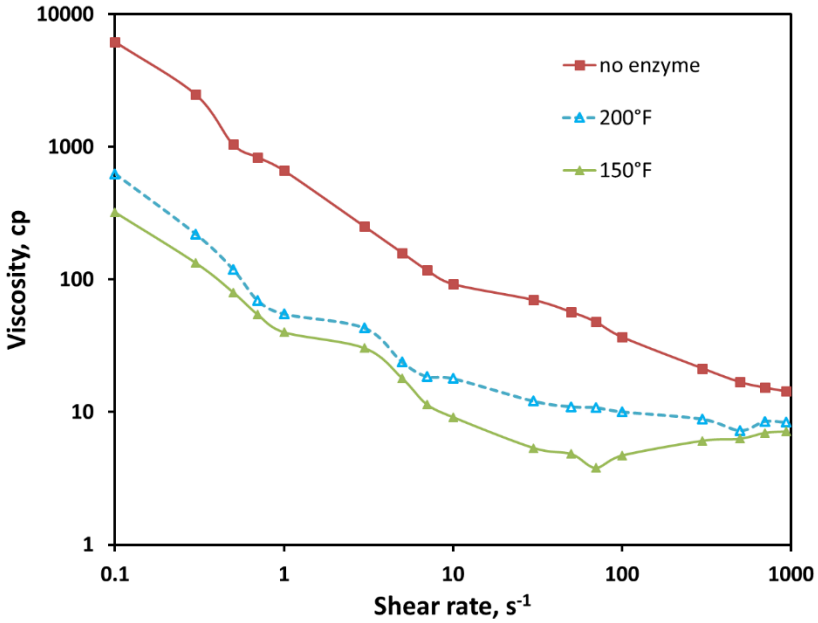

Fig. 92—The viscosity of ME-NFC fluids in the degradation tests with enzyme (0.05%) at 150 and 200ºF.

5.4.2. Degradation studies of KS-NFC and TEMPO-NFC fluids

Similarly, KS-NFC and TEMPO-NFC can also be degraded by oxidative breakers and enzymes. Three tests were performed with KS-NFC and different breakers (**Fig. 93**). One breaker, sodium persulfate (1 wt%), sodium bromate (1 wt%), or enzyme (0.5 vol.%), was used in each test. All tests were run for 24 h with different temperatures, since each breaker has a specific temperature preference. Viscosity was measured after degradation, and compared to the original viscosity of KS-NFC (40 lb/1000gal). The results have shown that the viscosity was reduced significantly for all three tests. However, the viscosity of the fluid using bromate and enzyme was lower than that with persulfate.

Three tests were also run with TEMPO-NFC fluid (40 lb/1000gal) under the same conditions (**Fig. 94**). The results have shown that all three breakers can degrade TEMPO-NFC fluid in similar ways as KS-NFC fluids.

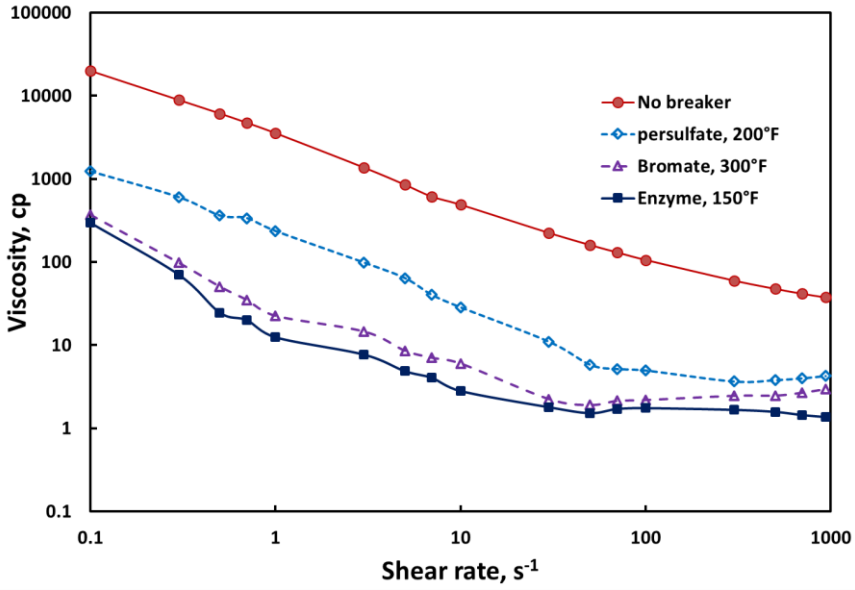

Fig. 93—The viscosity of KS-NFC fluids in the degradation tests with different breakers at 150, 200 and 300ºF.

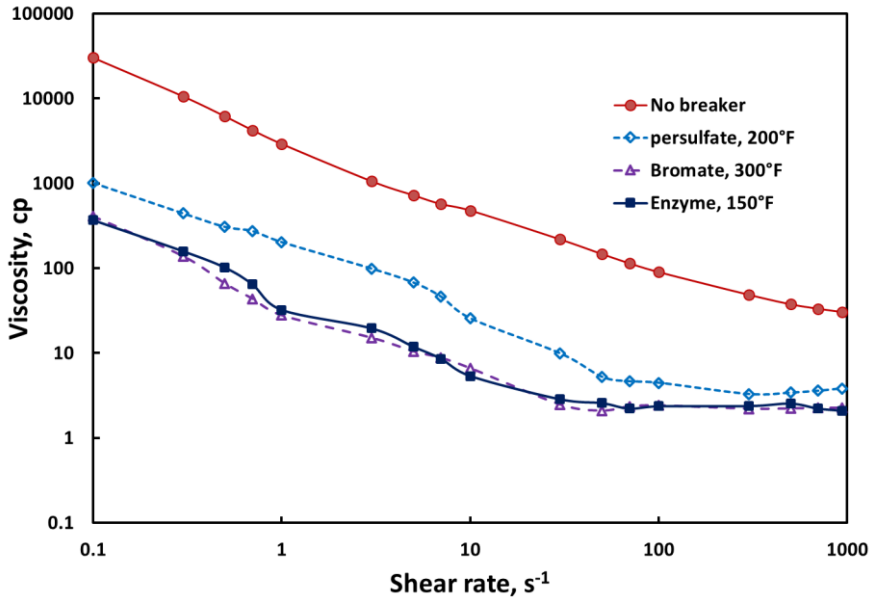

Fig. 94—The viscosity of TEMPO-NFC fluids in the degradation tests with different breakers at 150, 200 and 300ºF.

5.5. Formation damage evaluation of degraded NFC fluids

In this section, the formation damage of degraded fiber fluids has been evaluated using different types of cores in coreflood tests (**Table 19**). First of all, the fiber fluid was degraded with the enzyme at 150^{o}F for 24 h. Then the degraded fluid was injected into the core and the final permeability was calculated as the percentage of the initial permeability of the core. The percentage was compared to that in the test using the original fiber fluid.

From previous results in Section 4, all four fiber fluids caused severe damage to Indiana limestone cores. Therefore, Indianan limestone core was used to evaluate the degraded fluid. All four tests were run under the same conditions except using different types of fiber fluids. If the degraded fiber fluid would not cause severe damage to the limestone core, the enzyme may be used to remove/reduce the damage caused by the original fiber fluid. The results have shown that the final permeability of the cores using degraded fluids were higher than that using the original fluids (**Table 20**). For example, when the core was treated by the original KS-NFC fluid, the final permeability was only 18% of the initial permeability of the core. However, if the core was treated by degraded KS-NFC fluid, the final permeability increased to 93% of the initial permeability of the core. These results have shown that the degraded fiber fluids reduced the formation damage compared to the original fiber fluids.

One coreflood test using Boise sandstone core and degraded KS-NFC fluid was also performed. Similar results have been obtained. When the core treated with the degraded KS-NFC fluid, the final permeability was 92% of the initial permeability of the

core. The result has indicated that the degraded KS-NFC fluid did not cause damage to the core, which was completely different from the original KS-NFC fluid.

This method of coreflood tests using degraded fluids cannot represent the situation in the oilfield. However, combining the previous results of the degradation studies in this section, it can give us preliminary conclusion that breakers can be used to degrade the fiber fluids and remove/reduce the formation damage. The original fluid resulted in a low final permeability, only 36% of the initial permeability of Boise sandstone core.

Table 19—Coreflood tests using degraded fluids

Coreflood No.	Test 33	Test 34	Test 35	Test 36	Test 37
Fiber	ENZ-NFC	ME-NFC	TEMPO-NFC	KS-NFC	KS-NFC
Core Type	Limestone	Limestone	Limestone	Limestone	Boise
Porosity, vol%	11.8	13.2	12.1	11.9	27.3
Temperature, ºF	75	75	75	75	75
Fiber Concentration, ppt	8.3	8.3	8.3	8.3	8.3
Initial Permeability, md	321.1	425.4	381	415	1011
Final Permeability, md	297.8	309.0	197	385	930
Percentage, %	93	73	52	93	92

Table 20—Comparison between original and degraded fluids					
	Percentage, %				
Fiber	ENZ-NFC	ME-NFC	TEMPO-NFC	KS-NFC	KS-NFC
Core Type	Limestone	Limestone	Limestone	Limestone	Boise
Original Fluid	66	65	13	18	36
Degraded Fluid	93	73	52	93	92

One coreflood test using Boise sandstone core was performed to evaluate the damage of KS-NFC fluid containing enzyme at 150ºF. Enzyme, GBW-26C (1.0 ml), was added to 200 ml KS-FNC (40 lb/1000gal) fluid, and then 3 pore volume of the mixture fluid was injected to the Boise sandstone core. After 24 hours, the final permeability was measured at room temperature to compare with the initial permeability. The results have shown that the final permeability (815 md) of the core was 80% of the initial permeability (1011 md), indicating that the enzyme-loaded fiber fluid caused slight damage under the tested conditions. This was probably because that the fibers that could cause damage in the core were degraded into small molecules by the enzyme. When KCl brine was injected, the small molecules were flushed out easily, and a high final permeability was obtained.

5.6. Conclusion

The degradation studies of the fiber fluids have been performed using different types of breakers, including enzyme, acid, and oxidizers. The enzyme breaker has been

evaluated with the effects of temperature, enzyme concentration, and presence of KCl. Viscosity was measured after degradation and compared to the initial viscosity of the fluids. Filtration was used to separate the solid from the solution after degradation. HPLC was used to analyze the degraded products which were soluble in water. Scanning Electron Microscopy (SEM) was used to analyze the solid residue after degradation and filtration.

The fiber fluids were successfully degraded by the enzyme breaker, indicated by the significant decrease in the fluid viscosity. The presence of KCl did not affect the activity of the enzyme. Within a limited range, a higher enzyme concentration afforded a lower viscosity, suggesting a degradation of the polymer. The viscosity was lower when the tests were run at 150°F than 200°F. This is because the enzyme had a higher activity at 150°F.

After degradation, the fluids were filtered. The filtrates were analyzed by HPLC. These analyses have shown that the new viscosifier can be mostly degraded into soluble products with low viscosity, which can be flowed back after the treatment. The HPLC results were consistent with the results of the viscosity measurements of degraded fluids. A higher percentage of glucose was obtained at 150 than 200°F, which also indicated a more complete degradation. At the same temperature, a higher enzyme concentration produced a higher percentage of glucose in the degraded fluids, which agreed with the lower fluid viscosity. RAB tests have shown that the solid residue existed after degradation. However, SEM analysis of the solid residue has shown that there was no original fiber remaining after the treatment.

Coreflood tests were run with enzyme-degraded fiber fluids. Compared to the original fiber fluids, the degraded fluids caused much less damage under the same conditions. This is because the most of fibers were degraded into small water-soluble molecules which would not cause any damage. When the enzyme was added to the fiber fluid before injection, a high final permeability was obtained. These results have shown that the formation damage can be removed effectively by the enzyme breaker.

6. SUMMARY

In this project, we have investigated the properties of nanofibrillated cellulose (NFC) fibers in order to develop the potential applications of NFC in oil industry. The rheological properties, solid suspending ability, formation damage, degradation, and formation damage removal of four NFC-based fluids have been evaluated.

In section 2, the rheological properties of four NFC fluids were carefully studied using a rotational rheometer, Grace M5600. The viscosity measurements were performed to evaluate the effects of shear rate, salts, and temperature. The viscoelastic properties were examined by dynamic oscillatory tests. All four fluids were non-Newtonian, which can be described by the power-law model. This type of fluid had high thermal stability up to 350ºF, which was much better than guar fluid. TEMPO-NFC fluid had the highest viscosity within 200 minutes at 350ºF with 40 lb/1000gal fiber added. The viscosity of ENZ-NFC was stable in the presence of 10 wt% KCl or $CaCl_2$. The presence of KCl resulted in an obvious reduction of the viscosity of ME-NFC TEMPO-NFC, and KS-NFC fluids. This is because KCl can cause the collapse of the fiber chains by shielding the electrostatic repulsion between the negatively charged fiber chains. The zeta potential profiles of the fiber fluids confirmed that the fibers have negative charge and the presence of KCl reduced the zeta potential of the fibers significantly. The dynamic oscillatory tests have shown that the ENZ-NFC fluid behaved as an elastic material when the frequency was higher than 0.3 Hz. However, viscous modulus was still dominant for guar fluid until

2.3 Hz. The viscoelasticity of four fiber fluids were compared. TEMPO-NFC fluid has shown the best viscoelasticity under the same conditions.

In section 3, the solid suspending ability of the fiber fluids have been evaluated and compared to guar fluid using static sand settling tests. Fiber fluids had a much better solid suspending ability than guar fluid under the same conditions. An increase in the fiber concentration led to the improvement in the solid suspending ability. However, the temperature increase resulted in a faster sand settling. A correlation was found between the viscoelastic properties and the solid suspending ability for the fiber and guar fluids. The crossover frequency, where the viscous modulus is equal to the elastic modulus, was correlated to the solid settling time. The crossover frequency for the five fluid decreased in the following order: guar > ENZ-NFC > ME-NFC > KS-NFC > TEMPO-NFC. Correspondingly, the proppant suspending ability of these five fluids were as follows: guar < ENZ-NFC < ME-NFC < KS-NFC < TEMPO-NFC.

In section 4, the formation damage of four types of nanofibrillated cellulose fibers have been evaluated using different types of cores. The fiber fluids were injected into the cores. The final permeability of the core, expressed as a percentage of the initial permeability, was used to quantify the damage caused by the fiber fluid treatment. Generally, when low/moderate-permeability sandstone cores (Bandera and Berea) were treated with the cellulose fiber fluids, the damage was very small. However, guar-based fluids caused severe damage under the same conditions. When high-permeability cores (Indiana and Boise) were treated with the fiber fluids, the final permeability was reduced, especially for KS-NFC and TEMPO-NFC. KS-NFC and TEMPO-NFC fibers were

smaller than ENZ-NFC and ME-NFC in fiber diameter and length. Therefore, KS-NFC and TEMPO-NFC fibers could invade the core more easily and blocked the pore throats.

In section 5, the degradation studies of the fiber fluids have been performed using different types of breakers, enzyme, acid, and oxidizers. The enzyme has been evaluated with the effects of temperature, enzyme concentration, and presence of KCl. Viscosity was measured after degradation and compared to the initial viscosity. Filtration was used to separate the solid from the solution after degradation. HPLC was used to analyze the degraded products which were soluble in water. Scanning Electron Microscopy (SEM) was used to analyze the solid residue after degradation and filtration.

The fiber fluids were successfully degraded by the enzyme, indicated by the significant decrease in the fluid viscosity. The presence of KCl did not affect the activity of the enzyme. Within a limited range, a higher enzyme concentration afforded a lower viscosity, suggesting a degradation of the polymer. The viscosity was lower when the tests were run at 150°F than 200°F. This is because the enzyme had a higher activity at 150°F. After degradation, the fluids were filtered. The filtrates were analyzed by HPLC. These analyses have shown that the new viscosifier can be mostly degraded into soluble products with low viscosity, which can be flowed back after the treatment. The HPLC results were consistent with the results of the viscosity measurements of degraded fluids. A higher percentage of glucose was obtained at 150 than 200°F, which also indicated a more complete degradation. At the same temperature, a higher enzyme concentration produced a higher percentage of glucose in the degraded fluids, which agreed with the lower fluid viscosity. RAB tests have shown that the solid residue existed after degradation. However,

SEM analysis of the solid residue has shown that there was no original fiber remaining after the treatment.

Coreflood tests were run with enzyme-degraded fiber fluids. Compared to the original fiber fluids, the degraded fluids caused much less damage under the same conditions. This is because the most of fibers were degraded into small water-soluble molecules which would not cause any damage. When the enzyme was added to the original fiber fluid immediately before the injection to the core, a high final permeability of the core was obtained. These results have shown that the formation damage can be removed effectively by the enzyme breaker.

In conclusions, through evaluating the rheological properties, solid suspending ability, formation damage, and degradation of NFC fluids, the results have shown good performance of the NFC fibers as viscosifiers, which have provided some guidelines to develop the potential applications of NFC fibers in oil industry.

REFERENCES

Abdul Khalil, H.P.S., Davoudpour, Y., Islam, M.N. et al. 2014. Production and Modification of Nanofibrillated Cellulose Using Various Mechanical Processes: A Review. *Carbohydr. Polym.* **99** (0): 649-665. DOI: http://dx.doi.org/10.1016/j.carbpol.2013.08.069.

Acharya, A.R. Viscoelasticity of Crosslinked Fracturing Fluids and Proppant Transport. *SPE Prod Eng* **3** (4): 483 - 488. SPE 15937. DOI: 10.2118/15937-pa.

Almond, S.W. 1982. Factors Affecting Gelling Agent Residue under Low Temperature Conditions. Paper SPE 10658 presented at the SPE Formation Damage Control Symposium, Lafayette, Louisiana, 24-25 March. DOI: 10.2118/10658-ms.

Al-Muntasheri, G.A. 2014. A Critical Review of Hydraulic-Fracturing Fluids for Moderate- to Ultralow-Permeability Formations over the Last Decade. *SPE Prod & Oper* **29** (4): 243-260. SPE 169552. DOI: 10.2118/169552-pa.

Al-Yami, A.S., Nasr-El-Din, H.A., Bataweel, M.A. et al. 2008. Formation Damage Induced by Various Water-Based Fluids Used to Drill Hp/Ht Wells. Paper SPE 112421 presented at the SPE International Symposium and Exhibition on Formation Damage Control, Lafayette, Louisiana. 13-15 February. DOI: 10.2118/112421-ms.

Antoci, J.C. and Anaya, L.A. 2001. First Massive Hydraulic Fracturing Treatment in Argentina. Paper SPE 69581 presented at the SPE Latin American and Caribbean Petroleum Engineering Conference, Buenos Aires, Argentina, 25-28 March. DOI: 10.2118/69581-ms.

Audibert, A., Argillier, J.-F., Ladva, H.K.J. et al. 1999. Role of Polymers on Formation Damage. Paper SPE 54767 presented at the SPE European Formation Damage Conference, The Hague, Netherlands. 31 May-1 June. DOI: 10.2118/54767-ms.

Ayoub, J.A., Kirksey, J.M., Malone, B.P. et al. 1992. Hydraulic Fracturing of Soft Formations in the Gulf Coast. Paper SPE 23805 presented at the SPE Formation Damage Control Symposium, Lafayette, Louisiana, 26-27 February. DOI: 10.2118/23805-ms.

Bataweel, M.A. and Nasr-El-Din, H.A. 2012. Rheological Study for Surfactant-Polymer and Novel Alkali-Surfactant-Polymer Solutions. Paper SPE 150913 presented at the North Africa Technical Conference and Exhibition, Cairo, Egypt. DOI: 10.2118/150913-ms.

Bulova, M.N., Cheremisin, A.N., Nosova, K.E. et al. 2006. Evaluation of the Proppant-Pack Permeability in Fiber-Assisted Hydraulic Fracturing Treatments for Low-Permeability Formations. Paper SPE 100556 presented at the SPE Gas Technology Symposium, Calgary, Alberta, Canada. DOI: 10.2118/100556-ms.

Bulova, M.N., Nosova, K.E., Willberg, D.M. et al. 2006. Benefits of the Novel Fiber-Laden Low-Viscosity Fluid System in Fracturing Low-Permeability Tight Gas Formations. Paper SPE 102956 presented at the SPE Annual Technical Conference and Exhibition, San Antonio, Texas. DOI: 10.2118/102956-ms.

Brannon, H.D. and TjonJoePin, R.M. 1996. Characterization of Breaker Efficiency Based Upon Size Distribution of Polymeric Fragments Resulting from Degradation of Crosslinked Fracturing Fluids. Paper SPE 36496 presented at the SPE Annual Technical Conference and Exhibition, Denver, Colorado, 6-9 October. DOI: 10.2118/36496-ms.

Brannon, H.D., Tjon-Joe-Pin, R.M., Carman, P.S. et al. 2003. Enzyme Breaker Technologies: A Decade of Improved Well Stimulation. Paper SPE 84213 presented at the SPE Annual Technical Conference and Exhibition, Denver, Colorado. DOI: 10.2118/84213-ms.

Brannon, H.D. and Starks, T.R. 2009. Maximizing Return-on-Fracturing-Investment by Using Ultra-Lightweight Proppants to Optimize Effective Fracture Area: Can Less Be More? Paper SPE 119385 presented at the SPE Hydraulic Fracturing Technology Conference, The Woodlands, Texas. 19-21 January. DOI: 10.2118/119385-ms.

Burke, M.D. and Khan, S.A. 2000. Triggered Enzymatic Degradation of a Water-Soluble Polymer Solution Using a Novel Inhibitor. *Biomacromolecules* **1** (4): 688-695.

Bustos, O.A., Powell, A.R., Olsen, T.N. et al. 2007. Fiber-Laden Fracturing Fluid Improves Production in the Bakken Shale Multi-Lateral Play. Paper SPE 107979 presented at the Rocky Mountain Oil & Gas Technology Symposium, Denver, Colorado. 16-18 April. DOI: 10.2118/107979-ms.

Cawiezel, K.E. and Gupta, D.V.S. 2010. Successful Optimization of Viscoelastic Foamed Fracturing Fluids with Ultralightweight Proppants for Ultralow-Permeability Reservoirs. *SPE Prod & Oper* **25** (1): 80 - 88. SPE 119626. DOI: 10.2118/119626-pa.

Centurion, S.M., Rengifo, M., Cortona, M.N. et al. 2006. Successful Application of a Novel Fracturing Fluid in the Chicontepec Basin, Mexico. Paper SPE 103879 presented at the International Oil Conference and Exhibition in Mexico, Cancun, Mexico, 31 August-2 September. DOI: 10.2118/103879-ms.

Chatterji, J. and Borchardt, J.K. 1981. Applications of Water-Soluble Polymers in the Oil Field. *J Pet Technol* **33** (11): 2042 - 2056. DOI: 10.2118/9288-pa

Cheng, Y., Brown, K.M., and Prud'homme, R.K. 2002. Characterization and Intermolecular Interactions of Hydroxypropyl Guar Solutions. *Biomacromolecules* **3** (3): 456-461.

Cheng, Y. and Prud'homme, R.K. 2000. Enzymatic Degradation of Guar and Substituted Guar Galactomannans. *Biomacromolecules* **1** (4): 782-788.

Clark, J.B. 1949. A Hydraulic Process for Increasing the Productivity of Wells. *J Pet Technol* **1** (1): 1-8. SPE 949001. DOI: 10.2118/949001-g.

Coronado, J.A. 2007. Success of Hybrid Fracs in the Basin. Paper SPE 106758 presented at the Production and Operations Symposium, Oklahoma City, Oklahoma. 31 March-3 April. DOI: 10.2118/106758-ms.

Crews, J.B., Huang, T., Willingham, J.R. et al. 2008. Methods and Compositions for Fracturing Subterranean Formations. US Patent No. 7,723,272.

Crews, J.B., Huang, T., and Wood, W.R. 2008. New Technology Improves Performance of Viscoelastic Surfactant Fluids. *SPE Drill & Compl* **23** (1): 41-47. DOI: 10.2118/103118-pa.

de Kruijf, A.S., Roodhart, L.P., and Davies, D.R. Relation between Chemistry and Flow Mechanics of Borate-Crosslinked Fracturing Fluids. *SPE Prod & Fac* **8** (3): 165-170. SPE 25206. DOI: 10.2118/25206-pa.

DeVine, C.S., Tjon-Joe-Pin, R.M., Rickards, A.R. et al. 1998. Polymeric Damage and a Cost Effective Method for Damage Removal from Wells. Paper SPE 49249 presented at the SPE Annual Technical Conference and Exhibition, New Orleans, Louisiana, 27-30 September. DOI: 10.2118/49249-ms.

dos Santos, J.A.C., Cunha, R.A., de Melo, R.C.B. et al. 2009. Inverted-Convection Proppant Transport for Effective Conformance Fracturing. *SPE Prod & Oper* **24** (1): 187 - 193. SPE 109585. DOI: 10.2118/109585-pa.

Economides, M. and Nolte, K. 2000. *Reservoir Stimulation*. third edition. John Wiley & Sons Ltd, England.

Ellis, R.C. 1998. An Overview of Frac Packs: A Technical Revolution (Evolution) Process. *J Pet Technol* **50** (1): 66-68. SPE 39232. DOI: 10.2118/39232-jpt.

Farris, R.F. 1953. Fracturing Formations in Wells. U.S. Patent No. 2,596,843.

Fast, C.R., Holman, G.B., and Covlin, R.J. 1977. The Application of Massive Hydraulic Fracturing to the Tight Muddy &Quot;J&Quot; Formation, Wattenberg Field, Colorado. *J Pet Technol* **29** (1): 10-11. SPE 5624. DOI: 10.2118/5624-pa.

Fredd, C.N., Olsen, T.N., Brenize, G. et al. 2004. Polymer-Free Fracturing Fluid Exhibits Improved Cleanup for Unconventional Natural Gas Well Applications. Paper SPE 91433 presented at the SPE Eastern Regional Meeting, Charleston, West Virginia, 15-17 September. DOI: 10.2118/91433-ms.

Gadde, P.B., Liu, Y., Norman, J. et al. 2004. Modeling Proppant Settling in Water-Fracs. Paper SPE 89875 presented at the SPE Annual Technical Conference and Exhibition, Houston, Texas. 26-29 September. DOI: 10.2118/89875-ms.

Ghauri, W.K. 1960. Results of Well Stimulation by Hydraulic Fracturing and High Rate Oil Backflush. *J Pet Technol* **12** (6): 19-27. SPE 1382-G. DOI: 10.2118/1382-g.

Gheissary, G. and van den Brule, B.H.A.A. 1996. Unexpected Phenomena Observed in Particle Settling in Non-Newtonian Media. *J. of Non-Newtonian Fluid Mech.* **67** (0): 1-18. DOI: http://dx.doi.org/10.1016/S0377-0257(96)01436-X.

Gomaa, A.M., Cawiezel, K., Gupta, D.V.S.V.S. et al. 2011. Viscoelastic Evaluation of a Surfactant Gel for Hydraulic Fracturing. Paper SPE 143450 presented at the SPE European Formation Damage Conference, Noordwijk, The Netherlands, 7-10 June. DOI: 10.2118/143450-ms.

Goycoolea, F.M., Morris, E.R., and Gidley, M.J. 1995. Viscosity of Galactomannans at Alkaline and Neutral Ph: Evidence of 'Hyperentanglement' in Solution. *Carbohydrate Polymers* **27** (1): 69-71.

Grossman, W.L. 1951. Hydrafrac Operations in the Spraberry Production, West Texas. Paper SPE 128-G presented at the Fall Meeting of the Petroleum Branch of AIME, Oklahoma City, Oklahoma, 3-5 October. DOI: 10.2118/128-g.

Grubert, D.M. 1991. Evolution of a Hybrid Fracture/Gravel-Pack Completion: Monopod Platform, Trading Bay Field, Cook Inlet, Alaska. *SPE Prod Eng* **6** (4): 395-398. SPE 19401. DOI: 10.2118/19401-pa.

Haghshenas, A., and Nasr-El-Din, H. A. 2014. Effect of Dissolved Solids on Reuse of Produced Water and Proppant Handling in Hydraulic Fracturing Jobs in Tight Sand Gas Reservoirs. Paper SPE 168614 presented at the SPE Hydraulic Fracturing Technology Conference, The Woodlands, Texas. 4-6 February. doi:10.2118/168614-ms.

Hainey, B.W. and Troncoso, J.C. 1992. Frac-Pack: An Innovative Stimulation and Sand Control Technique. Paper SPE 23777 presented at the SPE Formation Damage Control Symposium, Lafayette, Louisiana, 26-27 February. DOI: 10.2118/23777-ms.

Harris, P.C., Morgan, R.G., and Heath, S.J. 2005. Measurement of Proppant Transport of Frac Fluids. Paper SPE 95287 presented at the SPE Annual Technical Conference and Exhibition, Dallas, Texas. 9-12 October. DOI: 10.2118/95287-ms.

Harris, P.C., Walters, H.G., and Bryant, J. 2009. Prediction of Proppant Transport from Rheological Data. *SPE Prod & Oper* **24** (4): 550 - 555. SPE 115298. DOI: 10.2118/115298-pa.

Hayatdavoudi, A., Mehdizadeh, A.M., Caothien, S. et al. 1994. Degradation Mechanisms of the Hec Gel in Connection with Prevention of the Formation Damage: Part I. Paper SPE 27366 presented at the SPE Formation Damage Control Symposium, Lafayette, Louisiana. 7-10 February. DOI: 10.2118/27366-ms.

Howard, G.C. and Fast, C.R. 1970. *Hydraulic Fracturing*, Monograph Series, Richardson, Texas, USA, Society of Petroleum Engineers.

Ibrahim, A., Romero, E.E., Woon, G.C. et al. 2014. High Angle Frac Pack Completions in Shallow Sands: A Case Study on Program Learnings and Operational Improvements. Paper IPTC 18220 presented at the International Petroleum Technology Conference, Kuala Lumpur, Malaysia, 10-12 December. DOI: 10.2523/18220-ms.

Irvine-Fortescue, J. and Shoufi, O. 2009. Massive Hydraulic Fracture Stimulation in South Oman. Paper IPTC 13335 presented at the International Petroleum Technology Conference, Doha, Qatar, 7-9 December. DOI: 10.2523/13335-ms.

Jennings, A., Jr., Darden, W., Wenzel, R. et al. 1977. Massive Hydraulic Fracturing in the Eastern United States. Paper SPE 6866 presented at the SPE Annual Fall Technical Conference and Exhibition, Denver, Colorado, 9-12 October. DOI: 10.2118/6866-ms.

Jardim Neto, A.T., Prata, F.G.M., Gomez, J. et al. 2012. Ultralightweight Proppants: An Effective Approach to Address Problems in Long Horizontal Gravel Packs Offshore Brazil. *SPE Drill & Compl* **27** (4): 613 - 624. SPE 150581. DOI: 10.2118/150581-pa.

Kapoor, M., Khandal, D., Gupta, R. et al. 2013. Certain Rheological Aspects of Functionalized Guar Gum. International Journal of Carbohydrate Chemistry 2013: 15. DOI: 10.1155/2013/463907.

Kelland, M. A. 2009. Production Chemicals for the Oil and Gas Industry. CRC Press, USA.

Khan, S., Kelly, R., Prud'homme, R. et al. 2002. Controlled Enzymatic Degradation of Guar Galactomannan Solutions Using Enzymatic Inhibition. US Patent no. US20020193343 A1.

Kostenuk, N.H. and Browne, D.J. 2010. Improved Proppant Transport System for Slickwater Shale Fracturing. Paper SPE 137818 presented at the Canadian Unconventional Resources and International Petroleum Conference, Calgary, Alberta, Canada. 19-21 October. DOI: 10.2118/137818-ms.

Krilov, Z., Wojtanowicz, A.K., and Tomic, M. 1996. Formation Damage in Horizontal Wells Caused by Polymer Mud. Paper SPE 31135 presented at the SPE Formation Damage Control Symposium, Lafayette, Louisiana. 14-15 February. DOI: 10.2118/31135-ms.

Lei, C. and Clark, P.E. 2007. Crosslinking of Guar and Guar Derivatives. *SPE J.* **12** (3): 316-321. SPE 90840. DOI: 10.2118/90840-pa.

Lei, Q., Jiang, T., Xu, Y. et al. 2008. The Study and Application of Low-Damage and Massive Hydraulic Fracturing Technique in Tight Gas Formations with High Temperature and High Pressure. Paper SPE 114303 presented at the CIPC/SPE Gas Technology Symposium 2008 Joint Conference, Calgary, Alberta, Canada, 16-19 June. DOI: 10.2118/114303-ms.

Li, E., Greenhorn, R.C., and Scarth, B.R. 1988. Measurement of Rheological Properties of Fracturing Fluids in Dynamic Mode. *J Can Pet Technol* **27** (4): 55-61. DOI: 10.2118/88-04-04.

Li, L., Nasr-El-Din, H.A., and Cawiezel, K.E. 2010. Rheological Properties of a New Class of Viscoelastic Surfactant. *SPE Prod & Oper* **25** (3): 355-366. DOI: 10.2118/121716-pa.

Liu, L., Deng, J., Ma, Y. et al. 2006. Single-Trip, Multiple-Zone Frac Packing Offshore Sand Control: Overview of 58 Case Histories. Paper SPE 103779 presented at the International Oil & Gas Conference and Exhibition, Beijing, China, 5-7 December. DOI: 10.2118/103779-ms.

Liu, Y. and Sharma, M.M. 2005. Effect of Fracture Width and Fluid Rheology on Proppant Settling and Retardation: An Experimental Study. Paper SPE 96208 presented at the SPE Annual Technical Conference and Exhibition, Dallas, Texas. 9-12 October. DOI: 10.2118/96208-ms.

Loveless, D., Holtsclaw, J., Saini, R. et al. 2011. Fracturing Fluid Comprised of Components Sourced Solely from the Food Industry Provides Superior Proppant

Transport. Paper SPE 147206 presented at the SPE Annual Technical Conference and Exhibition, Denver, Colorado. 30 October-2 November. DOI: 10.2118/147206-ms.

Ma, X. and Pawlik, M. 2007. Intrinsic Viscosities and Huggins Constants of Guar Gum in Alkali Metal Chloride Solutions. *Carbohydrate Polymers* **70** (1): 15-24.

Mahammad, S., Comfort, D.A., Kelly, R.M. et al. 2007. Rheological Properties of Guar Galactomannan Solutions During Hydrolysis with Galactomannanase and A-Galactosidase Enzyme Mixtures. *Biomacromolecules* **8** (3): 949-956.

Malhotra, S. and Sharma, M.M. 2011. A General Correlation for Proppant Settling in Ves Fluids. Paper SPE 139581 presented at the SPE Hydraulic Fracturing Technology Conference, The Woodlands, Texas. 24-26 January. DOI: 10.2118/139581-ms.

Malochee, S. and Comeaux, B. Case Study: Analyzing Bottomhole Temperature Gauge Data in Gulf of Mexico Frac Packs to Optimize Fracture Fluid Crosslink, Stability and Break Times. Paper SPE 84215 presented at the SPE Annual Technical Conference and Exhibition, Denver, Colorado, 5-8 October. DOI: 10.2118/84215-ms.

Martins, J.P., Leung, K.H., Jackson, M.R. et al. 1992. Tip Screenout Fracturing Applied to the Ravenspurn South Gas Field Development. *SPE Prod Eng* **7** (3): 252-258. SPE 19766. DOI: 10.2118/19766-pa.

Mayerhofer, M.J., Richardson, M.F., Walker, R.N., Jr. et al. 1997. Proppants? We Don't Need No Proppants. Paper SPE 38611 presented at the SPE Annual Technical Conference and Exhibition, San Antonio, Texas, 5-8 October. DOI: 10.2118/38611-ms.

Meese, C.A., Mullen, M.E., and Barree, R.D. 1994. Offshore Hydraulic Fracturing Technique. *J Pet Technol* **46** (3): 226-229. SPE 28159. DOI: 10.2118/28159-pa

Montgomery, C. 2013. Fracturing Fluids. Paper ISRM-ICHF-2013-035 presented at the ISRM International Conference for Effective and Sustainable Hydraulic Fracturing, Brisbane, Australia. 20-22 May.

Montgomery, C. 2013. Fracturing Fluid Components. Paper ISRM-ICHF-2013-034 presented at the ISRM International Conference for Effective and Sustainable Hydraulic Fracturing, Brisbane, Australia. 20-22 May.

Monus, F.L., Broussard, F.W., Ayoub, J.A. et al. 1992. Fracturing Unconsolidated Sand Formations Offshore Gulf of Mexico. Paper SPE 24844 presented at the SPE Annual Technical Conference and Exhibition, Washington, D.C., 4-7 October. DOI: 10.2118/24844-ms.

Morris, E.R., Cutler, A.N., Ross-Murphy, S.B. et al. 1981. Concentration and Shear Rate Dependence of Viscosity in Random Coil Polysaccharide Solutions. *Carbohydrate Polymers* **1** (1): 5-21.

Nasr-El-Din, H.A., Al-Mohammed, A.M., Al-Fuwaires, O.A. et al. 2007. Degradation of High Ph Borate Gels. Paper IPTC 11585 presented at the International Petroleum Technology Conference, Dubai. DOI: 10.2523/11585-ms.

Nor-Azlan, N., Sanchez, A.I., and Diyashev, I.R. 2003. Massive Hydraulic Fracturing - a Case History in Western Siberia, Russia. Paper SPE 84916 presented at the SPE International Improved Oil Recovery Conference in Asia Pacific, Kuala Lumpur, Malaysia, 20-21 October. DOI: 10.2118/84916-ms.

Norman, D. 2004. The Frac-Pack Completion: Why Has It Become the Standard Strategy for Sand Control? Paper SPE 101511 presented at the SPE Distinguished Lecture 2003-2004.

Norman, W.D., Jasinski, R.J., and Nelson, E.B. 1996. Viscoelastic Surfactant Based Aqueous Fluid Systems Using a Quaternary Ammonium Halide Thickener. US Patent No. 5,551,516.

Novotny, E.J. Proppant Transport. Paper SPE 6813 presented at the SPE Annual Fall Technical Conference and Exhibition, Denver, Colorado. 9-12 October. DOI: 10.2118/6813-ms.

Okoye, C.U., Onuba, N.L., Ghalambor, A. et al. 1991. Formation Damage in Heavy-Oil Formation During Steamflooding. Paper SPE 22980 presented at the SPE Asia-Pacific Conference, Perth. Australia. 4-7 November. DOI: 10.2118/22980-ms.

Oussoltsev, D., Butula, K.K., Klyubin, A. et al. 2008. Fiber-Based Fracture Fluid Technology a First for Oil Reservoirs in Western Siberia. Paper SPE 112438 presented at the SPE International Symposium and Exhibition on Formation Damage Control, Lafayette, Louisiana. 13-15 February. DOI: 10.2118/112438-ms.

Padgett, J.C. 1951. Information on Hydrafac Process. Paper presented at the 3rd World Petroleum Congress, The Hague, The Netherlands, 28 May-6 June. World Petroleum Congress. WPC-4142.

Palisch, T.T., Vincent, M., and Handren, P.J. 2010. Slickwater Fracturing: Food for Thought. *SPE Prod & Oper* **25** (3): 327-344. SPE 115766. DOI: 10.2118/115766-pa.

Parker, M.A., Vitthal, S., Rahimi, A. et al. 1994. Hydraulic Fracturing of High-Permeability Formations to Overcome Damage. Paper SPE 27378 presented at the

SPE IntI. Symposium on Formation Damage Control held in Lafayette, Louisiana, 7-10 February. DOI: 10.2118/27378-ms.

Parlar, M., Nelson, E.B., Walton, I.C. et al. 1995. An Experimental Study on Fluid-Loss Behavior of Fracturing Fluids and Formation Damage in High-Permeability Porous Media. Paper SPE 30458 presented at the SPE Annual Technical Conference & Exhibition, Dallas, 22-25 October. DOI: 10.2118/30458-ms.

Patel, P.S., Robart, C.J., Ruegamer, M. et al. 2014. Analysis of Us Hydraulic Fracturing Fluid System and Proppant Trends. Paper SPE 168645 presented at the SPE Hydraulic Fracturing Technology Conference, The Woodlands, Texas. 4-6 February. DOI: 10.2118/168645-ms.

Peebles, B., Kelley, R., Ritter, W. et al. 2002. Frac-Pack Completion of Gas-Storage Wells for Enhanced Deliverability. *SPE Drill & Compl* **17** (2): 107-117. SPE 78286. DOI: 10.2118/78286-pa.

Philipp, B., Jacopian, V., Loth, F. et al. 1979. Influence of Cellulose Physical Structure on Thermohydrolytic, Hydrolytic, and Enzymatic Degradation of Cellulose. In *Hydrolysis of Cellulose: Mechanisms of Enzymatic and Acid Catalysis*, first edition, Advances in Chemistry, American Chemical Society, USA.

Rae, P. and di Lullo, G. 1996. Fracturing Fluids and Breaker Systems—a Review of the State-of-the-Art. Paper SPE 37359 presented at the SPE Eastern Regional Meeting, Columbus, Ohio. 23-25 October. DOI: 10.2118/37359-ms.

Ramurthy, M., Lyons, B., and Magill, D.P. 2006. Hybrid Fracture Stimulation in Underpressured Coals. Paper SPE 100588 presented at the SPE Gas Technology Symposium, Calgary, Alberta, Canada. 15-17 May. DOI: 10.2118/100588-ms.

Rickards, A.R., Tjon-Joe-Pin, R.M., and Boles, J.L. 1993. Enzymatic Breaker System for Nondamaging Removal of Cellulose-Based Blocking Gels. Paper SPE 25488 presented at the SPE Production Operations Symposium, Oklahoma City, Oklahoma. DOI: 10.2118/25488-ms.

Rickards, A.R., Brannon, H.D., and Wood, W.D. 2006. High Strength, Ultralightweight Proppant Lends New Dimensions to Hydraulic Fracturing Applications. *SPE Prod & Oper* **21** (2): 212 - 221. SPE 84308. DOI: 10.2118/84308-pa.

Roger, B., Leuterman, A.J.J., and Cheryl, S. 1993. Drilling Fluids: Making Peace with the Environment. *J Pet Technol* **45** (1): 6 - 10. DOI: 10.2118/24553-pa

Roodhart, L.P. 1985. Proppant Settling in Non-Newtonian Fracturing Fluids. Paper SPE 13905 presented at the SPE/DOE Low Permeability Gas Reservoirs Symposium, Denver, Colorado. 19-22 March. DOI: 10.2118/13905-ms.

Roodhart, L.P., Fokker, P.A., Davies, D.R. et al. 1994. Frac-and-Pack Stimulation: Application, Design, and Field Experience. *J Pet Technol* **46** (3): 230-238. SPE 26564. DOI: 10.2118/26564-pa.

Rubinstein, M. and Colby, R.H. 2003. Polymer Physics. Oxford University Press, England.

Sahai, R., Miskimins, J.L., and Olson, K.E. 2014. Laboratory Results of Proppant Transport in Complex Fracture Systems. Paper SPE 168579 presented at the SPE Hydraulic Fracturing Technology Conference, The Woodlands, Texas. 4-6 February. DOI: 10.2118/168579-ms.

Salazar, F., Rachid, R., Milne, A. et al. 2013. Hydraulic Fracturing with Water-Based Fluids in Water-Sensitive Formations. Paper SPE 165082 presented at the 10th SPE International Conference and Exhibition on European Formation Damage, Noordwijk, The Netherlands, 5-7 June. DOI: 10.2118/165082-ms.

Samuel, M., Card, R.J., Nelson, E.B. et al. 1997. Polymer-Free Fluid for Hydraulic Fracturing. Paper SPE 38622 presented at the SPE Annual Technical Conference and Exhibition, San Antonio, Texas, 5-8 October. DOI: 10.2118/38622.

Samuel, M.M., Obianwu, C.W., Chao, G.W.-R. et al. 2007. An Engineered Fiber for the Fracturing of Unconsolidated Sand in Highly Deviated Wells in the Tali Field of Brunei. Paper SPE 108011 presented at the European Formation Damage Conference, Scheveningen, The Netherlands, 30 May-1 June. DOI: 10.2118/108011-ms.

Sarwar, M.U., Cawiezel, K.E., and Nasr-El-Din, H.A. 2011. Gel Degradation Studies of Oxidative and Enzyme Breakers to Optimize Breaker Type and Concentration for Effective Break Profiles at Low and Medium Temperature Ranges. Paper SPE 140520 presented at the SPE Hydraulic Fracturing Technology Conference, The Woodlands, Texas, 24-26 January. DOI: 10.2118/140520-ms.

Schein, G. 2005. The Application and Technology of Slickwater Fracturing. Paper SPE 108807 presented as a Distinguished Lecture during the 2004-2005 season. Society of Petroleum Engineers, USA.

Shaoul, J.R., Ross, M.J., Spitzer, W.J. et al. 2007. Massive Hydraulic Fracturing Unlocks Deep Tight Gas Reserves in India. Paper SPE 107337 presented at the European Formation Damage Conference, Scheveningen, The Netherlands, 30 May-1 June. DOI: 10.2118/107337-ms.

Siddiqui, M.A., Nasr-El-Din, H.A., Al-Anazi, M.S. et al. 2004. Formation Damage in Gas Sandstone Formations by High-Temperature Borate Gels Due to Long Term Shut-in Periods. Paper SPE 89476 presented at the SPE/DOE Symposium on Improved Oil Recovery, Tulsa, Oklahoma. DOI: 10.2118/89476-ms.

Sitdikov, S.S., Serdyuk, A., Nikitin, A. et al. 2009. Fiber-Laden Fluid: Applied Solution for Addressing Multiple Challenges of Hydraulic Fracturing in Western Siberia. Paper SPE 119825 presented at the SPE Hydraulic Fracturing Technology Conference, The Woodlands, Texas. 19-21 January. DOI: 10.2118/119825-ms.

Smith, M.B., Miller, W.K., II, and Haga, J. 1987. Tip Screenout Fracturing: A Technique for Soft, Unstable Formations. *SPE Prod Eng* **2** (2): 95-103. SPE 13273. DOI: 10.2118/13273-pa.

Smith, M.B. and Hannah, R.R. 1996. High-Permeability Fracturing: The Evolution of a Technology. *J Pet Technol* **48** (7): 628-633. DOI: 10.2118/27984-jpt.

Stewart, B.R., Mullen, M.E., Ellis, R.C. et al. 1995. Economic Justification for Fracturing Moderate to High Permeability Formations in Sand Control Environments. Paper SPE 30470 presented at the SPE Annual Technical Conference and Exhibition, Dallas, Texas, 22-25 October. DOI: 10.2118/30470-ms.

Suman, G., Ellis, R. and Snyder, R. *Sand Control Handbook*. 1985. Gulf Publishing Company, USA.

Sun, H., DeBenedictis, F., Zhou, J. et al. 2013. Field Case Histories of a Non-Damaging Guar Alternative for Linear Gel Application in Slickwater Fracturing. Paper SPE 165130 presented at the SPE European Formation Damage Conference & Exhibition, Noordwijk, The Netherlands. 5-7 June. DOI: 10.2118/165130-ms.

Talabani, S., Hatzignatiou, D.G., and Chukwu, G.A. 1993. Comprehensive Description and Evaluation of Polymers as Drilling Fluids. Paper SPE 26071 presented at the Western Regional Meeting, Anchorage, Alaska. 26-28 May. DOI: 10.2118/26071-ms.

Tayal, A., Kelly, R.M., and Khan, S.A. 1997. Viscosity Reduction of Hydraulic Fracturing Fluids through Enzymatic Hydrolysis. *SPE J.* **2** (2): 204-212. SPE 38432. DOI: 10.2118/38432-pa.

Tiner, R.L., Ely, J.W., and Schraufnagel, R. 1996. Frac Packs - State of the Art. Paper SPE 36456 presented at the SPE Annual Technical Conference and Exhibition, Denver, Colorado, 6-9 October. DOI: 10.2118/36456-ms.

Titov, K., Tarasov, A., Ilyin, Y. et al. 2010. Relationships between Induced Polarization Relaxation Time and Hydraulic Properties of Sandstone. *Geophys J Int* **180** (3): 1095-1106. DOI: 10.1111/j.1365-246X.2009.04465.x.

Tjon-Joe-Pin, R., Brannon, H.D., and Rickards, A.R. 1993. Remedial Treatment for Polymeric Damage Removal Provides Improved Well Productivity. Paper SPE 25385 presented at the SPE Asia Pacific Oil and Gas Conference, Singapore. 8-10 February. DOI: 10.2118/25385-ms.

Veatch, R.W., Jr. and Moschovidis, Z.A. 1986. An Overview of Recent Advances in Hydraulic Fracturing Technology. Paper SPE 14085 presented at the International Meeting on Petroleum Engineering, Beijing, China. 17-20 March. DOI: 10.2118/14085-ms.

Verret, R., Robinson, B., Cowan, J. et al. 2000. Use of Micronized Cellulose Fibers to Protect Producing Formations. Paper SPE 58794 presented at the SPE International Symposium on Formation Damage Control, Lafayette, Louisiana, 23-24 February. DOI: 10.2118/58794-ms.

Vitthal, S. and McGowen, J.M. 1996. Fracturing Fluid Leakoff under Dynamic Conditions Part 2: Effect of Shear Rate, Permeability, and Pressure. Paper SPE 36493 presented at the SPE Annual Technical Conference and Exhibition, Denver, Colorado, 6-9 October. DOI: 10.2118/36493-ms.

Walker, R.N., Jr., Hunter, J.L., Brake, A.C. et al. 1998. Proppants, We Still Don't Need No Proppants - a Perspective of Several Operators. Paper SPE 49106 presented at the SPE Annual Technical Conference and Exhibition, New Orleans, Louisiana, 27-30 September. DOI: 10.2118/49106-ms.

Wang, F., Zhang, Y., Liu, G. et al. 2012. The Horizontal Massive Multistage Fracturing Meet the Changling Tight Gas Field Development Strategy. Paper SPE 155911 presented at the IADC/SPE Asia Pacific Drilling Technology Conference and Exhibition, Tianjin, China, 9-11 July. DOI: 10.2118/155911-ms.

Weirich, J., Li, J., Abdelfattah, T. et al. 2013. Frac Packing: Best Practices and Lessons Learned from More Than 600 Operations. *SPE Drill & Compl* **28** (2): 119-134. SPE 147419. DOI: 10.2118/147419-pa.

Weng, D., Lei, Q., Ding, Y. et al. 2011. Case Study: Massive Hydraulic Fracturing in Volcanic Gas, China. Paper SPE 141543 presented at the SPE Production and Operations Symposium, Oklahoma City, Oklahoma, 27-29 March. DOI: 10.2118/141543-ms.

Westland, J.A., Lenk, D.A., and Penny, G.S. 1993. Rheological Characteristics of Reticulated Bacterial Cellulose as a Performance Additive to Fracturing and Drilling Fluids. Paper SPE 25204 presented at the SPE International Symposium on Oilfield Chemistry, New Orleans, Louisiana, 2-5 March. DOI: 10.2118/25204-ms.

Whalen, R.T. 2000. Viscoelastic Surfactant Fracturing Fluids and a Method for Fracturing Subterranean Formations. US Patent No. 6,035,936.

Yang, Y., Robart, C.J., and Ruegamer, M. 2013. Analysis of U.S. Hydraulic Fracturing Design Trends. Paper SPE 163875 presented at the SPE Hydraulic Fracturing Technology Conference, The Woodlands, Texas. 4-6 February. DOI: 10.2118/ 163875-ms.

Zhang, K. 2002. Fluids for Fracturing Subterranean Formations. US Patent No. 6,468,945.

Zhang, L.M., Zhou, J.F., and Hui, P.S. 2005. Thickening, Shear Thinning and Thixotropic Behavior of a New Polysaccharide-Based Polyampholyte in Aqueous Solutions. *Colloids and Surfaces A: Physicochemical and Engineering Aspects* 259 (1–3): 189-195.

Zhao, Z.-y., Cui, M., Conway, M.W. et al. 1995. The Rheology of Chinese Xd and Zw Borate Crosslinked Fracturing Fluids and Their Proppant Transport Capability. Paper SPE 29991 presented at the International Meeting on Petroleum Engineering, Beijing, China. 14-17 November. DOI: 10.2118/29991-ms.

APPENDIX A

In this part, all the figures of the coreflood tests which are not shown in the main part are listed for reference. The conditions and results have been included in tables in section 4.

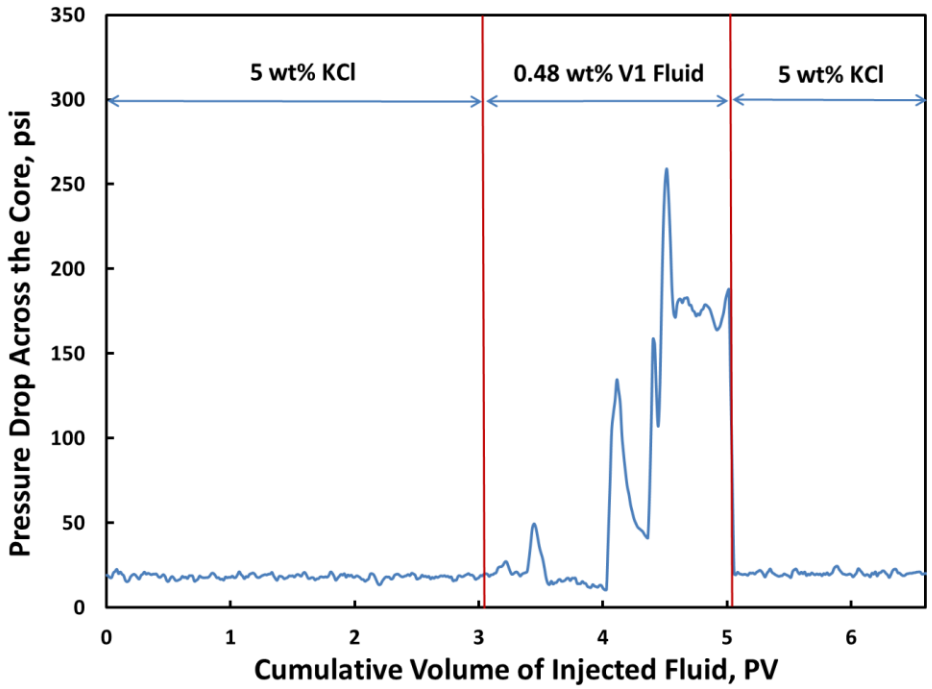

Fig. 95—Test 2: Pressure drop across the core with 40 lb/1000gal ENZ-NFC fluid and Berea core at 250°F.

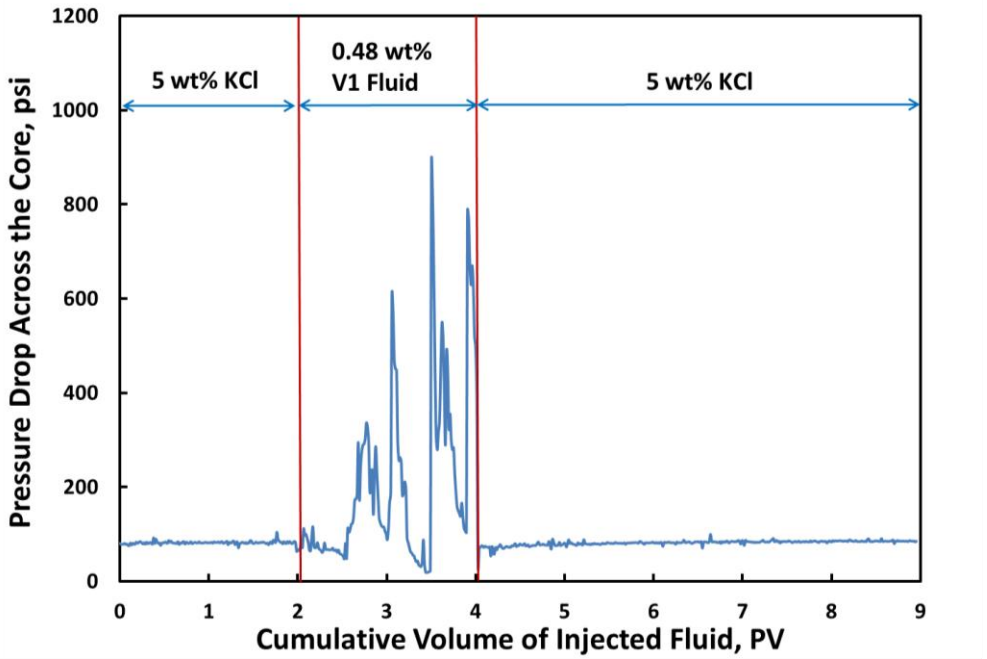

Fig. 96—Test 4: Pressure drop across the core with 40 lb/1000gal ENZ-NFC (V1) fluid and Bandera core at 250ºF.

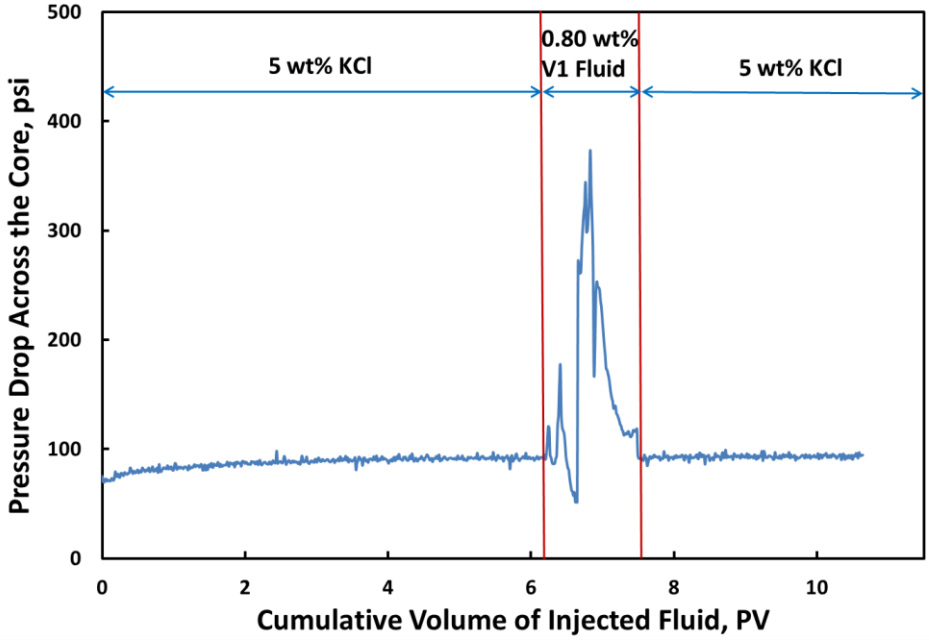

Fig. 97—Test 5: Pressure drop across the core with 67 lb/1000gal ENZ-NFC (V1) fluid and Bandera core at 250ºF.

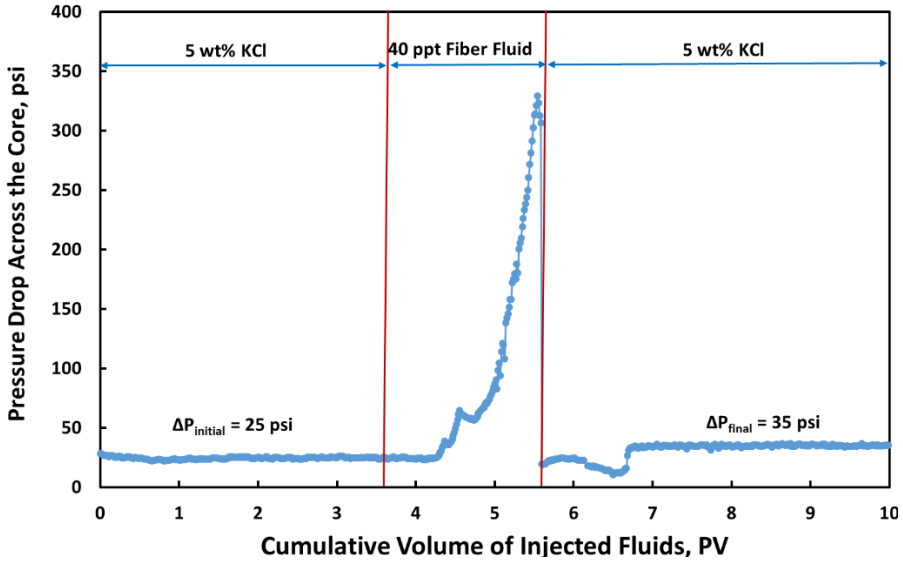

Fig. 98—Test 6: Pressure drop across the core with 40 lb/1000gal ENZ-NFC (V1) fluid and Beara core at 250ºF.

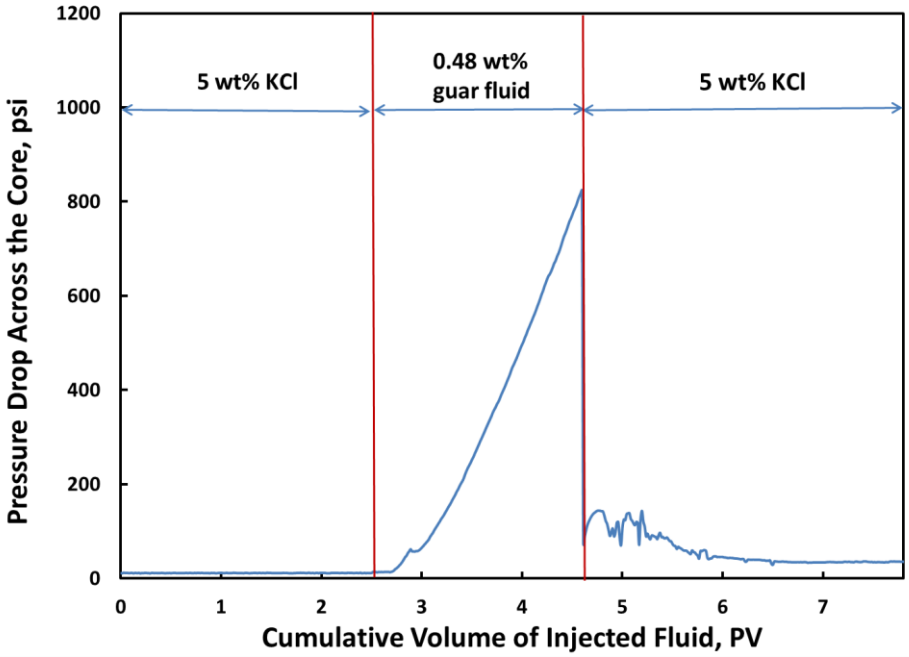

Fig. 99—Test 7: Pressure drop across the core with 40 lb/1000gal guar and Berea core at 75ºF.

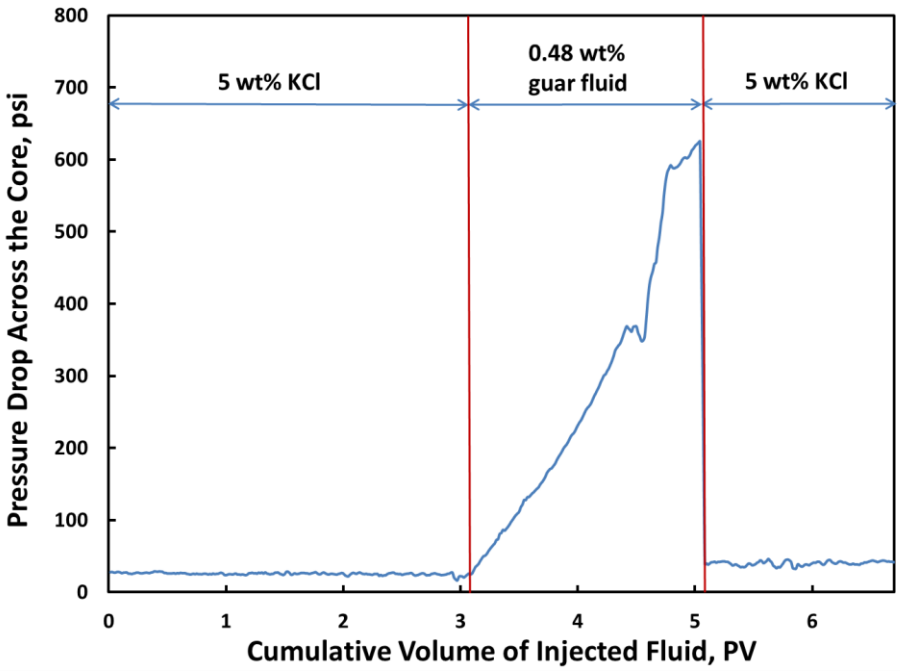

Fig. 100—Test 8: Pressure drop across the core with 40 lb/1000gal guar and Berea core at 250ºF.

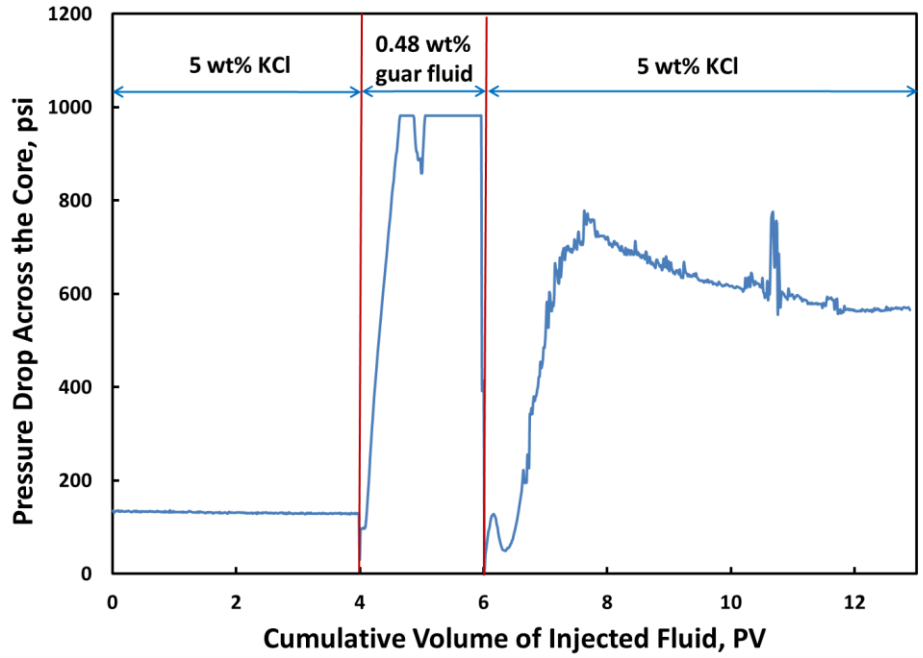

Fig. 101—Test 10: Pressure drop across the core with 40 lb/1000gal guar and Bandera core at 250ºF.

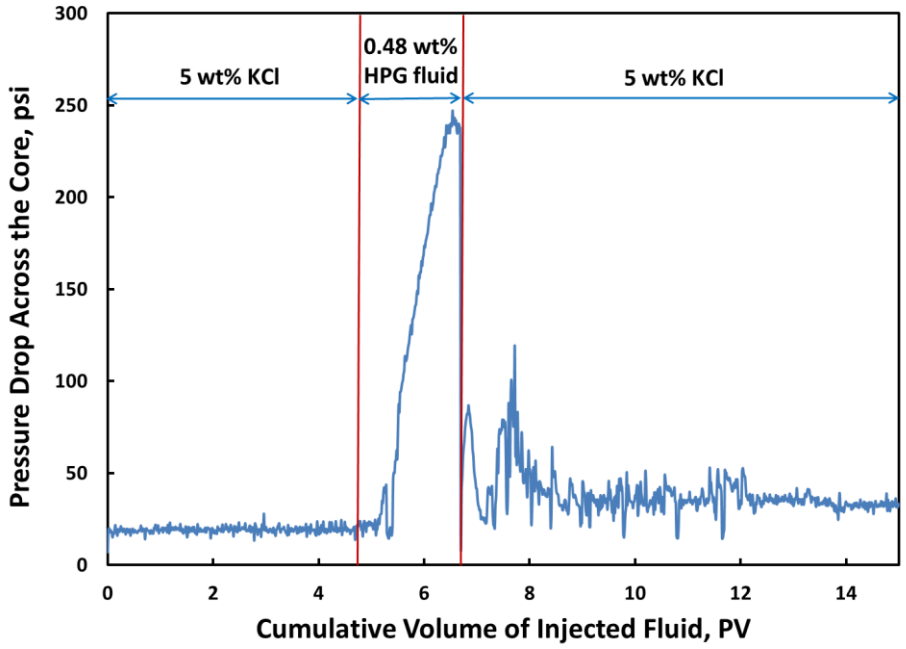

Fig. 102—Test 12: Pressure drop across the core with 40 lb/1000gal HPG and Berea core at 250°F.

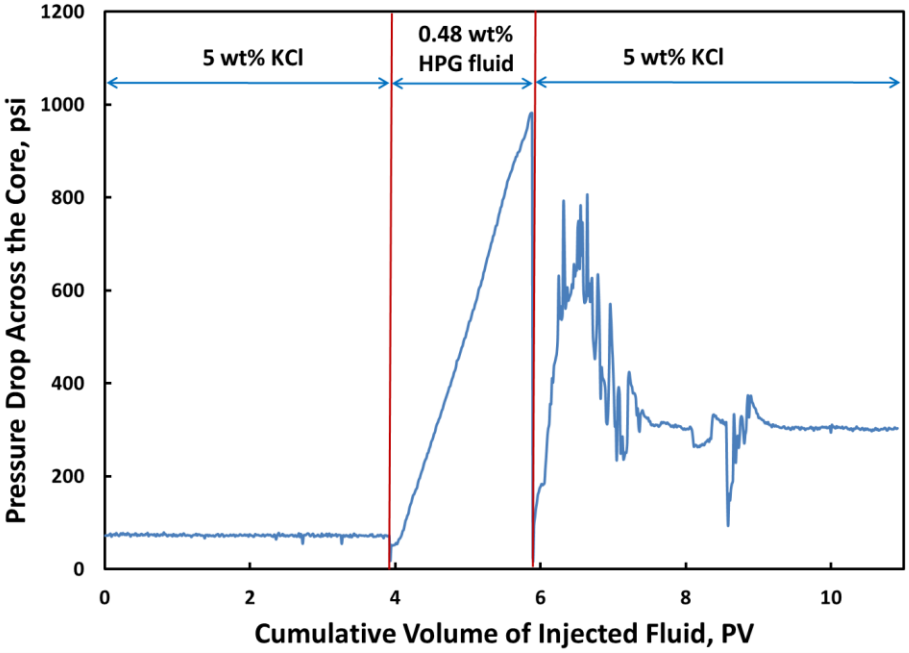

Fig. 103—Test 13: Pressure drop across the core with 40 lb/1000gal HPG and Bandera core at 250°F.

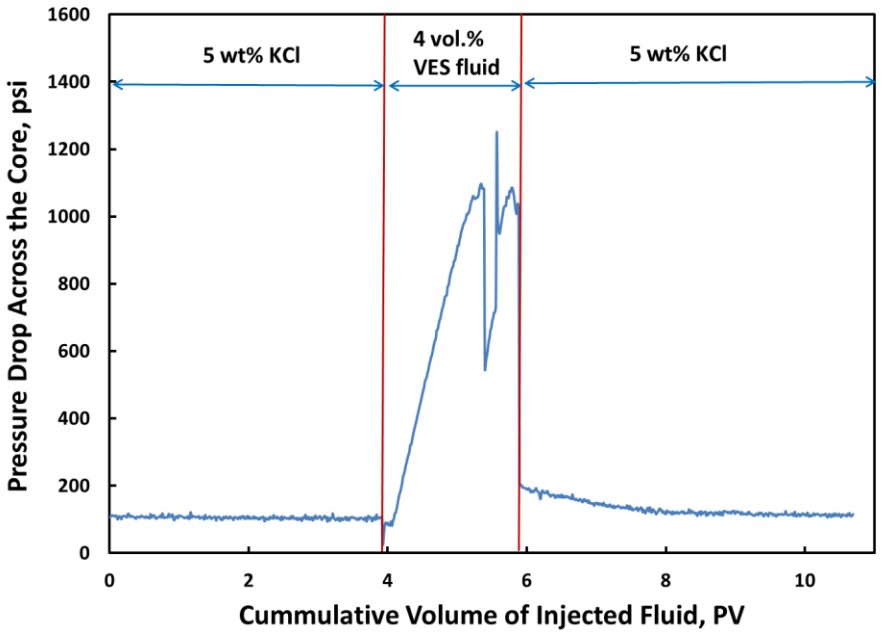

Fig. 104—Test 15: Pressure drop across the core with 40 gal/1000gal VES and Bandera core at 250°F.

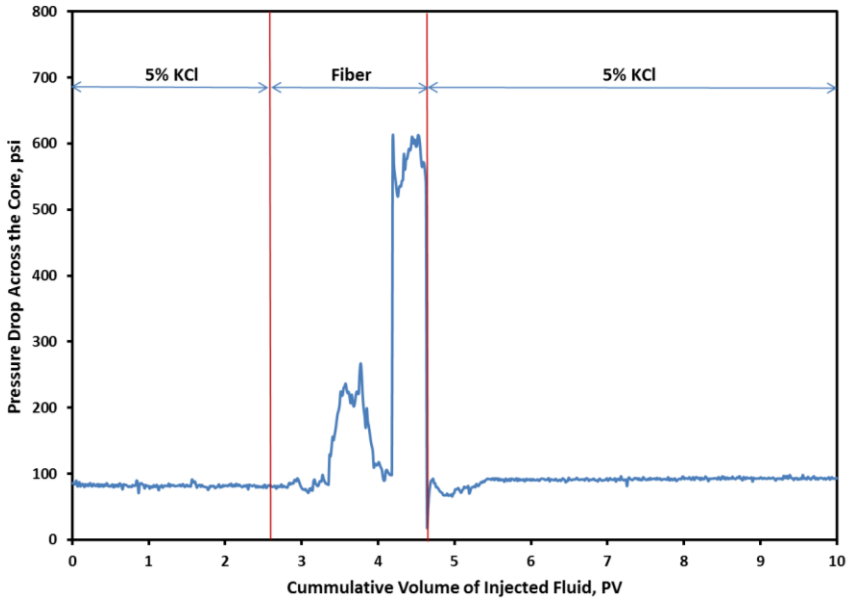

Fig. 105—Test 21: Pressure drop across the core with 40 lb/1000gal ME-MFC and Bandera core at 250°F.

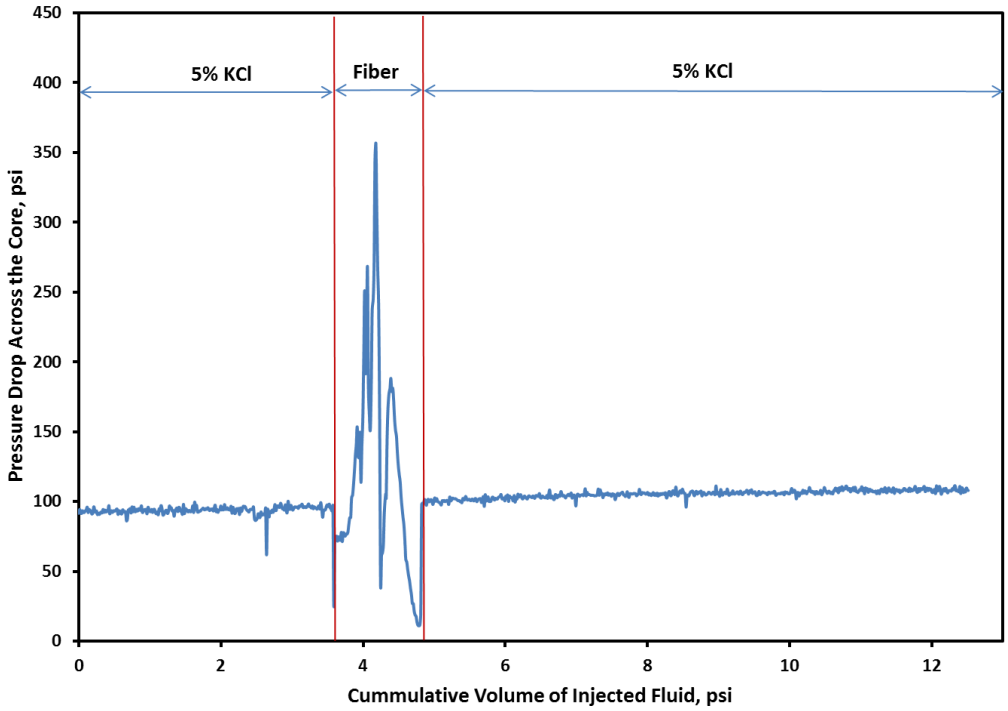

Fig. 106—Test 22: Pressure drop across the core with 67 lb/1000gal ME-MFC and Bandera core at 250ºF.